Albitization and oxidation of Variscan granitoid rocks related to the post-Variscan paleosurface in the Sudetes (Bohemian Massif, SW Poland)

Médard Thiry, Christine Franke, Kouakou Yao, Adam Szuszkiewicz, Carles Fàbrega, Maria Jeleńska, Magdalena Kądzialko-Hofmokl, Andrey Gurenko, David Parcerisa, Artur Sobczyk, et al.

To cite this version:

Médard Thiry, Christine Franke, Kouakou Yao, Adam Szuszkiewicz, Carles Fàbrega, et al.. Albitization and oxidation of Variscan granitoid rocks related to the post-Variscan paleosurface in the Sudetes (Bohemian Massif, SW Poland). International Journal of Earth Sciences, 2022, ⟨10.1007/s00531-022-02274-2⟩. ⟨hal-03902388⟩

HAL Id: hal-03902388
https://minesparis-psl.hal.science/hal-03902388v1

International Journal of Earth Sciences

Albitization and oxidation of Variscan granitoid rocks related the to Post-Variscan paleosurface in the Sudetes (Bohemian Massif, SW Poland)

--Manuscript Draft--

Manuscript Number:	IJES-D-22-00161R1
Full Title:	Albitization and oxidation of Variscan granitoid rocks related the to Post-Variscan paleosurface in the Sudetes (Bohemian Massif, SW Poland)
Article Type:	Original Paper
Keywords:	albitization; oxidation; granitoid; dating; paleosurface; Post-Variscan; Poland
Corresponding Author:	Médard Thiry, Ph.D Mines-Paris Fontainebleau, FRANCE
Corresponding Author Secondary Information:	
Corresponding Author's Institution:	Mines-Paris
Corresponding Author's Secondary Institution:	
First Author:	Médard Thiry, Ph.D
First Author Secondary Information:	
Order of Authors:	Médard Thiry, Ph.D
	Christine Franke, Ph.D
	Kouakou F.E Yao, Ph.D
	Adam Szuszkiewicz, Ph.D
	Carles Fàbrega, Ph.D
	Maria Jeleńska, Ph.D
	Magdalena Kądziałko-Hofmokl, Ph.D
	Andrey Gurenko, Ph.D
	David Parcerisa, Ph.D
	Artur Sobczyk, Ph.D
	Krzysztof Turniak, Ph.D
	Paweł Aleksandrowski, Ph.D
Order of Authors Secondary Information:	
Funding Information:	
Abstract:	The reddened granitoid facies in the basement of the Polish Sudetes exhibits two categories of alteration spatially arranged with respect to fractures: (1) saussuritization and sericitization within light-colored facies in the interior of fracture-bounded blocks and (2) albitization and hematitization in a reddened facies occurring adjacent to fracture walls. These alterations are associated with chloritization of primary ferromagnesian minerals and the development of secondary minerals such as quartz, K-feldspar, apatite, prehnite, calcite, and titanite. We link these parageneses and the observed zonation to a unique alteration event consisting of an interplay of chemical reactions of variable spatial extent. The complete albitization of the feldspars (plagioclase and K-feldspar) adjacent to fractures points to a significant supply of Na for the albite neoformation and availability of oxygen to form the associated hematite. The dating of the iron oxides by paleomagnetism and the secondary monazite associated with the albitized facies by U-Th-Pbtotal unambiguously indicates their

	Post-Variscan ages. In this context, the alterations are related to regionally widespread Post-Variscan paleosurface. Weathering profiles formed in phreatic groundwater environments downgradient of highlands that provided a hydrological head. Sodium supply was likely to origin from the gigantic salt playas that characterized Permian and Triassic lowlands. Weathering was interrupted by an advance of the Mesozoic transgression. The recognition of these weathering profiles over extensive parts of the Variscan Belt provides the basis for reconstructing the Post-Variscan paleosurface and constraining Triassic and Post-Triassic geodynamics, including erosion rates and geomorphological evolution of the Paleozoic massifs in Europe.

Albitization and oxidation of Variscan granitoid rocks related the to Post-Variscan paleosurface in the Sudetes (Bohemian Massif, SW Poland)

Médard Thiry(1*), Christine Franke(1), Kouakou F.E Yao(1), Adam Szuszkiewicz(2), Carles Fàbrega(3), Maria Jeleńska(4), Magdalena Kądziałko-Hofmokl(4), Andrey Gurenko(5), David Parcerisa(3), Artur Sobczyk(2), Krzysztof Turniak(2), Paweł Aleksandrowski(6)

(1) MINES Paris - PSL, Center of Geosciences and Geoengineering, 35 rue St Honoré 77305 Fontainebleau Cedex, France
(2) Institute of Geological Sciences, University of Wrocław, pl. M. Borna 9, 50-204 Wrocław, Poland
(3) Universitat Politècnica de Catalunya, Manresa, Spain
(4) Institute of Geophysics, Polish Academy of Sciences, Ks. Janusza 64, 01-452 Warsaw, Poland
(5) Centre de Recherches Pétrographiques et Géochimiques, UMR 7358, Université de Lorraine, F-54501 Vandoeuvre-lès-Nancy, France
(6) Polish Geological Institute – National Research Institute, Lower Silesia Branch, Al. Jaworowa 19, 53-122 Wrocław, Poland

*corresponding author: medard.thiry@free.fr https://orcid.org/0000-0003-2534-8882

Abstract:

The reddened granitoid facies in the basement of the Polish Sudetes exhibits two categories of alteration spatially arranged with respect to fractures: (1) saussuritization and sericitization within light-colored facies in the interior of fracture-bounded blocks and (2) albitization and hematitization in a reddened facies occurring adjacent to fracture walls. These alterations are associated with chloritization of primary ferromagnesian minerals and the development of secondary minerals such as quartz, K-feldspar, apatite, prehnite, calcite, and titanite. We link these parageneses and the observed zonation to a unique alteration event consisting of an interplay of chemical reactions of variable spatial extent. The complete albitization of the feldspars (plagioclase and K-feldspar) adjacent to fractures points to a significant supply of Na for the albite neoformation and availability of oxygen to form the associated hematite. The dating of the iron oxides by paleomagnetism and the secondary monazite associated with the albitized facies by U-Th-Pb$_{total}$ unambiguously indicates their Post-Variscan ages. In this context, the alterations are related to regionally widespread Post-Variscan paleosurface. Weathering profiles formed in phreatic groundwater environments downgradient of highlands that provided a hydrological head. Sodium supply was likely to origin from the gigantic salt playas that characterized Permian and Triassic lowlands. Weathering was interrupted by an advance of the Mesozoic transgression. The recognition of these weathering profiles over extensive parts of the Variscan Belt provides the basis for reconstructing the Post-Variscan paleosurface and constraining Triassic and Post-Triassic geodynamics, including erosion rates and geomorphological evolution of the Paleozoic massifs in Europe.

Keywords:

albitization, oxidation, granitoid, dating, paleosurface, Triassic, Poland.

Running title:

Albitization related to the Post-Variscan paleosurface

Statements and declarations:

The authors declare that they have no known competing financial interests or personal relationships that could have appeared to influence the work reported in this paper.

Acknowledgements:

This work is the result of a quest that was started more than 40 years ago at the Ecole des Mines de Paris. The French team likes to acknowledge the two participating Polish Institutions for the organization of the field work campaigns and for two scientific stays of K.Y. in the labs with access to CL. We acknowledge the IPGP Paleomagnetism group for access and help with 2G cryogenic magnetometer paleomagnetic and rock magnetic measurements as well as the CLIMAG group at the LSCE for access to the rock magnetic measurements performed in their laboratories. The authors thank Jean-Bernard Edel from the University of Strasbourg and an anonymous reviewer for their thoughtful comments, which significantly strengthened the earlier version of the article. Authors are also indebted to Tony Milnes from University of Adelaide for his discussions and language edition.

1 INTRODUCTION

In crystalline rocks, albitization is commonly considered to be a deep and high-temperature metasomatic alteration linked to granite cooling during exhumation (e.g. Putnis et al. 2007; Engvik et al. 2008; Sandström et al. 2010; Morad et al. 2010). Besides, in basaltic rocks, albitization with typical albite, chlorite, and epidote assemblage is considered to be relatated to pervasive alteration by deep circulation of heated seawater (spilitization) under relative lower temperature (Kelley et al. 1992; Alt et al. 2010; Richter and Diamond 2022). Studies of albitization in granitic and other basement rocks have been mostly undertaken by petrologists who usually consider its petrographical aspects and recognise the late-stage nature of the parageneses. However, the geometric aspects of the albitization phenomenon have never been thoroughly investigated. In this paper we describe the albitization as a result of superficial weathering, spatially and temporally associated with the Post-Variscan paleosurface, by analogy with situations described locally in the French Massif Central (Yerle and Thiry 1979; Schmitt 1986, 1992; Schmitt and Clement 1989; Parcerisa et al. 2009) and in NE Spain (Fàbrega et al. 2019).

We focus our study on the Polish Sudetes where paleomagnetic dating of Post-Variscan remagnetization overprints of the Paleozoic crystalline basement has already been well-reported in the literature (e.g. Edel et al. 1997). Our aim is to sort out whether the albitization observed in the Sudetic granitoids could have been of superficial (a weathering phenomenon) rather than of deep-seated hydrothermal origin. For this purpose, we describe detailed mineralogical and petrographical features of the albitized facies rocks. Special attention is payed to the petrographic evolution of the granitoids in relation to the reddened facies adjacent to fractures. The relationship between primary and secondary mineral phases is emphasized with the focus to establish a specific mineral paragenesis and geochemical conceptual model for the albitization, and to understand its association with the contemporaneous formation of hematite. Subsequently, the results of paleomagnetic dating of iron oxides and U-Th-Pb_{total} dating of monazites in the reddened facies are presented in order to explore their respective links with the Post-Variscan paleosurface.

2 GEOLOGICAL SETTING

2.1 Regional frame

The mountain range of the Sudetes is the topographic expression of a regional-size fault block, about 300 km long and 50 to 80 km wide, at the NE margin of the Bohemian Massif (Fig. 1). The Sudetic block was uplifted, together with the entire Bohemian Massif, in Late Cenozoic times along major NW-SE and NE-SW trending faults at the foreland of the Eastern Alps and Carpathians (e.g. Reicherter et al. 2008), while to the NE it is accompanied by the geologically similar Fore-Sudetic block that is currently not elevated.

The Sudetes occur on the norteastern periphery the internal zone of the Variscan belt of Europe, whose mostly crystalline, Late Neoproterozoic to Carboniferous basement rock complexes are arranged in a mosaic of a complex tectonic collage, amalgamated and deformed during Late Devonian through to Carboniferous Variscan tectonic events (Matte et al. 1990; Aleksandrowski and Mazur 2002; Kroner et al. 2008). The collage is intruded by syn- to late orogenic Carboniferous granitoid plutons, the most voluminous of which are those of Karkonosze, Strzegom-Sobótka and Kłodzko - Złoty Stok (e.g. Mazur et al. 2006, 2007).

The basement rocks are locally overlain by syn- to late-tectonic Carboniferous intramontane basins and remnants of a now much eroded post-orogenic Permo-Mesozoic sedimentary-volcanic cover (Fig. 1), which during Late Cretaceous – Early Paleogene times underwent compressional deformation: gentle folding and inversion-related faulting (Głuszyński and Aleksandrowski 2022). To the south, in the Intra-Sudetic Basin, Early Permian red beds and shales with volcanics up to 1250 m thick are followed by Late Permian and Early Triassic fluviatile deposits of Buntsandstein facies, wich do not exceed a few tens of meters in thickness (e.g. Dziedzic and Teisseyre 1990). To the north, in the North Sudetic Basin, there is a dominantly sedimentary series including Early Permian red beds with volcanics and Late Permian Zechstein facies carbonates, sulphates and clastics, averaging about 1000 m in thickness. The Early Triassic Buntsandstein of variegated sandstones, totalling about 600 m in thickness, are capped by Röt dolomites and later Keuper evaporites and Muschelkalk limestones (e.g. Baranowski et al. 1990; Chrząstek and Wojewoda 2011). In south-western and western Poland and eastern and northern Germany, the Early Triassic clastics that are accompanied locally by the Buntsandstein exceed 1000 m in thickness (Feist-Burkhardt et al. 2008). The Early Permian and Early Triassic clastic deposits reflect intense erosion and denudation of the southerly located Variscan internal massifs, including those of the Sudetes. The Late Permian Zechstein carbonates and sulphates as well as the late-Early to Middle Triassic carbonates, on the other hand, mark the episodes of marine transgression. The Late Permian transgression apparently left in the Sudetes only a thin sedimentary sequence of tens of metres thick, whereas that of the late-Early to Middle Triassic might have resulted in an originally much thicker sedimentary succession, similar to those in the adjacent areas (cf. e.g. Feist-Burkhardt et al. 2008). This is suggested by increasingly deepening facies of the now up to 100 m-thick Muschelkalk deposits towards their erosive top (Chrząstek and Wojewoda 2011). Also, the original presence of a relatively thick and extensive cover of marine Jurassic sediments in the Sudetes cannot be entirely ruled out, despite their present absence possibly due to pre-Cenomanian erosion.

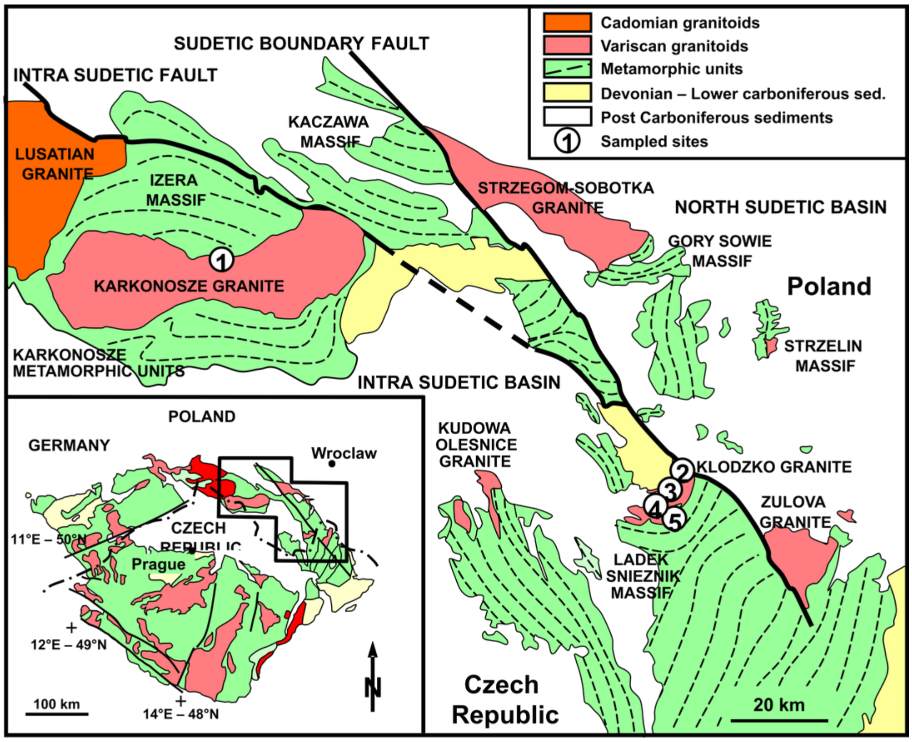

Fig.1 Geological map of the Sudetes (modified after Aleksandrowski et al. 1997). (1) Szklarska Poręba Huta quarry; (2) Laski quarry; (3) Laski village; (4) Chwalisław valley; (5) Mt Kopciowa.

2.2 Sampling

Our sampling was concentrated on the reddened granitic rocks in the quarry at Szklarska Poręba Huta on the Karkonosze pluton and in several exposures in the eastern part of the Kłodzko - Złoty Stok pluton, at Laski and in the Chwawlisław valley (Fig. 1). The focus was put on large exposures of rocks with distinct signs of reddening that are typically bound to fractures. In this study we use the term fracture to any brittle discontinuities in a rock, whether or not they imply fracture-parallel or -perpendicular displacement, i.e. various types of both joints and faults. Non-reddened rocks were also sampled in order to characterise differences between the reddened and non-reddened facies.

2.2.1 Karkonosze granitoid massif

The late-orogenic Karkonosze granitoid massif in the western part of the Sudetes is composed of a number of granitic facies thought to correspond to fractional crystallization, mixing with mafic magmas and hybridization processes (Žák and Klomínský 2007; Słaby and Martin 2008). The pluton resulted from sequential emplacement over a brief period of time at ca. 320-310 Ma (Machowiak and Armstrong 2007; Žák et al. 2013; Kryza et al. 2012, 2014; Kusiak et al. 2014).

Sampling of the Karkonosze pluton was undertaken in the Szklarska Poręba Huta quarry (N50°49’39’’, E15°29’38’’) on the NW margin of the Karkonosze massif, close to its contact with the metamorphic envelope (Fig. 1). Samples were obtained from a steep northern wall of the quarry where there was an exposure of two rock types in sharp intrusive contact: (1) a fine-grained equigranular leucocratic granite (so called aplogranite) and (2) a medium- to coarse-grained porphyritic biotite granite. Both granites contain thick (up to 25 cm) aplite veins and centimetre-wide quartz veins. According to Słaby et al. (2007), the granite from Szklarska Poręba Huta belongs to the geochemically furthest evolved granite types in the Karkonosze composite pluton.

The porphyritic granite from the Szklarska Poręba Huta quarry contains large phenocrysts (up to 10 cm) of perthitic K-feldspar (about 65-99% Or) mantled by plagioclase (about Ab ≥ 83%) and enclosed in medium-grained groundmass (Borkowska 1966; Słaby et al. 2002). Relative to the porphyritic granite, the aplogranite is enriched in quartz and plagioclase and impoverished in biotite and alkali-feldspar (Kozłowski et al. 1975).

2.2.2 The Kłodzko - Złoty Stok pluton

The Kłodzko - Złoty Stok (KZS) pluton, the largest composite intrusion in central Sudetes (Fig. 1), is composed off strongly diversified high-K metaluminous rocks, rich in mafic components (e.g. Lorenc 1994; Bachliński and Bagiński 2007; Jokubauskas et al. 2014). The small magma batches were emplaced between 349.0 ± 3.7Ma and 331.5 ± 2.6Ma. Short-lived late Carboniferous rejuvenation of magmatic activity along major fault zones caused intrusion of the the Laski monzogranite at 303.3 ± 3.8/4.2Ma (Jokubauskas et al. 2018 and references therein).

Exposures of reddened granitic rocks were sampled in the Laski quarry (N50°28’25” E16°48’34”), Laski village (N50°27’40” E16°48’12”) and a small old quarry near the creek of Mąkolnica (Chwalisław valley; N50°25’54” E16°49’42”). Jointly were sampled non reddened, relatively dark-grey medium-grained granodiorite wih relatively uniform plagioclase composition (36-46% An) typical of the Laski area (Wierzchołowski 1976). The quarry in the Chwalisław valley exposes granodiorite intruded by dykes (up to about. 1 m wide) of spessartite. Both rocks had been previously dated, yielding ages of 336.7 ± 2.3Ma and 321.1 ± 3.1Ma, respectively (Mikulski et al. 2013). Non-reddened granodiorite is a grey, medium- to fine-grained, equigranular rock with relative anorthite-rich plagioclase (39-44% An), whereas the fine-grained microporphyritic spessartite is composed of more sodic plagioclase (Wierzchołowski 1976; Awdankiewicz and Awdankiewicz 2010; Mikulski et al. 2013).

3 ANALYTICAL METHODS.

Powder X-ray diffraction (XRD) analyses were carried out at Mines-Paris, using a PANalytical X’Pert system fitted with a Cu-anode and X’celerator detector, on fragments of larger K-feldspar crystals separated by hand-picking from the bulk rock samples. XRD scans were run from 2 to 60° (2θ). The XRD diagrams were interpreted using the EVA© Bruker software. In the case of overlapping (131) and (1-31) peaks, deconvolution was undertaken using the FITYK software (Wojdyr 2010) with Pearson VII function applied to fit the peak shapes. Al-Si ordering of the K-feldspar structure was evaluated on the basis of the triclinicity parameter according to the method of Goldsmith and Laves (1954).

Selected thin sections from the reddened rock samples were studied using conventional petrographical microscopy and cathodoluminescence (CL) techniques at the Institute of Geological Sciences, University of Wrocław. The CL study made use of a CL MK3 cold cathode gun mounted on a polarizing optical microscope.

Systematic sampling for paleomagnetic analysis was performed focused on the reddened facies at four principal outcrops, three of them situated in the Kłodzko – Złoty Stok Massif (Laski quarry, Laski village, Chwalisław valley) and one in Szklarska Poręba Huta area. The samples for paleomagnetic analyses were drilled in the vicinity of principal fractures. The samples were collected as oriented drill cores using a petrol-driven hand drilling machine and as block samples oriented in field by measuring dip and dip azimuth.

They were cut into standard 2.5 x 2.5 cm cylinders for paleomagnetic experiments. Thermal demagnetization was subsequently performed on the cylinders either in the paleomagnetic laboratory of the Institute du Physique du Globe de Paris using a vertical three-axial 2G cryogenic magnetometer and at the Institute of Geophysics of the Polish Academy of Sciences in Warsaw using a 2G Enterprise SQIUD magnetometer. Stepwise demagnetization of the NRM was applied on the samples, starting at room-temperature, and if possible, embracing the complete temperature range up to the hematite temperature interval around 700°C. Alternatively, some selected samples were demagnetized using the alternating field technique at the Institute of Geophysics of the Polish Academy of Sciences in Warsaw. The resulting data are systematically corrected for the geographic position of each individual sample.

Further data processing was performed using either the PaleoMac5 software (Cogné 2003) or the PALMAG software provided by Lewandoski et al. (1997) Characteristic paleomagnetic directions were determined by a least-square fit of linear segments (Kirschvink, 1980) in orthogonal Zijderveld diagrams (Zijderveld 1967; see also supplementary material 2, Fig. S1 to S3), either on equal areas or in great circle fits. The PaleoMac5 and PALMAG software offer the opportunity to choose the groupped directions and to calculate respective site-mean directions and paleomagnetic pole statistics (Fischer, 1953; Mc Fadden and McElhinny 1988). The analyses of thermal demagnetization of NRM curves and thermomagnetic experiments (magnetization and saturation remanence during heating curves) allow the identification of magnetic carriers of the paleomagnetic directions (for instrumental details and rock magnetic results please see also supplementary material 2, Fig. S4 and S5).

The chemical compositions of feldspars and micas were analysed by EPMA (Electron Probe Micro Analysis) at the Scientific and Technological Centers of the Universitat de Barcelona (CCiTUB), using Cameca SX-51 and JEOL JXA-8230 electron microprobes, both operating at 15 kV and 1.5 nA. The CL images of the samples were used to guide the placing of the analyses. The table of EPMA results is included in the supplementary material 1.

Monazite dating was carried out using the EPMA U-Th-Pb$_{total}$ method following the recommendations included in Cocherie et al. (1998), Cocherie and Albarede (2001), and Williams et al. (2006). Monazite grains suitable for EPMA analysis were found by means of BSE imaging using a Hitachi TM-1000 electron microscope at the Manresa School of Engineering (Spain). U-Th-Pb$_{total}$ EPMA analyses were undertaken at the Scientific and Technological Centers of the Universitat de Barcelona (Spain) using a Jeol JXA-8230 electron microprobe operating at 15 kV, 40 nA of current intensity and a beam diameter of 1 µm. An in-house reference monazite from the Petaca District (Mexico), with an age of 1332 ± 5 Ma (2σ), was analyzed as a control standard jointly with the monazite samples. The age of each analysed monazite was calculated using the MonaziteAge software based on the works of Suzuki and Adachi (1991, 1994) and Suzuki et al. (1994) and which is included with the Jeol JXA-8230 instrument. The initial acquired data were prepared for subsequent statistical age analysis by eliminating the analyses which presented oxide totals higher and lower than 100 ± 5%. Subsequently, age outliers were discarded using a stepwise process based on box-plot graphs. The final ages of the different monazite generations were determined by deconvolution of the ages histogram using the Microsoft Excel add-in

ISOPLOT 4.15 from the Berkeley Geochronology Center (Ludwig 2003). A total of 189 EPMA analyses were made and 147 analyses (77% of the total) were retained including 18 from the Szklarska Poręba Huta quarry and 129 from the Chwalisław valley section. The table of monazite EPMA results is included in the Electronic Supplementary material 1.

The oxygen isotope composition of plagioclase and K-feldspar was determined by Seconday Ion Mass Spectrometry (SIMS) using a CAMECA IMS 1280HR ion microprobe at the Centre de Recherches Pétrographiques et Géochimiques (CRPG), Vandœuvre-lès-Nancy, France. Samples were mounted in 25 mm diameter epoxy mounts and the surface was metallographically polished. Afterwards the samples surfaces were imaged under optical cathodoluminescence to differentiate textural domains within the crystals. The detailed analytical conditions during the SIMS session are described in Fàbrega et al. (2017). The granite samples were analysed jointly with in-house plagioclase and K-feldspar standards. The analyses were placed in homogeneous luminescent domains in crack- and inclusion-free areas of the crystals. A total of 28 and 31 analyses were carried out on plagioclase and K-feldspar grains, respectively. Afterwards, the craters of the SIMS analyses were observed under BSE-imaging and analyzed by EPMA to check that the craters were homogeneously excavated and determine the chemical composition linked to each isotopic analysis. The instrumental mass fractionation (IMF) of the raw results was corrected by means of response surface methodology (RSM) following the procedures and using the response surface models described in detail by Fàbrega et al. (2017). The SIMS results including the instrumental setting, the raw and IMF-corrected $\delta^{18}O$ values, and the CL-images of the samples are included in the Electronic Supplementary Information. All the $\delta^{18}O$ values of this paper are relative to VSMOW.

4 SPATIAL DISTRIBUTION OF THE REDDENING

A process of granite reddening has resulted in both a pervasive coloration homogeneously distributed within the rock volume at some area and a more localised development of red to pinkish granite facies allied to the fracture network at other areas. The most typical and widespread type of alteration is a **fracture controlled reddening** with reddish/pinkish coloration restricted to narrow bands along fracture planes. The granodiorite of the Laski quarry and the aplogranite of the Szklarska Poręba Huta quarry are typical examples for this. The most intense alteration is a **pervasive and homogeneous reddening** with the entire rock impregnated by the reddish pigments, and fracture planes coated with dark red iron oxides. The Laski village section is typical of this pervasive reddened facies. The less intense alteration is a **red spotted facies** with pinkish spots distributed within non-reddened rock. The granite of Chwalisław valley outcrop is typical of this weakly altered facies.

In the Laski quarry the fractures are metre-spaced, cutting the rock into well-defined 0.5 to 1 m^3 blocks (Fig. 2a). The extent of fracture controlled reddening is closely related to the rank of the fracture, i.e. it is weak along minor fractures and more intense along major ones. The reddening penetrates the rock as deep as 1-10 cm. The coloration is most intense along fracture walls but fades further away from the fractures. There is also a direct relation between the frequency of the fractures and the intensity of coloration. In the SE part of the quarry, the most intensive reddened facies occur along a weakly defined metre-wide zone, characterized by particularly dense fracturing. Similarly, the porphyritic granodiorite exposed on Mt Kopciowa has fracture controlled reddening restricted to weak, narrow staining fronts, where its large K-feldspar phenocrysts are partly or entirely pink along the fractures.

In the Szklarska Poręba Huta quarry, the porphyritic granite is generally not reddened. However, the fine to medium-grained aplogranite exhibits a light pink reddening along steep N40° major and N135° related fractures, which penetrates the rock to a distance of 5-15 cm to 30-40 cm away from the fractures. Where fractures are sparse, the aplogranite is greenish in the center of the blocks (Fig. 2b) but in densely fractured (“chopping fractures”) zones the rock is pervasively pink.

The Chwalisław valley granodiorite outcrop is a typical example of the red spotted facies (Fig. 2c). A weak fracture controlled pinkish coloration has developed in narrow zones along fractures but further away from the fracture planes there is a scatter of spots together with small pinkish patches in the non-reddened rock. There is no obvious direct relationship between lamprophyre dikes and the reddening of the granodiorite. In fact the lamprophyre also has a faint pinkish coloration along the fracture planes, but their observance is hindered by the dark color of the rock.

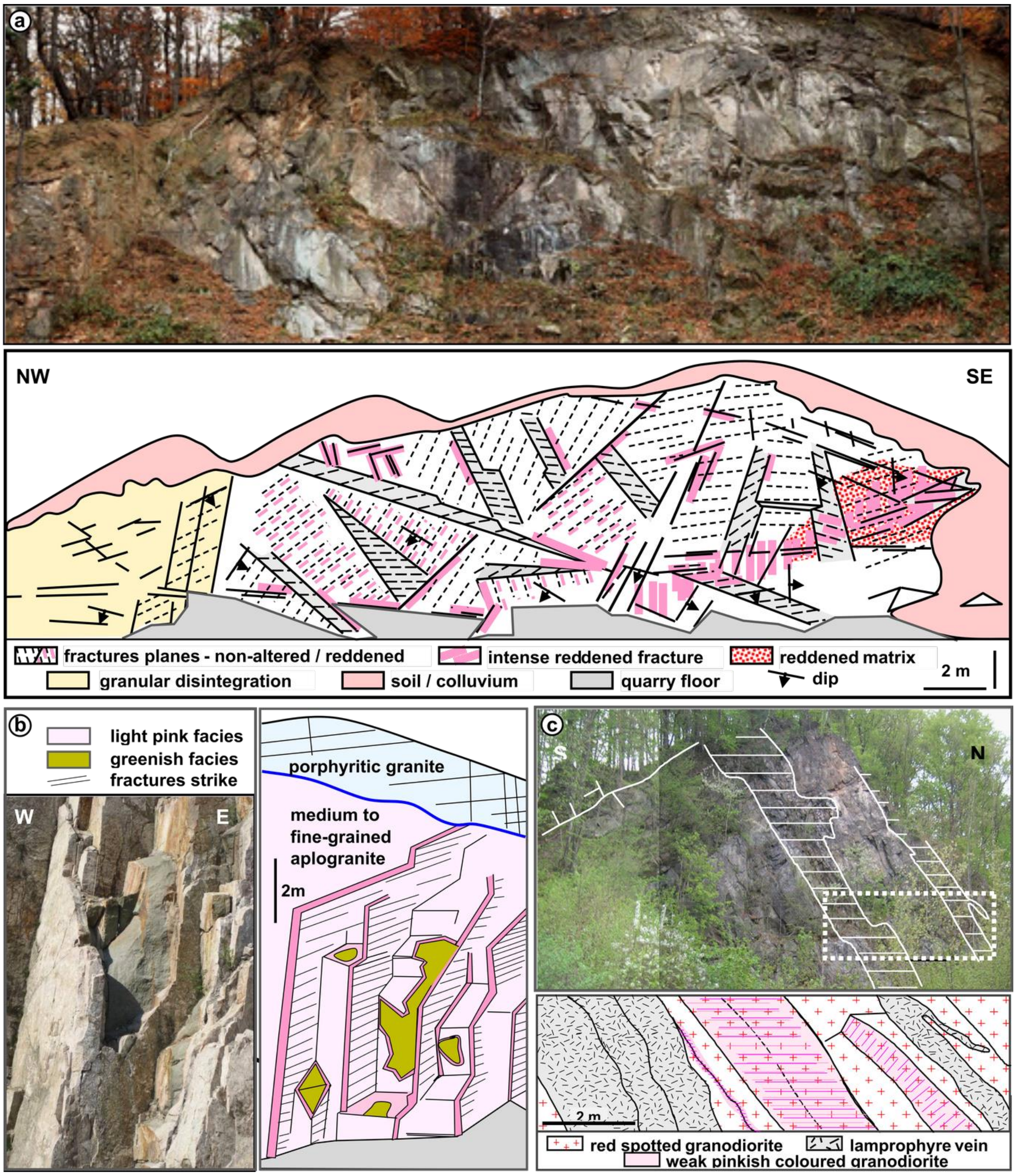

Fig. 2 Spatial arrangement of the reddening. (a) Photo and sketch of the fracture-controlled reddening in the Laski quarry. The highly fractured zones in the SE of the quarry are the most reddened. (b) Szklarska Poręba Huta quarry facies. The reddening proceeds along the steep fractures that cut the fine-grained aplogranite. (c) Sketch of the reddish alteration facies in the Chwalisław valley outcrop. The alteration is parallel to the lamprophyre veins that intruded the granodiorite.

5 MICROSCOPIC ASPECTS OF REDDENING

Optical and cathodoluminescence petrography reveal some systematic differences between the non-reddened and reddened rock facies. We present petrographical comparison of the affected mineralogical constituents, but thoses that are neither affected by nor related to the staining phenomenon are omitted from the comparison.

5.1 Plagioclase

In non-reddened granites plagioclase appears white to the naked eye. Large crystals are often normal-zoned with Ca-enriched cores and Ca-poor margins: some crystals are also rimmed with nearly pure albite. Polysynthetic twinning is common. It also occurs as inclusions in the K-feldspar phenocrysts (in porphyritic rock types) and constitutes most of the rock groundmass. The luminescence is typical for igneous plagioclase with yellow-green CL (Fig. 3a and 3b), that turns blue in the albitic rims. Regions with increased intensity of yellow-green CL correlates with a higher Ca content (cf. Słaby et al. 2002; Słaby and Götze 2004). Partial sericitization of primary plagioclase is often observed, especially in the Ca-enriched cores.

In reddened granites plagioclase appears pink to the naked eyes, due to hematite pigments which confer a red cloudiness to spots where primary plagioclase has been thoroughly altered to secondary untwined albite (i.e. albitization). While the hematite-free domains retain their primary CL characteristics, the pigmented plagioclase is non-luminescent (Fig. 3a and 3b), which is typical of neogenic feldspars formed at low temperatures (e.g. Marshall 1988; Götze et al. 2000; Leichmann et al. 2003; Powolny et al. 2022). Contrasting CL conveniently mark out the geometrical relationship between primary plagioclase and secondary albite: Ca-enriched crystal cores may be albitized leaving the outer Na-enriched zones unaffected (Fig. 3a) or secondary albite may be associated with microcracks, twinning and/or cleavage planes (Fig. 3b).

Primary plagioclase compositions range from An_{26} to An_{84}, and An_{14} to An_{51}, in the Chwalisław biotite-hornblende granodiorite and Laski valley granodiorite, respectively (Table 1). The oxygen isotope composition of the primary plagioclase, determined in the biotite-hornblende granodiorite of Chwalisław, shows $\delta^{18}O$ values ranging from +3 to +7 ‰ (Fig. 3c and Table 2), with no aparent correlation with the composition of plagioclase determined by EPMA in the SIMS points, that ranges from An_{36} to An_{43}.

Secondary albite shows a widespread micro porosity and a typical composition about $An_{0\text{-}2}$, independently of the type of parent rock and of the primary plagioclase composition (Table 1). In crystals were the completeness of albitization has not been totally reached, a slightly higher Ca content was observed, with An% values ranging from 6 to 14% (Table 1). The oxygen isotope composition of the secondary albite, determined in the Chwalisław sector, is significantly heavier than the primary plagioclase, with $\delta^{18}O$ values ranging from +7 to 11‰ (Fig. 3d and Table 2).

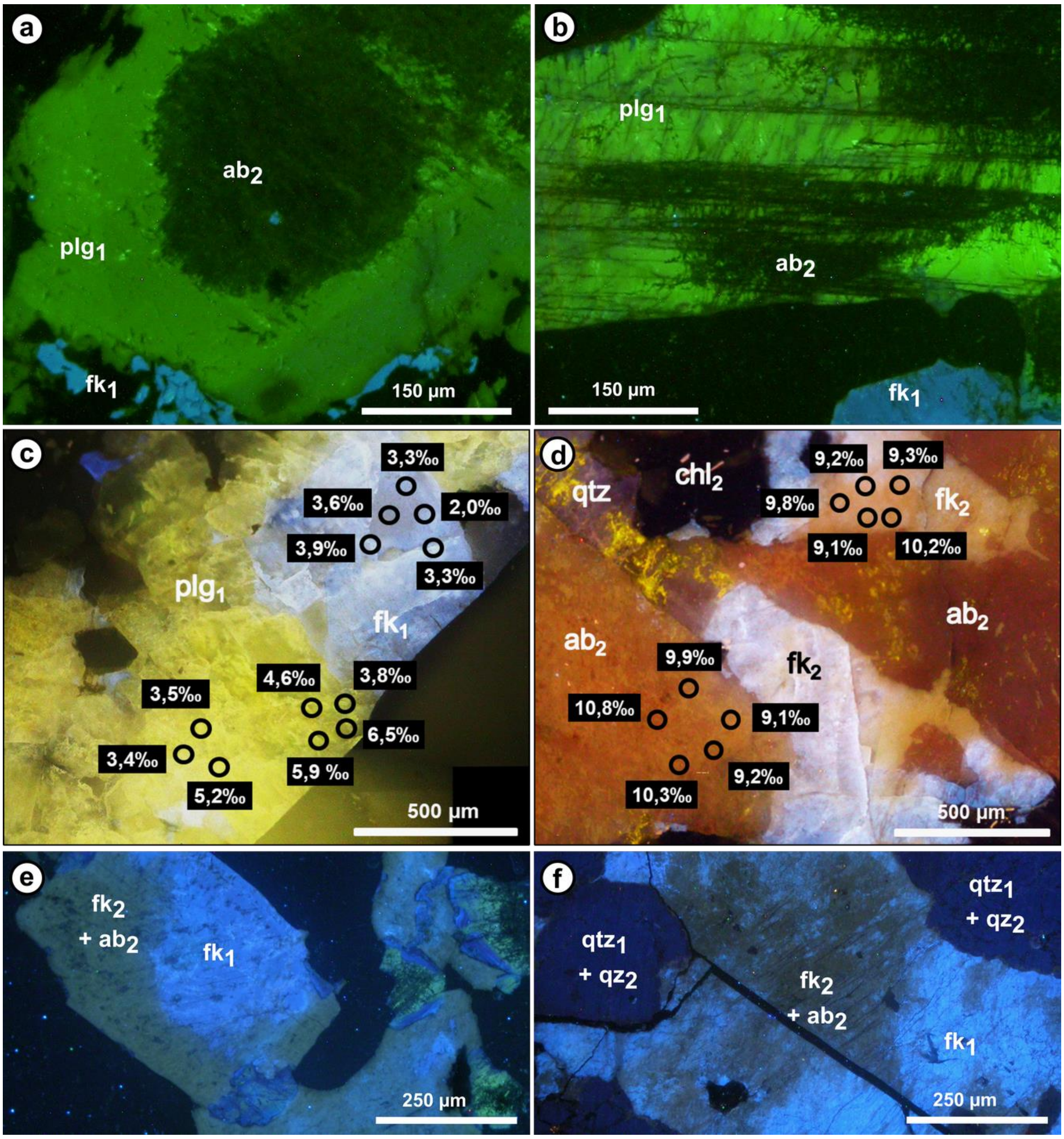

Fig. 3 CL Petrography and oxygen isotope composition of albitized plagioclase and K-feldspar. (a) Plagioclase with a non-luminescent albitized core and yellow luminescent rim. (b) Albitization along the major twinning planes and micro-fractures. (c) δ18O values of yellow luminescent primary plagioclase and blue luminescent primary K-feldspar and (d) non-luminescent secondary albite and turbid microclinized K-feldspar. (e) Cathodoluminescence images of partially albitized K-feldspar showing non-luminescent areas containing secondary microcline, patch perthites and quartz patches on the crystal rims. (f) Albitization of K-feldspar along microfractures. plg$_1$: primary plagioclase; ab$_2$: secondary stained albite; fK$_1$: primary K-feldspar; fK$_2$: secondary K-feldspar; qtz$_1$: primary quartz; qtz$_2$: secondary quartz.

Table 1 Mole % of feldspar components of plagioclase and K-feldspar.

site	rock	plagioclase		K-feldspar	
		primary / albitized	**An %**	**primary / microclinized**	**Or %**
Reddened facies					
Szklarska Poręba	porphyritic granite	primary albitized	1 - 3 0 - 3	microclinized	94 - 98
Laski Quarry	granodiorite	albitized	0 - 2	microclinized	95 - 98
Spotted facies					
Szklarska Poręba	porphyritic granite	primary albitized	8 - 14 4 - 6	partially microclinized	78 - 93
Laski Quarry	granodiorite	primary albitized	21 - 59 6 - 14	partially microclinized	79 - 92
Fresh rock					
Laski Valley	granodiorite	primary	14 - 51	primary	85 - 91
Chwalislaw Valley	hornblende-biotite granodiorite	primary	26 - 84	primary	72 - 93

* EPMA analyses converted to mole percent of the feldspar components by normalizing to eight oxygen atoms per formula unit.

Table 2 $\delta^{18}O$ ‰ results of plagioclase and K-feldspar.

site	rock	plagioclase		K-feldspar	$\delta^{18}O$ ‰
		primary / albitized	**$\delta^{18}O$ ‰**	**primary / microclinized**	
Reddened facies					
Chwalislaw Valley	hornblende-biotite granodiorite	albitized	6 - 11	microclinized	5 - 11
Fresh rock					
Chwalislaw Valley	hornblende-biotite granodiorite	primary	3 - 7	primary	2 - 4

Apart from hematite pigments, neogenic albite is sometimes associated with calcite and prehnite. Secondary albite is not twinned - its development erased the polysynthetic twinning in the primary plagioclase. This is in contrast to “classical” saussuritization in which the petrographic features of the primary plagioclase are preserved, at least partially (de la Roche 1957; Sandström et al. 2010; Jenkin et al. 1992; Morad et al. 2010).

5.2 K-feldspar

In non-reddened granites, K-feldspar is white to grey and often Carlsbad-twinned with varying amounts of microperthitic albite. In the porphyritic granitoids it is present as large (several centimeters) phenocrysts and as a constituent of the groundmass (<< 1 cm). Cross-hatch twinning is not a common feature but, if present, is developed in domains rather than whole crystals.

As observed using CL, any alteration of primary crystals is manifested by a change in the blue luminescence typical of igneous K-feldspar (cf. Słaby et al. 2002; Słaby and Götze 2004; Powolny et al. 2022). The hematite-stained parts of K-feldspar crystals correspond to regions of quenched, sometimes dark-brownish luminescence, similar to the previously shown secondary albite (Fig. 3e and 3f). Such CL characteristics match secondary feldspars formed in low-temperature diagenetic and supergenic environments (e.g. Götze et al. 1999; González-Acebrón et al. 2010; González-Acebrón et al. 2012).

There is a clear relationship between hematite staining and albitization of K-feldspar. Semi-quantitative measurements of the intensity of XRD reflections from the two feldspar species reveal that a low and rather constant albite content in K-feldspar phenocrysts in non-reddened granitoids increases and becomes highly variable in the reddened facies (Yao 2013). Primary light-colored K-feldspar phenocrysts are predominantly formed of orthoclase but an increase in albite content is generally marked by its transformation (recrystallization) to microcline, as indicated by an increasing triclinicity. Since triclinicity reflects the state of Al-Si ordering of K-feldspar structure it is likely that the increase of Al-Si ordering, albitization and hematite-staining of the K-feldspar are interrelated processes.

The composition of the primary K-feldspar ranged from Or_{72} to Or_{93} in the the Chwalisław sector and from Or_{85} to Or_{91} in the Laski valley (Table 1). The oxygen isotope composition of the primary K-feldspar (Table 2), determined in crystals from the biotite-hornblende granodiorite of Chwalislaw valley, present $\delta^{18}O$ values ranging from +2 to +4 ‰. The $\delta^{18}O$ values show a positive trend versus the increase in K^+ content of the K-feldspar (see Electronic Supplementary Information). In the quenched luminescence regions, the primary orthoclase is replaced by secondary microcline showing aboundant micro porosity, with typical composition varying from Or_{94} to Or_{98}, indepentdently of the parent rock and the composition of the primary K-feldspar. The microclinization process is accompanied by the development of patch perthites of highly pure albite, with typical composition of An_0. The oxygen isotope composition of the microclinized K-feldspar (Table 2), also determined in the biotite-hornblende granodiorite of Chwalislaw, presents $\delta^{18}O$ values, ranging from +5 to +11 ‰ and also shows a positive trend versus the orthoclase content (0r %) of the K-feldspar.

5.3 Albitization propagation

Albitization of primary plagioclase occurred along microcracks and cleavage planes (Fig. 4a). The albitized zones are patchy and amoeboid, with no relation to the crystallographic directions in the primary plagioclase. Often albitization developed from the margins towards the central parts of a crystal, leaving the core as well as the primary albitic outer rim unaffected (Fig. 4b). A common albitization pattern is observed in some of the compositionally zoned plagioclases in which the Ca-enriched core has been altered but the Ca-poor rims remains unaffected (Fig. 4c). The albitized core often contains scattered sericite which corresponds to an earlier phenomenon than albitization as it is also observed in non-albitized plagioclase from the non reddened facies. In most altered facies, primary plagioclase is perversavely albitized exept outer rims composed of primary albite (Fig. 4d). These altered facies are intensely reddened and often show micro-fractures filled with iron oxides.

Albitization of primary K-feldspar proceeds in a similar way as in palgioclases: from the margins of the crystals along microcracks, twinning and/or cleavage planes. In the reddened granitoids, euhedral to sub-euhedral K-feldspar phenocrysts are partly or entirely pink (Fig. 4e and 4f). There is a direct correlation between the intensity of staining in the granitoids and the amount and distribution of hematite pigmenting phenocrysts and smaller K-feldspar crystals.

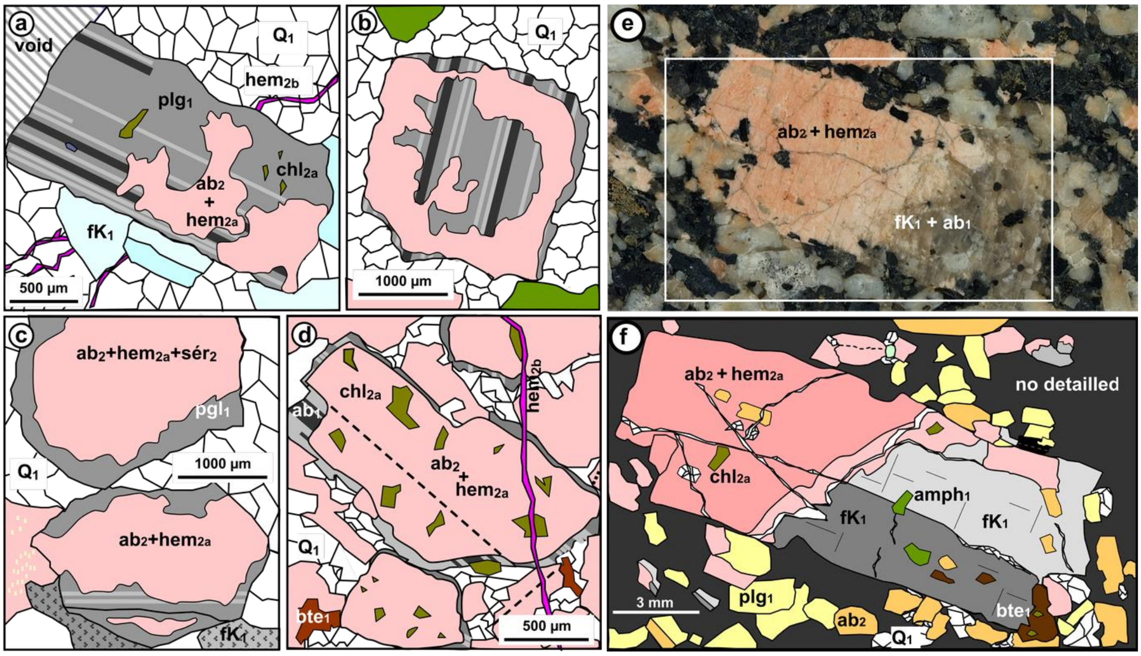

Fig. 4 Sketches of albitized red/pinkish plagioclase and K-feldspar. (a) Plagioclase albitization along microfractures. (b) Irregular albitization of the outer rim of the primary plagioclase: the primary albitic rim remains unaffected. (c) Albitization of the seritized core of the primary plagioclase. (d) Complete albitization of the primary plagioclase crystal except the outer rim which is composed of primary albite. (e) Polished section of a partially reddened orthoclase phenocryst. The upper part of the phenocryst is pink and dull whereas the lower part is translucent. (f) Sketch of (e). The orthoclase phenocryst exhibits classic Carlsbad twinning in the translucent part and has inclusions of hornblende, chlorite, biotite, and plagioclase. In the pinkish part the twinning is erased, and the orthoclase is albitized and hematized. fK_1: primary K-feldspar; plg_1: primary plagioclase; Q_1: primary quartz; bte_1: biotite; amph1: amphibole; ab_2: untwined secondary albite; chl_{2a}: secondary chlorite after biotite; hem_{2a}: pigmentary hematite; hem_{2b}: coarser-crystalline hematite.

5.4 Fe-Mg minerals

Light to dark brown biotite is the main mafic mineral and minor greenish hornblende is commonly present in samples from the Kłodzko - Złoty Stok massif. In non-reddened samples both biotite and hornblende show signs of chloritization, though hornblende appears more resistant to this alteration.

Chloritization is significantly more intensive in the reddened granitoids where all stages of the replacement process, from initial weak alteration along the edges and cleavage planes of the primary crystals to the formation of complete chlorite pseudomorphs, could be observed. Biotite inclusions in hematite-stained plagioclase are invariably replaced by chlorite. There is no clear evidence for a volume change during the chloritization of the primary Fe-Mg minerals. Secondary microcrystalline and flaky chlorite also occurs in microfractures and intergranular boundaries. Pyrite, Ti-oxides and titanite are often associated with secondary chlorite.

5.5 Fe-minerals

Fe-sulphides and oxides in the granitoids include pyrite, hematite, maghemite, and magnetite. Pyrite occurs irrespective of hematite pigmentation as relatively large (50-200 µm) euhedral crystals and lens-shaped aggregates in the cleavages of chloritized biotite and hornblende. Late anhedral grains fill also microfractures. The margins of most of the observed pyrite grains are replaced by hematite.

Pigmentary hematite is responsible for red cloudiness observed in plagioclase from the reddened granitoïd facies under microscope. In the red spotted facies plagioclase exhibits coexisting hematite-pigmented and hematite-free domains which are primary igneous plagioclase (Fig. 5a) and in pervasively reddened facies and in fracture controlled reddened facies the plagioclase is entirely hematite-stained (Fig. 5b). Dusty hematitic pigment is confined to albitized domains in plagioclase and K-feldspar. Some observations suggest that the hematitic pigments are not directly related to microporosity in the altered feldspars. Firstly, the pigment is absent from the porous saussuritized feldspars of the non-reddened granitoid facies. Secondly, it is not concentrated along the albitization front which is enriched in micropores that relate to the volume-loss replacement of the primary feldspar by secondary albite. Instead, hematite is distributed more or less homogeneously through all of the albitized feldspar. Microscopic flaky aggregates and subhedral larger grains of hematite are often observed in intergranular boundaries located close to chloritized biotite and hornblende (Fig. 5b) and in microfractures (Fig. 5c) and, as well as in the cleavage of some chloritized biotite (Fig. 5e), sometimes together with secondary quartz and/or calcite.

Maghemite and magnetite could not be recognized unequivocally under the microscope nor by XRD analyses but their presence was unmistakably detected by thermal demagnetization experiments (paleomagnetic experiments, this study). In contrast to hematite, magnetite is restricted to the non-reddened facies. Maghemite, on the other hand, was detected mainly in the weakly reddened facies. Thus, maghemite may be regarded as a ‘transitional’ Fe-mineral between the magnetite-dominated non reddened granitoids and hematite-dominated reddened facies.

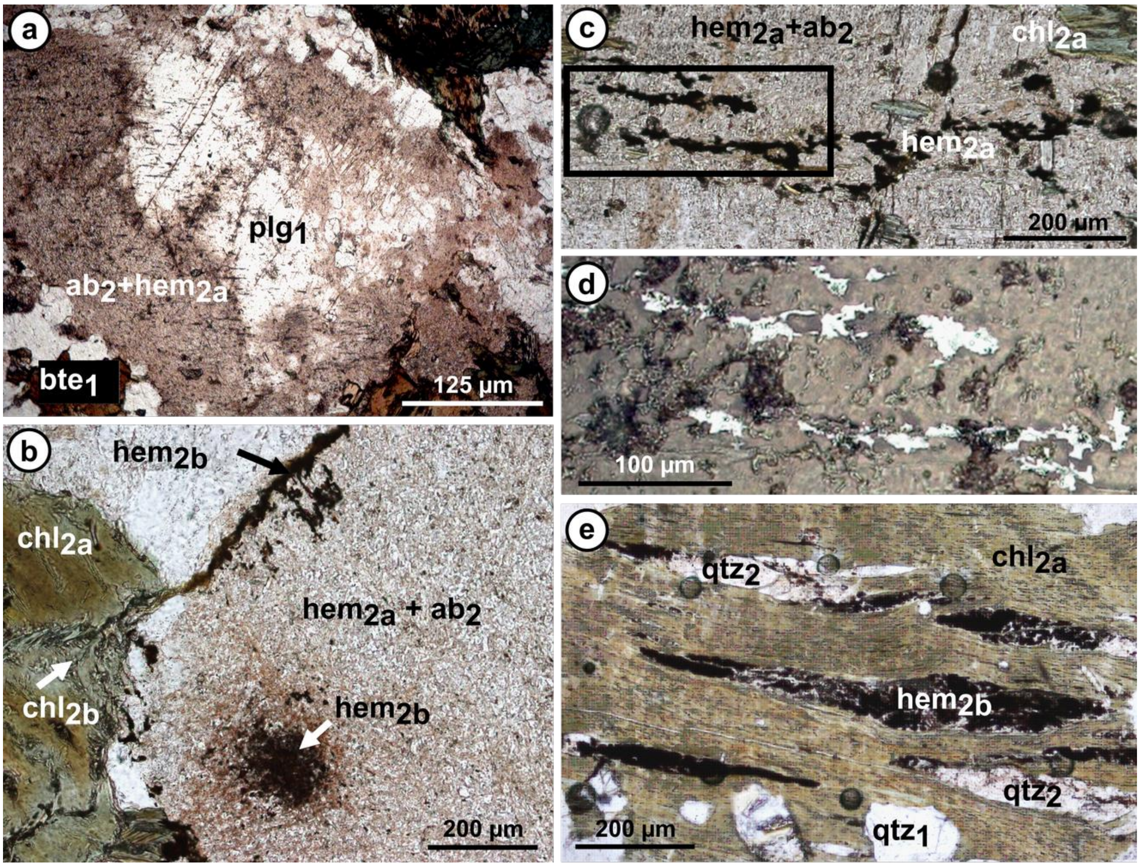

Fig. 5 Hematite occurrences within albitized granitoids. a) Light pink albitized plagioclase away from reddened fracture walls with light colored relict of primary plagioclase. (b) Plagioclase entirely reddened and albitized from pervasively reddened facies; hematite appears as pigments within the secondary albite and as granules within microfractures. (c) Fine red hematite pigments and elongated hematite flakes within secondary albite; plane polarized. (d) Enlargement of (c); reflected light. (e) Hematite lenses within the cleavage of a chloritized biotite crystal, notice lenses of secondary quartz in similar position; plane polarized. plg$_1$: primary plagioclase; ab$_2$: secondary albite; bte$_1$: primary biotite; chl$_{2a}$: secondary chlorite after biotite; chl$_{2b}$: neogenic chlorite in micro-fracture; hem$_{2a}$: secondary hematite pigment; hem$_{2b}$: secondary granular and flaky subhedral hematite.

5.6 Other minerals

Quartz of the non-reddened facies is essentially unaltered, presenting a homogeneous dull-luminescence. Differently, the quartz grains of the reddened facies are significantly altered, presenting a network of micron sized non-luminescent veins of secondary quartz displaying in a cobweb texture. Internal zoning of quartz have already been described in the chloritized facies of the Sudetic Karkonosze granite (Wilamowski 2002), and similar quartz alteration has been observed in the red albitized facies of NE Spain (Fàbrega et al. 2019).

Sericite is more abundant in non-reddened samples and in weakly-reddened rock away from fractures. It occurs mostly in plagioclase and emphasizes the compositional zoning as it has preferentially developed in the Ca-enriched plagioclase cores but is entirely absent from the albitic rims. Sericitization obliterates the primary polysynthetic twinning in the plagioclase host. Tiny sericite crystals (5 µm) occur in plagioclase in the aplogranite of Szklarska Poręba Huta and less fractured granodiorites of the Kłodzko – Złoty Stok massif. This form of sericite is associated with secondary albite but not with Ca-bearing minerals such as prehnite and epidote. However, larger sericite flakes (10-20 µm) formed at the expense of Ca-enriched plagioclase in the reddened granodiorite from Chwalisław and Laski are associated with secondary prehnite, albite, and sometimes also calcite. Sericite is rare in K-feldspars.

Prehnite and less commonly calcite are either present as secondary minerals associated with saussuritization of plagioclase and chloritization of Fe-Mg minerals or as late primary phases healing fractures. While calcite is observed exclusively in the reddened rock facies, disseminated prehnite is more abundant in the non-reddened granitoids. Secondary prehnite, apart from prehnite-sericite-albite aggregates in the saussuritized Ca-enriched plagioclase cores, occurs also as monomineralic fan- and bowtie-shaped aggregates in intergranular boundaries and as elongated lenses in biotite. The latter are concordant with cleavage and the inflation of the lenses disturbs the parallel alignment of the mica flakes. They are observed only in partially chloritized biotite in the non-reddened granitoids but are absent in the proximity of reddened fracture walls. Similar lenses of secondary calcite are present in chloritized biotite and hornblende in the reddened rock facies. Both prehnite and calcite, sometimes accompanied by laumontite, are also observed as late primary minerals healing microfractures cutting across the mineral framework of the reddened granitoids.

Magmatic apatite is commonly present as small inclusions in biotite and hornblende or as inherited inclusions in their chlorite pseudomorphs. Nonetheless, in some chlorite pseudomorphs, we also observe apatite inclusions that were considerably larger and at the same time less abundant than typical apatite inclusions in unaltered primary Fe-Mg minerals. They are likely a second generation of apatite resulting from recrystallization and also dissolution of smaller crystals during chloritization, such as those shown in the albitized facies in the Morvan (Parcerisa et al., 2009) and in NE Spain (Fàbrega et al.,2019) and those linked to low-temperature spilitic albitization in the Intra‐ Sudetic Basin (Powolny et al. 2022).

REE-bearing minerals, mostly epidote and monazite, are typically subhedral to euhedral crystals around 50-200 µm in size, in the non-reddened. The REE-rich epidote is more abundant in the reddened facies than in the unaltered rocks and occurs as larger grains up to 200-400 µm. Monazite in the reddened facies occurs in two different forms depending on its position with respect to the reaction front. The crystals in a cm-scale zone inside the reddish/pinkish facies in contact with the albitization reaction front are mostly pseudomorphed by secondary monazite. This secondary monazite has corroded grain boundaries and micron-sized porosity, suggesting that the replacement occurs via a dissolution-reprecipitation process. In contrast, in strongly reddened rocks, monazite grains can be pseudomorphed by secondary apatite.

5.7 Summary of petrographic observations

Petrographic analyses of the reddened and non-reddened granitoids provide a basis for discerning major differences in the mineralogical composition of the two granitoid facies. Apart from hematite, which is responsible for the red pigmentation, and quartz, the content of which is fairly constant, the relative abundances of major and some minor constituents vary with increasing reddening (Fig 6). In particular, the amount of Ca-enriched plagioclase decreases largely at the expense of secondary albite and is practically undetectable in the most intensely reddened sample. While plagioclase in the non-reddened rocks is partially sericitized, the plagioclase in the reddened facies is predominantly albitized. To some extent K-feldspar follows the same pattern, with albitization and microclinization of primary K-feldspar in the reddened facies. Weak chloritization of biotite and amphibole is observed already in the non-reddened granitoids but the process is dramatically more intense with increasing reddening and leads to a complete disappearance of the primary Fe-Mg minerals in the most reddened facies. Chloritization of biotite, in particular where the alteration is intense, is often coupled with the formation of secondary titanite and Fe-minerals along cleavage planes and microfractures. Similarly, chloritized amphibole often contains calcite along cleavages, indicating the removal of Ca from the chloritized crystal.

Small amounts of prehnite occur in the unpigmented granitoids but it becomes more abundant with reddening. However, its presence also depends on the initial rock type as it is absent from the aplogranite of Szklarska Poręba Huta and the granodiorite of Laski village, irrespective of the extent of staining. The sericite content seems to be unaffected by reddening. Dispersed calcite and laumontite are detected exclusively in the reddened facies, though they are present as late fracture fillings in both stained and unstained granitoids.

The presence of hematite pigments in feldspars is directly related to albitized domains. For instance, we have not observed albitized plagioclase that is hematite-free. Also, hematite pigments in K-feldspars were not observed in non-albitized regions. The crystallization of hematite pigments seems to be synchronous with albitization. If hematite formed later in micropores within secondary albite, it is expected that the migration of the hematitizing fluids followed some pathways. No such possible pathways were observed. Thus, assuming that hematite and secondary albite are contemporaneous, the albitization must have taken place under oxidizing conditions. Furthermore, secondary minerals related to albitization near the fractures are stained with iron oxides whereas secondary saussuritization minerals, corresponding to albite-sericite-prehnite aggregates, are not affected by the reddening. Albitization-saussuritization alterations grade progressively from fractures inwards into the fracture blocks; they do not overlap or cut across each other as expected if they were distinct unrelated alteration stages.

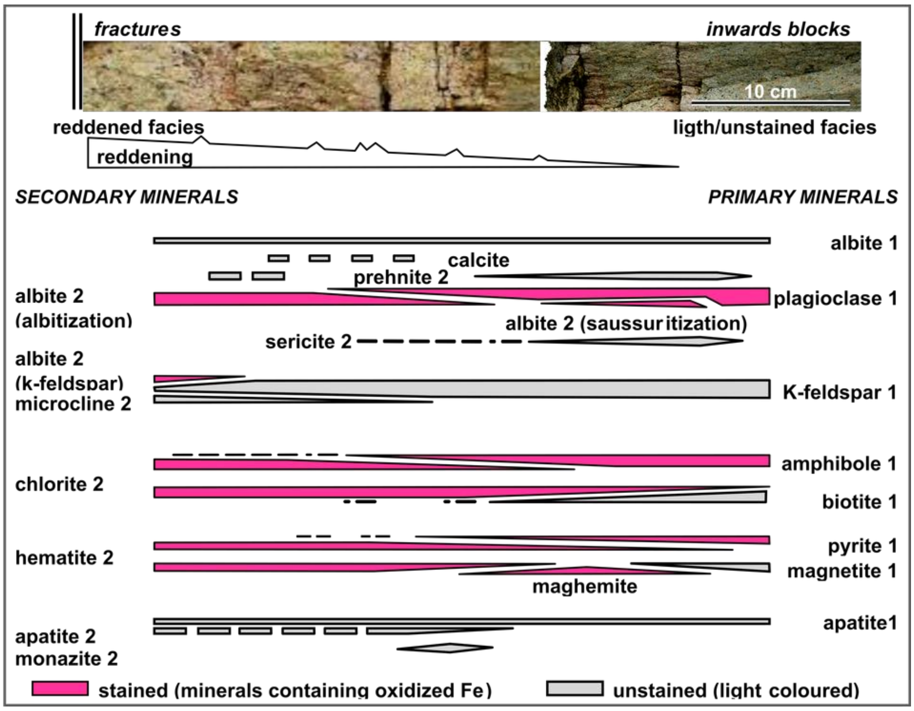

Fig. 6 Spatial distribution of mineral parageneses in relation to marginal fractures and core of granitoid fracture blocks.

6 AGE DATING AND GEODYNAMICS

Dating of the albitization provides a clear tool for determining if it could be related to deep, high-temperature metasomatic processes linked to granite cooling or alternatively a product of weathering on uplift and exposure of the granitoid mass. We compared the results of two independent methods of dating: on one hand paleomagnetic dating of iron minerals and on the other hand U-Th-Pb$_{total}$ radiochronology of monazite, a phosphate able to incorporate high U and Th concentrations.

6.1 Monazite dating

The Szklarska Poręba Huta quarry section provided only one sample containing mainly unaltered monazite. Deconvolution of the monazite U-Th-Pb$_{total}$ ages histogram (Fig. 7a) provides an average age of 314 ± 56 Ma (2σ). Although we cannot discard the possibility that some of these points could represent a mix of primary and secondary mineral ages. The Chwalisław valley section provided two samples containing numerous monazite grains for U-Th-Pb$_{total}$ radiochronology. The deconvolution of the monazite U-Th-Pb$_{total}$ ages histogram (Fig. 7b) yields two distinct age peaks, one at 254 ± 24 Ma (2σ) and a second at 321 ± 8 Ma (2σ) with a relative misfit of 0.988.

The textural analyses of samples from the Chwalisław valley section show that the older ages occur in well preserved grains from the non-reddened facies as well as in primary domains preserved within altered grains of the slightltly reddened/pinkish facies. On the other hand, the younger ages (centered around 254 Ma) are almost observed in the monazite grains with dissolution-reprecipitation features in the reddish/pinkish facies close to the reaction front (Fig. 7d and 7e). The resseting of the monazite geochronometer is accompanied with compositional changes, including an increase in the Huttonite component [Th,Si(PO$_4$)], Fe and Al, and a loss of

REE+Y (Fig. 7c). These compositional changes in relationship with younger ages, and the systematic occurrence of the younger ages in the more altered monazite grains close to the reaction front strongly support that primary monazite in the reddish/pinkish albitized facies were variably recrystallized at about 254 Ma. The broad distribution observed in the 254 Ma peak relative to the 321 Ma peak is caused by less younger age data (in comparison with older age data).

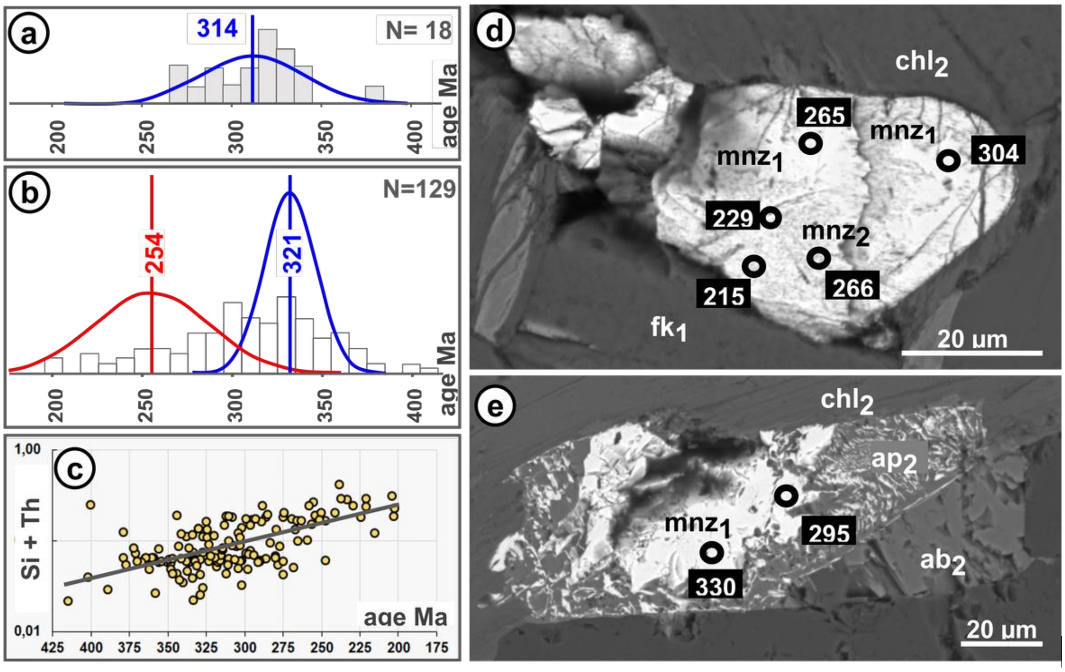

Fig. 7 Dating of monazite. (a) Mean age obtained from the histogram of ages of samples from the Szklarska Poręba Huta quarry, sample WL 006. (b) Deconvolution ages obtained from the histogram of ages of samples from the Chwalisław valley section, samples WL 018 and WL 018a. (c) Single U-Th-Pb$_{total}$ age of a monazite grain in the pinkish facies near the albitization front showing primary monazite (clear patches) partially replaced by microporous secondary monazite, BSE image. (d) Single U-Th-Pb$_{total}$ age of a monazite grain in the strongly reddened rocks partially replaced by secondary apatite, BSE image. mnz$_1$: primary monazite; mnz$_2$: secondary monazite; ap$_2$: secondary apatite; ch$_2$: chloritized biotite; fk$_1$: primary K-feldspar, ab$_2$: secondary albite.

6.2 Paleomagnetic dating

Albitization and reddening caused by the presence of hematite, are shown to be closely associated as they reveal no spatial discrepancy at outcrop or microscope scale. We thus consider albitization and hematization to be cogenetic. The dating of the hematite formation is possible by dating the paleomagnetic secondary remagnetization signal. This would then allow to date the albitization event.

The different components of the paleomagnetic signal recorded within the analyzed oriented samples have been separated by stepwise thermal demagnetization experiments and are related to their specific magnetic carriers (see also supplementary material 2). According to the respective temperature interval at which a specific decay in the magnetic intensity curve was observed, one or a sucession of several magnetic carriers were identified in the sample. In principle, thermomagnetic and microscopic analysis showed three different types of magnetic mineral assemblages were observed within the analyzed samples: (1) hematite dominated in pervasive reddened facies and in fracture controlled reddened facies; (2) coexisting hematite-maghemite mostly in fracture controlled reddened facies further away from the fractures; and (3) maghemite dominated mainly in spotted facies.

In addition, maghemite-bearing mineral assemblages sometimes register residual, presumably primary magnetite. This was mainly observed in samples distant from fracture zones and in the less reddened spotted facies. As well, a weak contribution of goethite was sometimes observed which was demagnetized after application the 120°C demagnetization step. Goethite is considered as negligible component compared to the other magnetic carrier minerals and is most likely linked to a weak recent overprint by surface weathering of the outcropping rock sections.

The stepwise thermal demagnetization allowed us to obtain the vector directions recorded by the magnetic carrier minerals at the moment of their formation. These directions were considered to be characteristic for either the maghemite or hematite components, or both, if their inclination and declination values were stable according to the respective considered temperature intervals. It is thus possible to sometimes extract two slightly different directional intervals from one single sample if the two main carriers diverge in their mean direction. The results were 'sub-grouped' according to their directional information.

The extracted directional information was then transformed into magnetic paleopoles (e.g. Butler 1998) that were subsequently projected onto the apparent polar wander path (APWP) reference curve for Eurasia (Edel and Duringer 1997; Besse and Courtillot 2003). In total 275 individual samples were analyzed for the calculation of the mean paleopoles carried by hematite or hematite-maghemite.

The severe rejection criteria for paleomagnetic samples in our dataset are mainly due to high error defined by values of α 95 (Kirschvink 1980; Fisher et al. 1987). Additionally, we eleminated samples that did not show any linear segments of the demagnetization vector on a Zijderveld diagram or a clear stable endpoint near the origin of a Zijderveld plot, as described by McFadden and McElhinny (1988). The resulting 18 averaged paleopoles all show acceptable α 95 values (< 15) according to the recommendations of e.g. Fisher et al. (1987) and very often plot directly on or close to the Apparent Polar Wander Path (APWP; Table 3). Six paleopoles were calculated for one or two directions only. For these paleopoles the mean angle deviation (MAD) values are given instead. All poles were listed in the Table 3. The paleomagnetic data set also includes additional paleopoles that correspond to the primary Devonian magnetization of the granitoid rocks, carried by primary magnetite (not shown here).

Table 3 Results from paleomagnetic data analyses, corresponding to the averaged site-wise paleopoles plotted in Fig. 8. MAD = mean angle deviation; TH = thermal demagnetization; AF = alternating field demagnetization; mgt = magnetite; mhm = maghemite; hm = hematite; goe = goethite; LC = low coercivity compounds; HC = high coercivity compounds.

paleo-poles	site outcrop	age	Nb of samples	α 95	MAD	type of analysis	pole latitude	pole longitude	magnetic carriers
1	Sklaska Poreba	Late Carboniferous	3	8.9		TH	20	125	mgt, mhm, hm
2	Chwalisław	Late Carboniferous	2		10.1	AF	23	126	LC+HC
3	Laski quarry	Late Carboniferous	3	8.7		TH	27	141	mgt, mhm, hm
4	Laski quarry	Middle Permian	4	8.7		TH	41	182	mhm, hm
5	Laski quarry	Late Permian	2		6.7	TH	53	161	goe*, hm
6	Laski village	Late Permian	1		3.8	TH	55	170	hm
7	Sklaska Poreba	Late Permian	3	10.1		TH	47	157	mhm
8	Laski quarry	Late Triassic	4	5.1		AF	54	127	LC+HC
9	Laski quarry	Triassic/Jurassic	2		7.7	AF	51	107	HC
10	Chwalisław	Triassic/Jurassic	3	3.3		AF + TH	49	118	mhm
11	Chwalisław	Triassic/Jurassic	3	7.3		TH	42	99	mhm, hm, goe*
12	Sklaska Poreba	Triassic/Jurassic	3	7.2		TH	36	104	mhm, hm
13	Laski quarry	Early Jurassic	4	9.1		TH	53	74	mhm
14	Chwalisław	Early Jurassic	8	5.9		TH	58	83	mhm, goe*
15	Laski quarry	Early Jurassic	2		6.6	AF + TH	73	93	mhm, hm
16	Sklaska Poreba	Early Jurassic	3	5.9		AF	74	67	LC+HC
17	Laski village	Middle Jurassic	6	5.0		TH	73	170	hm
18	Laski village	Middle Jurassic	1		10.4	TH	79	114	hm

Figure 8 shows the mean paleopoles for all four studied outcrops including Laski quarry, Laski village, Chwalisław valley, and Szklarska Poręba Huta. Four main groups of paleopoles and more ‘isolated’ average paleopoles plot along the APWP curve for Eurasia:

(1) Samples from paleopoles 1, 2, and 3 have a mixed magnetic assemblage which is dominated by primary magnetite. These represent the oldest group with Late Carboniferous ages (between 320 to 303 Ma) and are represented in all outcrops (with exception of Laski Village, that exhibits exclusivly pervasive reddened facies) whichpresumambly correspond to the primary age of the granitoid. All other paleopoles record secondary remagnetization ages.

(2) An ‘isolated’ average paleopole of Middle Permian age near the 270 Ma reference point from Laski quarry (paleopole 4).

(3) A cluster of Late Permian ages close to 258 Ma from the Szklarska Poręba Huta quarry, Laski quarry and the basal part of the Laski village section (paleopoles 5, 6, 7).

(4) A relatively ‘isolated’ average paleopole of Late Triassic age close to 225 Ma from Laski quarry (paleopole 8).

(5) A group of ages near Triassic/Jurassic boundary (arround 205 Ma) comprising four sets of paleopoles from the Laski quarry (paleopole 9), Chwalisław valley (paleopoles 10 and 11) and Szklarska Poręba Huta (paleopole 12) samples.

(6) A group of paleopoles of Middle Jurassic ages (between 175-165 Ma; paleopoles 17 and 18). This group is clearly different because it is solely carried by samples from the upper part of the Laski village section that is pervasively reddened/hematized. The intense remagnetization of these samples seems to have erased the

primary magnetization carried by magnetite and the potential Permo-Triassic overprint. The lower part of the section still retains the Permo-Triassic signal.

(7) A group of Early Jurassic paleopoles (13, 14, 15, 16) plots between the 195 to 187 Ma reference point, but they show a significant S to SW offset from the APWP. Part of this directional offset may be due to the fact that these samples (from the Laski quarry, Chwalisław valley, and Szklarska Poręba Huta) may have been remagnetized successibly multiple times during the Permo-Triassic and later again during Early Jurassic times. If so, the hematite in these samples could carry a mixed cumulative age signal that is probably less well extractable than the initial remagnetization from primary magnetite to maghemite and/or hematite during the Permo-Triassic alteration phase.

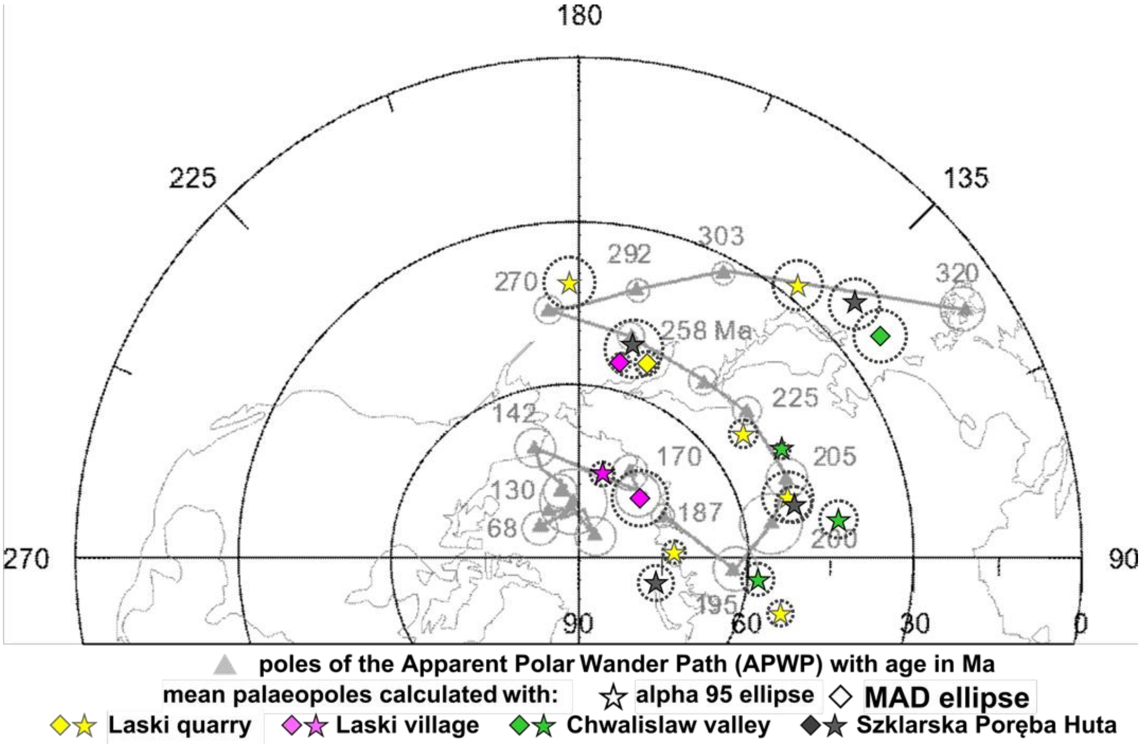

Fig. 8 Stereographic projection of the paleomagnetic results for the calculated average paleopoles for the study sites. The paleopoles are compared to the APWP for Eurasia (grey line) using the combined curve of Edel and Duringer (1997) from the Permian to Middle Jurassic (grey circles) and Besse and Courtillot (2003) from the Middle Jurassic until present (grey triangles). Star symbols represent mean poles with their respective α 95 confidence circle, diamond symbols are paleopoles with their respective MAD confidence circle, corresponding to Table 3.

In our petrographic studies magnetite was solely found in the non-reddened facies whereas the magnetite detected by thermal demagnetization in samples of the weakly reddened facies probably relates to residual tiny crystals included in quartz. Maghemite is mainly detected in the weakly to intermediately pigmented facies distant from the reddened fractures at Laski and Szklarska Poręba Huta and in red spotted facies from Chwalisław valley. According to the literature, maghemite is metastable with respect to hematite and is considered to have formed by the slow oxidation of magnetite under weak oxidative conditions (Steinthorsson and Helgason 1992; Bowles et al. 2011). Hematite is dominant in the pervasively reddened facies in the Laski village section and is indicative of strong oxidative environments.

A chronology appears between the different magnetic facies of alteration. The less reddened spotted facies which is mainly dominated by maghemite carries the oldest remagnetization ages while the pervasively reddened and albitized facies shows the youngest ages. In the mean time, incipient reddening and albitization appears as the less intensely altered facies and conversely the pervasively reddened and even pervasively albitized without primary plagioclase and K-feldspar relict appears as the most intensely altered facies. This conjonction and the fracture controled reddening that diminish obviouly from most intensely altered facies towards the less altered spotted facies led us to consider that these various gradiens agree with a succession of facies from the base to the top of the alteration profiles. This suggests also that, with time, the active alteration front progressively retreated upwards into shallower weathering horizons.

It is of particular note that the Late Permian U-Th-Pb$_{total}$ age at 254 ± 24 Ma obtained for secondary monazites in samples from the Chwalisław valley section corresponds to the paleomagnetic poles 10, 11, and 14 near 258 Ma on the Eurasian APWP (Fig. 8). These paleomagnetic poles, were obtained for weakly pigmented facies from Lasky quarry, Sklarska Proeba Huta, and Laski village, from samples taken further away from reddened fractures that contain significant amounts of maghemite. On one hand, maghemite developed in the early stages of albitization, under less oxidative conditions. On the other hand, secondary monazite formed in the immediate vicinity of the albitization front and was rapidly altered away from this front. The consistency in independed ages of the albitizing and oxidizing environments obtained from completely different secondary minerals and by means of distinctly different dating methods provide confidence in datation results. This does not contradict with the younger paleomagnetic ages obtained in this study for which we do not have access to separately datable minerals.

6.3 Links to other age determinations

The older age obtained for monazite from the Chwalisław valley section (321±8 Ma) is within the range of the previously published primary crystallization ages for the Kłodzko - Złoty Stok (KZS) Pluton between 349.0±3.7 Ma and 331.5±2.6 Ma (U-Pb, zircon; Jakubauskas et al. 2018 and references therein). The younger age (254±24 Ma) reflects growth of secondary monazite via dissolution-reprecipitation process. Similar Permian K-Ar ages between 256-268 Ma (K-Ar isochron age, 4 points: 261 Ma) were reported by Depciuch (1972) for KZS diorites from Mąkolno affected by chloritization/sericitization and interpreted as time of hydrothermal solutions activity. Unaltered samples representing main varieties of KZS igneous rocks provided significantly older K-Ar ages ranging from 291 to 303 Ma (K-Ar isochron age, 14 points: 295 Ma).

Our mean value of the monazite age (314 Ma) for Szklarska Poręba Huta aplogranite is consistent with high precision ID-TIMS U-Pb zircon ages 312.5 ± 0.3 Ma and 312.2 ± 0.3 Ma indicating crystallization of two main granite varieties (porphyritic and equigranular) of the Karkonosze Pluton (Kryza et al. 2014). Similar 40Ar/39Ar ages of 312 ± 4 Ma reported by Marheine et al. (2002) suggest fast cooling below closure temperature of the K-Ar system. It has to be mentionned, even if of poor quality, an age of 271 ± 20 Ma obtained on monazite from the same aplogranite at Szklarska Poręba Huta (Mikulski et al. 2004). This dating deserves to be linked to the 254 ± 24 Ma obtained on the secondary monazite of the Chwalisław valley section. The Karkonosze granite underwent fast uplift to the surface as evidenced by granitic detrital material in Upper Carboniferous sediments of the North Sudetic Basin (Milewicz 1968, Milewicz 1970).

Previous paleomagnetic dating aimed to determine the primary age of the emplacement of several Carboniferous plutonic units of the Polish Sudetes and led to the detection of Permo-Triassic (re)magnetizations (Edel et al. 1997). Even if the study did not plan to determine the age of the albitization, and even if sampling of the obviously altered (reddened) facies was avoided, re-magnetization events, younger than the age of the emplacement of the granitoïd, were present in some of the samples from the Chwalisław valley amphibolites in contact with the Kłodzko - Złoty Stok intrusion and in the Izera dolerite close to the the Szklarska Poręba Huta quarry (Edel et al. 1997). The authors identified paleomagnetic carriers of these Permo-Triassic paleopoles as hematite and maghemite, while the Carboniferous paleopoles reported by Edel et al. (1997) are carried by (primary) magnetite. Further paleomagnetic studies ~~of Kądziałko-Hofmokl et al. (2003)~~ on the Kłodzko Metamorphic Complex report on Triassic and Jurassic directions for similar magnetic mineral assemblages (Kądziałko-Hofmokl et al. 2003).

The Permian-Triassic age in the Kłodzko – Złoty Stok massif and the Szklarska Poręba area recurs systematically despite the different dating techniques. Thus, there is consistency between the results of paleomagnetic dating of the reddened/albitized facies in this study and other published age determinations on the various facies which were simply described as ‘altered’ but not clearly characterized as albitized.

6.4 Link to the Post-Variscan paleosurface

The Sudetic area, together with the southern part of the Germanic Basin of central Europe, is assed to have been emergent during Permian and Trias on the basis of stratigraphic and sedimentological evidence (Feist-Burkhardt et al. 2008; Głuszyński and Aleksandrowski 2022). At the same time, Permian and Triassic ZHe cooling ages reported by Danišik et al. (2010) and Sobczyk et al. (2015) are consistent with the idea of exposure of some parts of the Karkonosze granite during the Triassic (see also Migoń and Danišik 2012). Similarly, Carboniferous to Triassic ZHe data reported by Danišik et al. (2012) show that certain parts of the Kłodzko - Złoty Stok granitoid massif may have been close to the Earth surface during the Triassic (249.8 ± 20.0 – 209.4 ± 4.1 Ma) and reflect the record of progressive cooling through the zircon helium partial retention zone.

Results of zircon (U-Th)/He (ZHe) dating available for the Western Sudetes area revealed i.a. Triassic (248.2 ± 16.6 – 212 ± 14.2 Ma) cooling signals (Sobczyk et al. 2015). They have been interpreted as a record of bedrock slow exhumation or alternatively as an apparent ages due to zircon thermal system rejunevation, as a result of burial (see discussion in Sobczyk et al. 2020) or an advective heat flow under crustal extensional conditions (Botor et al. 2017). Noteworthy, ZHe datings for the Permian sandstones from the Fore-Sudetic Homocline (Sobczyk et al. 2013) provided a single Mid-Triassic cooling age (244 ± 5.0 Ma) within a Weissliegendes series, correlating with paleomagnetic datation which was interpreted, due to its clear post-depositional origin, as a probable age of Kupferschiefer mineralization. Therefore, low-temperature thermochronological data, even if not providing indisputable proof for the Post-Variscan paleosurface exposure during Trias, give some arguments for linking Triassic bedrock cooling with a regional crustal instabillity during the post-orogenic unroofing. Also the local sedimentological record for the Early Triassic lithofacies within the Intra-Sudetic and North Sudetic synclinoriums indicates channel flow and river bed depositionial environments (Kowalski 2020), suggesting the predominance of continental conditions for this period with local source areas located mainly in the Karkonosze-Izera Massif. Noteworthy, strongly kaolonized undisturbed Triassic (Buntsandstein) sandstones from the Sudetes are interpreted as a record of *in situ* chemical weathering profiles at the Triassic paleosurface (Kowalski 2020 and references therein). Finally, regional review studies indicate that during the Late Triassic to Early Cretaceous the Sudetes landforms were steaty sustained by the Post-Variscan paleosurface that formed a vast land mass undergoing slow erosion and denudation resuling i.a. in formation of deep weathering mantles, known also from central and northern Europe (Migoń and Lidmar-Bergström 2001). Powolny et al. (2022) advocated a late to post-magmatic low-temperature fluid-rock interactions controlling the process of albitization within the Permian trachyandesites from the Intra-Sudetic Basin. Based on apatite fission-track central ages obtained for three samples, these authors proposed a Jurassic (182 – 161 Ma) time interval for this thermal event. Closer inspection of apatites analyzed by Powolny et al. (2022) show that >50% of all dated grains revealed a Triassic cooling age, which indicates a possible two stage post-Variscan albitization in the Sudetes.

In the absence of any major Triassic magmatic event in the Sudetes and adjacent areas, we link the reddening alteration of the Kłodzko – Złoty Stok and of the Karkonosze granites, as well as their albitization, to a Post-Variscan/Pre-Triassic paleosurface, similar as described for the French Massif Central (e.g. Schmitt and Clement 1989; Parcerisa et al. 2009) and in NE Spain (Fàbrega et al. 2019). It follows then that the most pervasively reddened/albitized facies were formed near the paleosurface while at depth the granites were progressively less affected by the alteration process. It is of note that the conspicuous reddened and albitized fractures are never cut by any fractures that do not exhibit this alteration. Hence, we regard the lack of non-albitized fractures as evidence that the alteration is relatively recent and post-dates the exhumation of the granite bodies.

Moreover, the superficial origin of albitisation and reddening via weathering explains the spread of the paleomagnetic data along the APWP curve for 100 Ma from the Permian to the Jurassic. This distribution of palaeomagnetic ages is not the result of successive phases of alteration, but rather a single event that is heterogeneously recorded in the rock. It relates to the progression of weathering along fractures and even around kilometer sized massive rock volumes. But presumably there were times of more active and less active phases during this long period, mainly under the influence of climate and eustatic sea level changes, which could explain some clustering of paleomagnetic ages during distinct periods.

7 INTERPRETATION OF THE PARAGENESES

In general, our observations agree with earlier data on fracture related hydrothermal alterations with the development of albitization and saussuritization (e.g. De Jong and Williams 1995; Lee and Parsons 1997; Engvik et al. 2008; Plümper and Putnis 2009; Sandström et al. 2010; Morad et al. 2010; Powolny et al. 2022). The direct relationship of albitization and related alterations with the Post-Varisacan paleosurface completely changes the paleoenvironmental conditions that prevailed for these alterations compared to quoted studies that ascribe them a deep and relatively high temperature environment. Nevertheless, in the context of a direct relationship with the Post-Varisacan paleosurface, the alterations discussed in this study do not exhibit any typical regolith features, such as illuviation structures related to water percolation in vadose environments, bioturbation, or pallid or iron stained mottles. On the contrary, the isotropic structures around blocks evoke an aquifer environment and recall saprolite from the lower zones of regolith horizons corresponding to deep weathering of bedrock. The most astonishing characteristic is the alteration around the fracture blocks. This occurs without modification of the primary fabric of the rock and without any obvious development of porosity. However, the alteration developed systematically via a hierarchical net of fracturing from the macro-scale, demarking fracture blocks, to intergrain microcracks, giving to the albitization front at outcrop scale a dendritic aspect of fresh unaltered blocks surrounded by reddened fractures (Fig. 9a). Here we examine the geochemical grades, coupled dissolutions, precipitations and water-rock interactions in order to identify the nature of the fluids that triggered these alterations and ultimately the nature of the related paleoenvironment.

7.1 Fracture-bound geochemical grades

The alteration primarily and intensively affects the plagioclase and only to a lesser extent K-feldspar and ferromagnesian minerals (biotite and amphibole). The alteration of plagioclase is of three kinds (Fig. 9a and 16b).

1) Albitization of the primary feldspars is causally linked to proximity to the fractures. Some late Ca-bearing silicates may be associated with this alteration, but they rather fill in microcracks and their origin may not be directly related to the albitized plagioclases.
2) Saussuritization of the primary plagioclases accompanied by the development of Ca-bearing prehnite is typical of the non reddened and lightly reddened facies away from fractures. Secondary albite has developed along with saussuritization of the primary plagioclase.
3) Invasive development of sericite (sericitization) affects in places the primary plagioclases from the non reddened and lightly reddened facies and is associated with the formation of small neogenic albite but without any Ca-bearing silicates.

The alteration of ferromagnesian minerals is connected to the alteration of plagioclase. There is a progressive chloritization of biotite in the non reddened and lightly reddened facies as the fractures are approached. Chloritization seems to occur either under volume conservation or with a slight decrease of the volume of the biotite with secondary minerals such as quartz, K-feldspar, prehnite, and iron-bearing minerals embedded in the cleavage planes. The amphiboles appear to be less sensitive to chloritization than biotite, remaining practically unaltered in the unaltered and lightly reddened saussuritized facies.

These alterations result in a strong geochemical overprint between the core and the boundaries of the fracture-isolated blocks (Fig. 9c). The margins of the blocks are strongly Na-enriched due to albitization of plagioclase, and depleted in K due to chloritization of biotite and partial albitization of K-feldspar. The cores of the blocks are relatively enriched in K, Ca and Al compared to the albitized facies (taking into consideration the saussuritization of the plagioclases).

The secondary mineral parageneses, especially albitization and sausuritization, never exhibit an interruption or clear alteration front but appear rather as continuum, grading from one to another. There is no obvious temporal succession between the parageneses. By contrast, the parageneses are overlapping, with small sericites in the albitized/hematitized plagioclase crystal cores formed due to alteration of the plagioclase before albitization. The secondary parageneses appear more like an expression of the geochemical gradients between fluids circulating within the fractures and the massive granitoid blocks. Thus, the observed sequences of neogenic minerals result from the progressive encroachment of the reaction front towards the cores of the fracture blocks while their outer margins are gradually altered in equilibrium with the interstitial fluids. It is appropriate at this juncture to refer to metasomatic sequence or zonation rather than paragenesis involving successive or different alteration processes.

The albitization as well as the iron oxide pigmentation becomes less intense away from the walls of the fractures towards the inner parts of the fracture blocks. This gradient reflects a decreasing Na^+ and O_2 (and/or Fe) content of the fluids circulating in the intergranular crystal boundaries (Fig. 9d). In contrast, the K^+ and Ca^{++} content of the interstitial fluids would have decreased in the opposite direction: K-bearing minerals (K-feldspar, biotites) and Ca-bearing plagioclases were altered by leaching of K^+ and Ca^{++} at the fracture walls and sericite formed within the lightly reddened and unaltered facies progressively more distant from them.

7.2 Coupled dissolution-precipitation reactions

It is well known, plagioclase with a high An content is susceptible to preferential dissolution due to enhanced instability in the presence of water (Matthews and Goldsmith 1984; Stillings and Brandtley 1995). Thus, destabilization of plagioclase could be a trigger resulting in a chain of reactions in the altered granitoids.

Albitization of plagioclase proceeds at constant volume (with low porosity) given a Na-supply, additional silica, and with the release of Ca and some Al (Ramseyer et al. 1992; Parcerisa et al. 2009; Hövelmann et al. 2010). In the vicinity of the fractures, the released cations would have been leached and evacuated by the circulating fluids. As the reaction continued, fluid circulating in the rock by diffusion and convection would have become gradually depleted in Na, and albitization diminished and or even ceased at low Na-content (Fig. 9d).

Biotites are destabilized and transfromed into chlotite in the vicinity of the fractures, probably through a double effect of the leaching of the K interlayer cations and oxidation of the Fe2+ in octahedral sheets (Fig. 9e). Here leaching of $Si(OH)_4$ takes place because the cation/Si ratio is equal to ~1 within the biotite, whereas it is between 1 and 1,5 within the replacement chlorite. Detailled study of the Karkonosze granite’s chloritization (Wilamowski 2002) showed that “The rate of potassium removal from biotite during the progress of chloritization is not constant. The rapid removal of K is observed at initial stages of chloritization. After the replacement of 20% of the biotite, K removal is much slower.” The released silica could have nourished the albitization of the plagioclase. If the chloritization occurred without an additional cation supply, the volume loss would have been about 30%, whereas if additional cations were introduced (such as the Al released by plagioclase alteration) the volume loss may have been less substantial (Ferry 1979).

Amphiboles appear to be less "sensitive" to chloritization than the biotites, probably because their structure does not contain any unstable or mobile cations such as K^+. The destabilization of the amphiboles is most likely a result of leaching of Mg and perhaps oxidation of Fe^{2+}. It might be that amphiboles, and in particular hornblendes (which are calcic), are relatively protected against chloritization because of the Ca liberated by albitization of the plagioclase. For that reason the chloritization of amphiboles occurs only in the more intensively altered facies in which plagioclases are albitized and therefore no longer provide Ca^{++} to the fluids.

Hematitization is systematically associated with the albitization. Hematite occurs mainly as pigments within the neogenic albite or as coarser crystalline material associated with the ferromagnesian minerals. There is no iron oxide precipitation in the fractures, so the fluids circulating in the fractures appear unlikely to have been iron-bearing. Hematite has likely been nourished by the iron released by alteration of ferromagnesian minerals.

The formation of sericite depended mainly on the availability of K^+. Chloritization of biotite was the quasi-exclusive source of K in the system because albitization of K-feldspar was not pervasive. Besides, K released by chloritization in the early stage of the alteration and in the vicinity of fractures would have been evacuated by convective fluid flow. Sericitization is present away from the fractures where diffusion was dominant with respect to the movement of the chemical elements. Thus, sericitization is dominant in the non reddened and moderately reddened facies where the Na-content was lowered in the interstitial fluids due the increasing distance from the fractures that are the major source of Na. Yet, where the K/Na ratio was higher, albitization was limited and K competed with Na to form K-bearing silicates (mainly secondary K-feldspars and/or sericite) in combination with Si and Al (Ben Baccar et al. 1993; Perez and Boles 2005).

Euhedral crystals of prehnite within altered plagioclase indicate epigenetic replacement with the main chemical component directly supplied in situ by the plagioclase. On the other hand, prehnite finning in microfractures witnesses the mobility of these components over some distance. If the mobility of Ca and Si is to be expected, it is rather unusual for Al , typical fairly immobile in a medium close to neutral pH, except in presence of complexing agents (Castet et al. 1993; Farmer and Lumsdon 1994 ; Oelkers et al. 1994). In any case, Al appears to have been fairly mobile, at least in some cases, but it is difficult to assess whether or not Al was evacuated from the fractures by fluid circulation.

Recrystallization of monazite was also apparently triggered by calcium availability. Initially, primary monazite recrystallized into secondary monazite at the early stages of albitization but later, during advanced stages of the albitization, primary and secondary monazite recrystallized into apatite in concert with the increase in calcium availability in the system.

These alterations can be considered to be topochemical: the saussuritization of plagioclase provided Ca for prehnite development and the chloritization of biotite is the likely source of K for sericitization. However, the complete albitization of the plagioclases and in particular the albitization of the K-feldspars in the vicinity of the fractures testify for the supply of Na, and the hematite associated with albite registers the oxidative capacity of the alteration and therefore a supply of oxygen.

7.3 Fluid-rock interactions

The geochemical exchanges between reaction zones are determined by the transport of the ions in the fluids. Exchanges in fractures record the circulation of the transport fluids by convection. The circulation may have been relatively rapid in the major fractures but slower as the dimensions of the fractures decreased. Away from the open micro-fractures, the quantity of fluid is reduced and mainly limited to ‘thin films’ at the boundaries of mineral grains and the dissolution-recrystallization interface. Such confined fluids may be very different in chemical composition and behavior from bulk fluids (Putnis and Ruiz-Agudo 2013). Within thin films, the circulation would have been minimal, diffusion prevailed over convection and ion mobility was extremely reduced.

In this context, the coupled-reactions described above are not part of a global geochemical equilibrium related to the fluids in the fractures but they are rather part of a spatially-linked dynamic geochemical equilibrium. The balances are not determined by the kinetics of the mineralogical reactions but rather by the kinetics of the diffusion of ions in the rock. The system was only partially open. A geochemical zoning developed and progressed in a chromatographic way: with displacement of ions at diverse rates and according to fronts governed by distinct reactions. This is characteristic of a metasomatic system (Korzhinskii and Oestreich 1965; Brinhall and Dietrich 1987; Guy 1993). Thus, thermodynamic reactions that originally seem incompatible with a global context may occur. Temperature is not a limiting factor but it allows speeding up of the reactions by accelerating diffusion. The reaction rate is controlled by the diffusion rate and is extremely slow, but not impossible from a thermodynamical point of view.

Thus, within a block of massive rock bounded by fractures, a zoning of the ion transport that determines the geochemical zoning is primary established (Fig. 9g). Along the fracture walls, exchanges by convection prevail and are relatively fast; the mineralogical parageneses formed in equilibrium with the fluid and thereby reveal the geochemical characteristics of the fluid. Further away from the fracture walls, exchanges are slow and are driven by diffusion; the mineralogical parageneses are controlled by local balances that are far from the balance within the fluid. This alteration of massive blocks differs entirely from alteration of porous rock where ion mobility is practically exclusively provided by fluid flowthrough.

7.4 Geochemistry of the fracture fluids.

Albitization of plagioclase and K-feldspar reflects an interaction with Na-enriched and relatively K-depleted fluids (Saigal et al. 1988; Aagaard et al. 1990; Ben Baccar et al. 1993; Schmitt 1994; Perez and Boles 2005). The association with hematite indicates that the fluids were also enriched in oxygen. There seems to have been a relatively low CO_2 fugacity since only minor calcite was formed, in spite of the abundance of Ca released during plagioclase alteration. The fluids were also relatively under-saturated in SiO_2, Al and Mg, since chlorite coating the fractures is sometimes entirely altered to hematite. On exiting the system, fluids were depleted in Na and O_2. However, they were enriched in K because, in the early stages of the alteration, little or no sericite was formed within plagioclases during the chloritization of biotite. The chemical balance is more difficult to establish for SiO_2, Al and Ca. Significant amounts of silica were liberated during chloritization of biotite so it is likely that it was exported from the system, at least in the granodioritic facies that is rich in biotite. It could be that Al and Ca were in balance between the altered plagioclases and the formation of prehnite and calcite, even if a quantified balance is not available. Nevertheless, it is obvious that the Ca was easily exported from the cortical reactional zones during the early stage of the alteration. The mobility of Al is unlikely to have occurred on a significant scale because the major fractures never show any alumino-silicate mineralization. In conclusion, it appears clear that the fluids responsible for the alteration were oxidized, Na-rich and relatively depleted in K in comparison to Na.

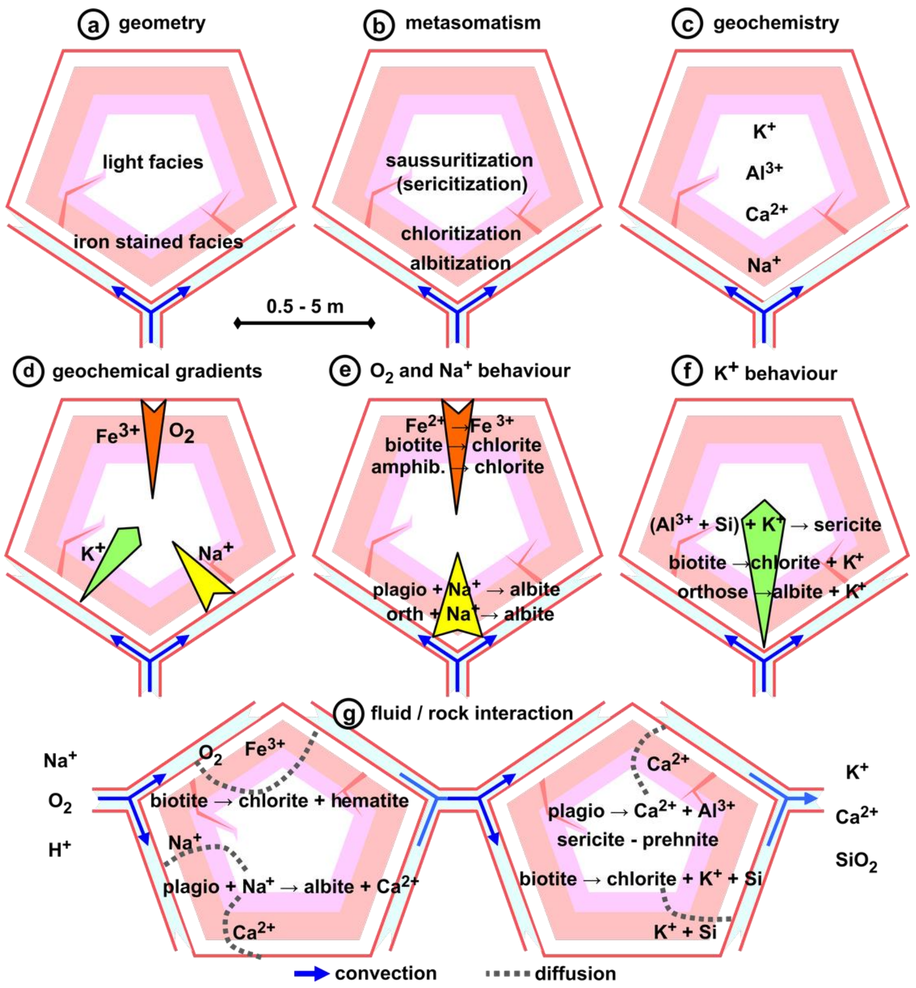

Fig. 9 Schematic interpretative sketch of the various petrographic parageneses related to reddening and albitization of the granitoid rocks in the Sudetes at the outcrop scale.

7.5 Iron oxide behavior

Maghemite is considered to be metastable with respect to hematite (Waychunas 1991; Majzlan et al. 2003). In addition, it is generally admitted that slow and incomplete oxidation of magnetite favours the topotactic formation of maghemite whereas faster oxidation of magnetite, under highly oxidizing conditions, results in hematite formation (Steinthorsson and Helgason 1992; Bowles et al. 2011). The maghemite-hematite transition during albitization may be attributed to changes in the alteration environment during the oxidation of magnetite. In this case the alteration commenced with the formation of maghemite under low oxidizing conditions in the non-reddened and slightly reddened granitoids and continued with the formation of hematite in the reddened facies under stronger oxidizing conditions, when ferrous silicates (biotite and amphibole) were being oxidized. Thus, the occurrence of maghemite and hematite suggests that the oxidizing conditions changed during the alteration of the granitoid and the spatial distribution of hematite and maghemite provides a tool to estimate the gradient of these conditions. The distribution of the alteration environments substantiates the idea that reddened albitized facies and non reddened saussuritized/sericitized facies reflect gradational changes during a single event.

From a geochemical point of view there is no contradiction in the spatial discrepancy between the zones of alteration of the silicate minerals and the distribution of the iron oxides. The physico-chemical properties that constrain their reactions are not the same. A key-factor in the alteration and crystallization of the silicates is the pH, whereas Eh and the oxygen fugacity controls the oxidation state of the iron oxides. Theses two parameters may vary independently. Nevertheless, the precipitation of iron oxides is also facilitated by the elevated pH. Thus, local lowering of the H^+ activity at the sites of feldspar alteration will favour the localized precipitation of hematite as inclusions within the feldspars (Boone 1969). This also explains the local distribution of pigmentary hematite inclusions in albite during the alteration of both plagioclase and K-feldspar. On the other hand, the intensity of the reddening, or the abundance of the pigmenting hematite, is related to oxygen fugacity and therefore is likely to decrease away from the fractures. From the geochemical point of view, the hematite distribution is consistent with the alteration sequence of the silicate minerals.

7.6 Origin of the oxidizing fluids

In general, post-magmatic alterations are explained by a hydrothermal model which uses large convective circuits to bring the superficial fluids in contact with the warm rock complexes, in particular granitic intrusions, in which the alterations then take place (Taylor 1977; Jenkin et al. 1992; Putnis et al. 2007; Drake et al. 2008). The magmatic intrusions provide heat to the fluids and the subsequent loss in fluid density causes the upwelling, maintaining the circulation between the landsurface and depth. Fluids with a deeper origin may be also mixed into this circulation model.

In the hydrothermal model, the superficial origin of the fluids, or at least the participation of meteoric water, has been evoked by oxygen and hydrogen isotope studies on the alteration minerals (Simon and Hoefs 1987; Sun and Eadington 1987; Jenkin et al. 1992; Boyce et al. 2003). These models usually consider superficial oxygen-rich fluids descending very deeply (more than 10 km) before they interact with the rock matrix. However, some reactive transport models strongly suggest that this form of fluid percolation leads to a rapid depletion of the oxygen fugacity in the circulating fluids, so fluids at great depths are very likely to be under-saturated in oxygen (MacQuarrie et al. 2010).

Here we have documented the Permian-Triassic-Jurassic age of the alteration and provided arguments that it is necessarily related to the Post-Variscan paleosurface and *de facto* involved infiltration of weathering solutions and/or groundwater flow.

7.7 Temperature and depth of formation

The $\delta^{18}O$ results allow to estimate the fluid temperature during plagioclase albitization and K-feldspar microclinization. Assuming a local isotopic equilibrium between minerals and the fluid at the reaction interface, the isotopic mass balance was calculated for each reaction using the equation of Taylor (1977), by (Eq. 1):

$$\delta^{18}O_f^w = \delta^{18}O_i^w + \frac{R}{W} \times \left(\delta^{18}O_i^m - \delta^{18}O_f^m\right) \qquad (1)$$

Where $\delta^{18}O^w_i$ and $\delta^{18}O^w_f$ $\delta^{18}O^w_i$ are the initial and final oxygen isotope compositions of the fluid, respectively, R and W the percentage of oxygen atoms in the rock (or mineral) and water, respectively, and $\delta^{18}O^m_i$ and $\delta^{18}O^m_f$ the oxygen isotope composition of the initial and final minerals, respectively. For the rock-to-water oxygen mass ratio (R/W), conservative estimates of 0.5 and 1 were applied. The applied values for the oxygen isotope composition of the initial fluid ($\delta^{18}O^{w}{}_{i}$) were -8 and -12‰ (VSMOW), which are typical $\delta^{18}O$ values observed in deep groundwaters hosted in stable granitic basements (Stober & Bucher 1999a and b; Barth 2000; Kloppmann et al. 2002).

Two options of reactions paths were considered, (1) sequential reactions, with a fluid moving across a steeped sequence of albitization and microclinization, so that the mass balance of albitization is calculated first and subsequently the mass balance of microclinization is calculated using as initial fluid isotopic composition the $\delta^{18}O$ value of the final fluid obtained from the mass balance of previous albitization or, (2) concomitant reactions, were the fluid is renewed at the beginning of each reaction. After the isotopic mass balance estimation for each reaction, a temperature was calculated for each reaction using the plagioclase-water (Eq. 2) and K-feldspar-water (Eq. 3) equilibrium fractionation equations of Zheng (1993).

$$1000 \ln \alpha_{Ab-H2O} = \frac{4.33}{T^2} \times 10^6 - \frac{6.15}{T} \times 10^3 + 1.98 \qquad (2)$$

$$1000 \ln \alpha_{Kfs-H2O} = \frac{4.32}{T^2} \times 10^6 - \frac{6.27}{T} \times 10^3 + 2.00 \qquad (3)$$

Using the two reaction paths and the crossed combinations of the different applied values for R/W and $\delta^{18}O^{w}{}_{i}$, the estimated interaction temperatures of water during albitization and microclinization range between 32 and 89ºC (average of 60ºC). Significantly, and despite the large relative variations in the values applied to R/W and $\delta^{18}O_{if}$, and the two different reaction paths, the temperature estimates present a narrow range of variability, supporting that the mineral reactions developed in by interaction with “low” temperature groundwaters. Thus, considering the Permian-Triassic age and the relatively low temperature of the alteration, the hypothesis that the alteration fluids were closely related to the paleosurface and *de facto* “vertical” infiltrations of a weathering solution is a plausible possibility. Similar reaction temperatures (45 to 65ºC) were obtained for plagioclase albitization and K-feldspar microclinization in Permian-Triassic age red-stained albitized profiles in NE Spain (Fàbrega et al. 2019), that are similar in field layout, petrographic characteristics and age to the Polish sections of this study.

Regardless of the lack of accuracy of these temperature estimates, these estimated values show that the temperatures of the reactions associated with the development of red-stained albitized rocks are significantly below temperatures suggested for albitization formed under hydrothermal alteration (Cathelineau 1986; Boulvais et al. 2007) and tardi-magmatic alteration (Lee and Parsons 1997; Fiebig and Hoefs 2002). Instead, the low temperature range accords with the geological settings, age and association of the red-stained albitized profile developped on the Post-Variscan paleosurface during the Permian-Jurassic period. We suggest that the albitized profile developed a few hundred metres beneath the Post-Variscan paleosurface by interaction with relatively ‘low’ temperature groundwaters, and was subsequently exposed at the landsurface after erosion of the uppermost weathering mantle.

8 PALEOENVIRONMENTAL SETTING OF THE ALBITIZATION

The absence of mesoscale- and microscale-geopetal structures, together with clues of directional water flow combined with the isotropic structures around fracture blocks within the macro-scale profiles, evoke an aquifer environment at the origin of the albitization. Boreholes in the Massif Central (Schmitt 1986) and field exposures in the Morvan (Parcerisa et al. 2009) and NE Spain (Fàbrega et al. 2019) show that the albitized profiles may generally reach 100 m in thickness and may even exceed 200 m. Such profiles are comparable to those of weathering profiles with thick basal saprolite horizons in tropical soils (Boulangé 1984; Vasconcelos et al. 1994; Ruffet et al. 1996; Grimaud et al. 2015) and deep groundwater saprolites in dry saline environments as well as in periglacial environments (Thiry et al. 2006; Thiry et al. 2017). Nevertheless, the primary profiles were probably much thicker because only the deep indurated horizons have survived the erosion that preceded the Mesozoic transgression. The profiles were certainly at some stage surmounted by non-indurated horizons and regolith materials. On the other hand, the functioning of the albitization profiles and thus landscape stability spreading over ~50 Ma in the Sudetes is comparable to the duration of the deep tropical weathering profiles and related landscapes rooted in old cratons mentioned above.

Reaction temperatures calculated from the oxygen isotope composition of minerals, and hypotheses about the oxygen isotope composition of reactant fluids and their circulation, led us to an estimation of the mean temperature of albitization and associated reactions of about 60°C in the Sudetes albitized profiles and 55°C in the Catalan albitized profiles (Fàbrega et al. 2019). Based on this temperature, and considering a geothermal gradient of about 25–30°C km^{-1} and a surface temperature of ~30°C, in consideration of the high paleotemperature proposed at the Permian–Triassic boundary, led to calculate a mean depth of about 1 km for the environment in which albitization occurred.

There is indeed a systematic vertical profile organization for the sections we have studied, specifically with a more albitized and ferruginized upper part, a less-altered and reddened lower part where albitization occurred under weakly oxidizing conditions, and the progressive weakening and disappearance of alteration with depth. In connecting this geometry to the Pre-Triassic paleosurface, its is clear that the albitization represents a climatic weathering process of great magnitude. The low mobility of most of the involved chemical elements could point to deep groundwater table with very low outflow. But even if the alteration occurred at a greater depth, reactant solutions would have to have been renewed to provide at least sufficient O_2 and Na^+. Therefore, there must have been water flow within fractures between the fractured blocks which implies a hydraulic gradient. In particular, a regional hydraulic gradient with meteoric water infiltrating the upstream profiles and groundwater outflowing downstream would have been necessary. As albitization developed, water changed composition from entrance to outflow with loss of O_2, Na^+, and H^+ and a likely increase in K^+, Ca^{++}, and possibly SiO_2 content, as deduced from the geochemistry of the mineral transformations (Fig. 9g). The lateral evolution of such albitized profiles has been documented in the SW of the French Massif Central (Yerle and Thiry 1979; Clément 1986; Schmitt 1986). Here, (1) profiles on basement heights are thin and albitization is mainly restricted to fracture walls (such as described herein), and (2) lowland profiles rooted in Carboniferous and Permian deposits are much thicker with upper horizons albitised and oxidized whereas deeper albitized horizons remain anoxic and are the site of K-feldspar neoformations (Fig. 10).

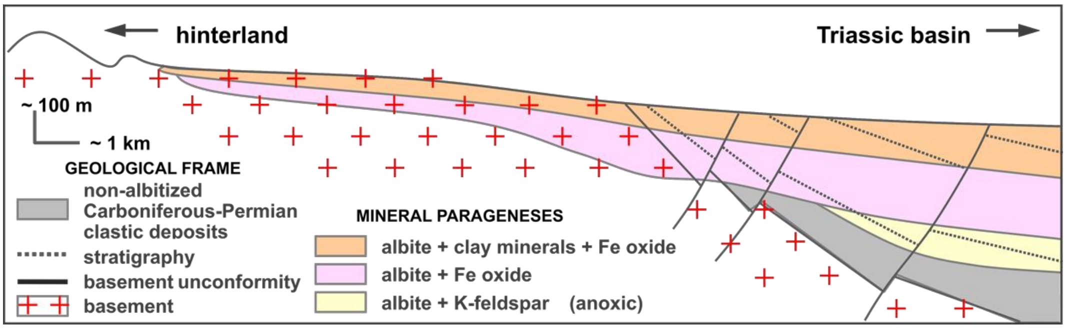

Fig. 10 Arrangement of mineral parageneses on the southern edge of the Massif Central. Albitized profiles thicken from crystalline heights towards Carboniferous and Permian basin lowlands where K-feldspar forms at depth. Modified after Clément (1986).

Two fundamental elements must be taken into account: (1) the presence of relief to ensure the hydrological gradient, and (2) the origin of sodium that triggers the whole chain of alteration. In terms of the groundwater dynamics, it could be that albitization developed in landscapes of intermediate relief, perhaps on large piedmonts between a mountain range and sea level. Petrographic data indicate that sodium was imported without potassium enrichment. Early modeling attempts (Schmitt 1994) also indicated that a high Na$^+$/K$^+$ ratio was probably required. The Na$^+$ enrichment is most likely to be linked with the peculiar geochemical setting of the Permian-Triassic environments in the region. Sodium could have originated from the gigantic salt deposits of these periods and may have been imported in large quantities and over long distances by successive phases of eolian reworking from littoral and endoreric basins during dry periods (Bourquin et al. 2011).

It should be stressed that the albitization started long before the recorded dating, possibly as early as Mid-Permian, with the development of the Zechstein evaporite deposits in the Germanic basin. It is the final stage that we have dated: previous stages have likely been overprinted by succeeding reactions. Classically, weathering profiles progress from top to base and result in older ages in the uppermost horizons and younger ages at depth, as evidenced in numerous long-lasting paleoweathering sequences (Vasconcelos et al. 1994; Dammer 1995; Ruffet et al. 1996). However, paleomagnetic dating of the profiles we have studied here show an inverse polarity, with the oldest ages in the weakly albitized and reddened bottom horizons and the youngest ages in the more albitized and ferruginized uppermost horizons. This points to a ‘regressive’ weathering sequence, in which the weathering profile did not continue to deepen but was ‘blocked’ with only the upper horizons continuing to be weathered. This profile form relates in some way to the specific evolution of the landscape in the region in relation to the widespread Mesozoic transgression. It would have corresponded to a rise in basal hydrological level which induced rising watertables across the continent. The rising watertables would have limited the infiltration of surficial waters, changed the hydrodynamic gradients and effectively stopped the alteration at depth. Thus, the regional geodynamics during the Late Permian and Triassic period strongly influenced weathering and regolith processes while the climate was steadily warm and semi-arid.

Weathering toposequences should be considered on a continental scale as shown by Fàbrega et al. (2019). In the case of our study area, the toposequence is arranged between the relief of the Varsican Belt that provided the hydraulic gradient and the Permian and Triassic basins that probably supplied the salt. Albitization was initiated and probably gradually invaded the entire Post-Varisacan paleosurface across several 10’s of Ma during which both landscape and climate were relatively stable. Indeed, the overall ages determined up to now for the albitization span a relatively long period, between 270 and 170 Ma, that corresponds to the Middle Permian to the Middle Jurassic (Table 4). The distribution of the now-dated albitized profiles along the Post-Variscan paleosurface between the Zechstein Sea in the North and the Tethys in the South (Fig. 11), shows that:

4) the profiles closest to the marine environments, namely the Sudetes and NE Spain, show the oldest ages (this study; Fàbrega et al. 2019);

5) the Vosges massif, which was connected to the marine environment through the threshold passage of the Triassic transgression coming from the North, also show relatively old albitized profiles (Vercruysse 2011);

6) the area most distant from the sea, namely the Rouergue heights overlay by infra-Jurassic deposits, comprises the youngest albitized profiles (Schmitt et al. 1984) while the Permian graben covered with coarse Triassic deposits on lower plateaux in Rouergue (Bonhomme et al. 1980) and Morvan (Ricordel et al. 2007) have older ages; and

7) in the Sudetes, the highly evolved ferruginous albitized facies currently in hillside positions are relatively young while the valley-bottom sections are older. This differentiation is possibly related to local morphologies whereby raised tectonic blocks remained emerged during the Mesozoic transgression.

The concordance between age and relative position in the Triassic paleogeography is striking. The areas covered early by the Triassic transgression have the oldest albitized profiles whereas the highlands distant from the sea have the youngest ages. It is actually the interruption of weathering by the Triassic transgression that is dated. These datings could in future be used as a tool to better enhance the mapping of the Triassic transgression and the geodynamics of the basement as well as its post-Triassic evolution.

Paleolandscape and paleoweathering features of the Post-Varican paleosurface in Western Europe may be compared to regolith features existing today on the African, Australian and South American cratons inherited from Pangea break out. Combined radiogenic dating and geomorphological analyses allowed us to document paleolandscape and paleoweathering profiles that functioned for more than 100 Ma in these cratonic regions (Vasconcelos et al. 1994; Dammer 1995; Ruffet et al. 1996; Pillans, 2007; Beauvais et al. 2008; Peulvast et al. 2008 ; Beauvais and Chardon 2013; Jean et al. 2020). This is the spatial and temporal scale of the albitization and hematization paleoweathering profiles that we studied on the Western European Post-Variscan paleosurface. Persistance of the Post-Variscan paleosurface is conforted by the widespread magnetic overprinting phase due to secondary hematite formation (related or not to albitization) that affected widely the Variscan belt during the 235-250 Ma time-span Edel et al. (2018).

Table 4 – Age of the reddened/albitized rocks related to the Post-Variscan paleosurface on the Variscan Belt.

area	location	geomorph	rockl	sample	method	age	reference
Sudetes	Szklarska Poręba	hill	granitoide	2.5 x 2.5 cm	palaeomag	256-190	herein
	Laski quarry	valley	granitoide	2.5 x 2.5 cm	palaeomag	270-190	herein
	Laski village	hill slope	granitoide	2.5 x 2.5 cm	palaeomag	258-170	herein
	Chwalisław	valley	granitoide	2.5 x 2.5 cm	palaeomag	205-195	herein
	Chwalisław	valley	granitoide	monazite	U-Th-Pb$_{tot}$	254	herein
	Chwalisław	valley	granitoide	2.5 x 2.5 cm	palaeomag	250	Edel et al. (1997)
Vosges			granitoide	2.5 x 2.5 cm	palaeomag	255-235	Vercruysse (2011)
Morvan			granitoide	2.5 x 2.5 cm	palaeomag	235	Ricordel et al. (2007)
Rouergue	Bertholène	high	orthogneiss	minerals	K-Ar	210-200	Schmitt et al. (1984)
	Brousse	basin	sediments	clay fraction	K-Ar	230	Bonhomme et al. (1980)
NE Spain	Guilleries Massif		granite	monazite	U-Th-Pb$_{tot}$	251	Fàbrega et al. (2019)
	Roc Frausa Mass.		granite	monazite	U-Th-Pb$_{tot}$	254	Fàbrega et al. (2019)
	Hortmoier Massif		granite	K-F crystals	K–Ar	240	Fàbrega et al. (2019)

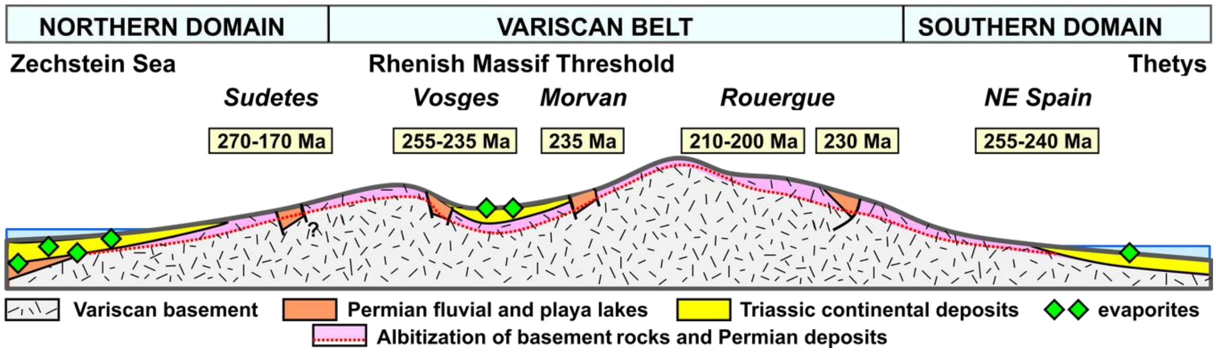

Fig. 11 Position and age of the studied albitized profiles on a schematic N–S geomorphological section of the Post-Variscan paleosurface and associated sedimentary basins during Permian-Triassic times. The oldest ages occur nearest the sea and youngest away the sea and in highland areas that were later buried. Paleogeography after Bourquin et al. (2011).

9 CONCLUSIONS

The oxidized and albitized facies of the Polish Sudetes granitoids exhibit two types of ‘classical’ petrographical parageneses: a saussuritization-sericitization and an albitization-hematitization. The chloritization of amphiboles and biotites that is associated to these alterations is intermediate between both. These alterations are always closely associated without any break or spatial discordance between them. They are controlled by the presence of fractures and are spatially arranged with respect to the configuration of these fractures. Albitization and hematitization are preferentially intense close to the walls of the fractures whereas the saussuritization and the sericitization of plagioclase become more important further away from the fractures and towards the center of the massive blocks. These alterations can be considered as topochemical. However, the complete albitization of the plagioclase and K-feldspar in the vicinity of the fractures signifies a supply of Na. Hematite associated with albite is an indication of oxidative capacity and therefore the supply of oxygen via the alteration.

Paleomagnetic dating of the reddened and albitized facies reveal Late Permian to Early Jurassic ages for the iron-oxides and radiochronological dating of associated monazite using the U-Th-Pb$_{total}$ method indicates Late Permian recrystallization ages. Given the ages of the alteration, it can clearly be related to the extensive Post-Variscan paleosurface in the region, since the altered granitoids were already outcropping during from Late Permian to Early Jurassic. Therefore, these reddened and albitized profiles can be considered a consequence of deep weathering.

As there was clearly a requirement to renew solutions to feed chemical reactions, it is likely that the alteration profiles were downstream of highlands in order to generate a hydrological head. The sodium supply that triggered albitization could well have come from the gigantic salt playas that characterized the lowland paleogeography of the Permian and Triassic in the region. Thus, we suggest that the reddened and albitized profiles developed on a wide glacis shaped in the basement rocks upstream of the evaporatic basins. The deep weathering was interrupted and preserved by the Mesozoic transgression.

The age dating shows that the oldest examples of the alteration profiles (Late Permian to Early Triassic) are proximal to the Zechstein and Tethys seas, while the youngest (late Triassic to basal Jurassic) are further away and appear to be located on the highlands that were more recently covered by the Mesozoic transgression. Thus, this alteration of the crystalline rocks is an important marker to constrain Triassic and post-Triassic geodynamics in the region, including erosion rates and the geomorphic evolution of the Paleozoic massifs.

Albitized and oxidized facies of crystalline basement are widespread throughout the world. Until now, this subject has attracted relatively little interest from petrographers. A re-examination of all existing data could involve a reconsideration of questions such as prehnite and sericite paragenesis, particularly from the viewpoint of temperature of formation, since they have in the past been used as an indicator of 'high temperatures'. It may be that the formation of sericite and prehnite is not part of a unique alteration leading to albitization, but the fact remains that proximity to the paleosurface is clearly indicated by the presence of hematite.

We suggest that particular attention should be paid to the radiochronological and paleomagnetic dating results that some have considered to be "obviously too young" in the context of the age of emplacement of the crystalline massifs. These "too young" dates have been systematically rejected as false in the past and rarely noted in publications; consequently this information was lost. A new consideration of these dates may realise their consistency, as shown for example by Edel and Schneider (1995) for the Permian formations that endured a Triassic rejuvenation highlighted by paleomagnetism.

It should be noted that the formation of secondary apatite in the reddened albitized Sudetes rocks has previously been reported in conjunction with albitization and chloritization related to the Triassic paleosurface in the French Massif Central (Parcerisa et al. 2009) and in NE Spain (Fàbrega et al. 2019). It also formed during metasomatic albitization in a metagabbro from Norway (Engvik et al. 2009). The formation of significant amounts of secondary apatite during albitization must be taken into account if fission track analysis or (U–Th)/He dating is carried out on these reddened albitized rocks.

References:

Aagaard P, Egeberg PK, Saigal GC, Morad S, Bjørlykke K (1990) Diagenetic albitization of detrital K-feldspars in Jurassic, Lower Cretaceous, and Tertiary clastic reservoir rocks from offshore Norway, II. Formation water chemistry and kinetic considerations. Journal of Sedimentary Petrology 60:575–581.

Aleksandrowski P, Kryza R, Mazur S, Żaba J (1997) Kinematic data on major Variscan strike-slip faults and shear zones in the Polish Sudetes, northeast Bohemian massif. Geological Magazine 133: 727-739.

Aleksandrowski P, Mazur S (2002) Collage tectonics in the northeasternmost part of the Variscan Belt: the Sudetes, Bohemian Massif). In: Winchester, J., Pharaoh T. & Verniers J. (eds), Palaeozoic Amalgamation of Central Europe, Geological Society, London, Special Publications 201: 237-277.

Alt, J.C., Laverne, C., Coggon, R.M., Teagle, D.A., Banerjee, N.R., Morgan, S., Smith-Duque, C.E., Harris, M., Galli, L. (2010) Subsurface structure of a submarine hydrothermal system in ocean crust formed at the East Pacific Rise, ODP/IODP Site 1256. Geochemistry, Geophysics, Geosystems, 11(10).

Awdankiewicz M, Awdankiewicz H (2010) Spessartites of the Kłodzko Złoty-Stok dyke swarm. Mineralogia Special Papers 37: 135-139.

Bachliński R, Bagiński B (2007) Kłodzko-Złoty-Stok granitoids massif. In Kozłowski A., Wiszniewska J (eds) In Granitoids in Poland, Archiwum mineralogiczne, Monograph 1: 261-273.

Baranowski Z, Haydukiewicz A, Kryza R, Lorenc S, Muszynski A (1990) Outline of the geology of the Góry Kaczawskie (Sudetes, Poland). Neues Jahrbuch für Geologie und Paläontologie, Abhandlungen 179: 223-257.

Barth SR (2000) Geochemical and boron, oxygen and hydrogen isotopic constraints on the origin of salinity in groundwaters from the crystalline basement of the Alpine Foreland. Applied Geochemistry 15:937–952. https://doi.org/10.1016/S0883-2927(99)00101-8

Beauvais A, Chardon F (2013) Modes, tempo, and spatial variability of Cenozoic cratonic denudation: The West African example, Geochem. Geophys. Geosyst., 14, 1590–1608, doi:10.1002/ggge.20093.

Beauvais, A., Ruffet G, Henocque O, Colin F (2008) Chemical and physical erosion rhythms of the West African Cenozoic morphogenesis: The 39Ar-40Ar dating of supergene K-Mn oxides, J. Geophys. Res., 113, F04007, doi:10.1029/2008JF000996.

Ben Baccar M, Fritz B, Madé B (1993) Diagenetic albitization of K-feldspar and plagioclase in sandstone reservoirs: thermodynamic and kinetic modeling. Journal of Sedimentary Petrology 63:1100–1109.

Besse J, Courtillot V (2003) Apparent true polar wander and the geometry of the geomagnetic field over the last 200 Myr: Correction. Journal of Geophysical Research 108: 2300.

Bonhomme M, Yerle J.-J, Thiry M (1980) Datation K-Ar de fractions fines associées aux minéralisations. Le cas du bassin uranifère permo-houiller de Brousse-Broquiès (Aveyron, France).- C.R. Académie Sciences Paris 291D: 121-123.

Boone GM (1969) Origin of clouded red feldspars, petrology contrasts in a granitic porphyry intrusion. American Journal of Science 267: 633-668.

Borkowska M, (1966) Petrografia granitu Karkonoszy (Petrography of the Karkonosze Granite). Geologia Sudetica 2: 7-119. (in Polish with English extended summary)

Botor D, Dunkl I, Anczkiewicz A, Mazur S (2017) Post-Variscan thermal history of the Moravo-Silesian lower Carboniferous Culm Basin (NE Czech Republic - SW Poland). Tectonophysics 712-713: 643-662.

Boulangé B (1984) Les formations bauxitiques latéritiques de Côte d'Ivoire. Travaux et Documents ORSTOM 175, 341 p.

Boulvais P, Ruffet G, Cornichet J, Mermet M (2007) Cretaceous albitization and dequartzification of Hercynian peraluminous granite in the Salvezines Massif (French Pyrénées). Lithos 93: 89-106.

Bourquin S, Bercovici A, López-Gómez J, Diez J-B, Broutin J, Ronchi A Amour F (2011) The Permian–Triassic transition and the onset of Mesozoic sedimentation at the northwestern peri-Tethyan domain scale: palaeogeographic maps and geodynamic implications. Palaeogeography Palaeoclimatology Palaeoecology 299: 265-280.

Bowles JFW, Howie RA, Vaughan DJ, Zussman J (2011) Non-Silicates: Oxides, Hydroxides and Sulphides. Rock-Forming Minerals, 2nd edn, Geological Society of London 5A: 920 p.

Boyce AJ, Fulignati P, Sbrana A (2003) Deep hydrothermal circulation in a granite intrusion beneath Larderello geothermal area (Italy): constraints from mineralogy, fluid inclusions and stable isotopes. Journal of Volcanology and Geothermal Research 126: 243-262.

Brinhall G, Dietrich W (1987) Constitutive mass balance relations between chemical composition, volume, density, porosity, and strain in metasomatic hydrochemical systems: Results on weathering and pedogenesis. Geochimica et Cosmochimica Acta 51: 567-587.

Butler RF (1998) Paleomagnetism: Magnetic domains to geologic terranes. Electronic edition, 237 p.

Castet S, Dandurand J-L, Schott J, Gout R (1993) Boehmite solubility and aqueous aluminium speciation in hydrothermal solutions (90-350°C): Experimental study and modeling. Geochimica et Cosmochimica Acta 57: 4869-4884.

Cathelineau M (1986) The hydrothermal alkali metasomatism effects on granitic rocks: quartz dissolution and related subsolidus changes. Journal of Petrology 27: 945-965.

Chrząstek A., Wojewoda J (2011) Mezozoik południowo-zachodniej Polski - synklinorium północnosudeckie (Mesozoic of SW Poland, the North Sudetic Synclinorium). In: Żelaźniewicz, A., Wojewoda, J., Ciężkowski, W. (eds), *Mezozoik i kenozoik Dolnego Śląska*. Polskie Towarzystwo Geologiczne, Wrocław, 1-10 (in Polish, English abstract).

Clément J-Y, (1986) Minéralogie, pétrologie et géochimie du Permien de Lodève (Hérault, France) : diagenèse précoce, altération feldspathisante et mise en place des minéralisations uranifères. E.N.S.M.P. Mémoire Sciences de la Terre 2: 137 p.

Cocherie A, Albarede F (2001) An improved U-Th-Pb age calculation for electron microprobe dating of 845 monazite. Geochimica et Cosmochimica Acta 65:4509–4522, https://doi.org/10.1016/S0016-7037(01)00753-0 846

Cocherie A, Legendre O, Peucat J-J, Kouamelan AN (1998) Geochronology of polygenetic monazites 847 constrained by in situ electron microprobe Th-U-total lead determination: Implications for lead 848 behaviour in monazite. Geochimica et Cosmochimica Acta *62*: 2475-2497, https://doi.org/10.1016/S0016-7037(98)00171-9

Cogné J-P (2003) PaleoMac: a Macintosh^{TM} application for treating paleomagnetic data and making plate reconstructions. Geochemistry Geophysics Geosystems 4: 1007.

Dammer D (1995) Geochronology of chemical weathering processes in the northern and western Australian regolith. PhD thesis, Australian National University: 214 p.

Danišík M, Migoń P, Kuhlemann J, Evans NJ, Dunkl I, Frisch W (2010) Thermochronological constraints on the long-term erosional history of the Karkonosze Mts, central Europe, Geomorphology 117: 78–89.

Danišík M, Štěpančíková P, Evans NJ (2012) Constraining long-term denudation and faulting history in intraplate regions by multisystem thermochronology: An example of the Sudetic Marginal Fault (Bohemian Massif, central Europe). Tectonics 31: TC2003, https://doi.org/10.1029/2011TC003012

De Jong G., Williams PJ (1995). Giant metasomatic systems formed during exhumation of mid-crustal Proterozoic rocks in the vicinity of the Cloncurry fault, northwest Queensland. Australian Journal of Earth science 42: 281-290.

De La Roche H (1957) Eléments pour l’étude de la saussuritisation. Mémoires de l’Institut Scientifique de Madagascar 7D: 217-223.

Depciuch T (1972) Wiek bezwzględny (K-Ar) granitoidów Kłodzko Złotostockich i strefy Niemczy. Kwartalnik Geologiczny 16: 103-111.

Drake H, Tullborg EL, Annersten H (2008) Red-staining of the wall rock and its influence on the reducing capacity around water conducting fractures. Applied Geochemistry 23: 1898-1920.

Dziedzic K, Teisseyre AK (1990) The Hercynian molasse and younger deposits in the Intra-Sudetic Depression, SW Poland. Neues Jahrbuch für Geologie und Paläontologie, Abhandlungen 179: 285–305.

Edel J-B, Schneider J-L (1995) The Late Carboniferous to Early Triassic geodynamics evolution of the Variscan Europe in the light of magnetic overprints in Early Permian rhyolites from the northern Vosges (France) and the central Black Forest (Germany). Geophysical Journal International 122: 858-876.

Edel J-B, Duringer P (1997) The apparent polar wander path of the European plate in Upper Triassic-Lower Jurassic times and the Liassic intraplate fracturing of the Pangea: New palaeomagnetic constraints from NW France and SW Germany. Geophysical Journal International 128: 331-344.

Edel J-B, Aifa T, Jelenska M, Kadzialko-Hofmokl M, Zelazniewicz A (1997) Réaimantations des formations paléozoïques des Sudètes polonaises et courbe de dérive des pôles géomagnétiques d'Europe du Carbonifère moyen au Jurassique moyen. Comptes Rendus de l'Académie des Sciences - Séries IIA - Earth and Planetary Science Letters 325: 479-486.

Edel J B, Schulmann K, Lexa O, Lardeaux J-M. (2018) Late Palaeozoic palaeomagnetic and tectonic constraints for amalgamation of Pangea supercontinent in the European Variscan belt. Earth-science reviews, 177: 589-612

Engvik AK, Golla-Schinder U, Berndt J, Austrheim H, Putnis A (2009) Intragranular replacement of chlorapatite by hydroxy-fluor-apatite during metasomatism. Lithos 112: 236-246.

Engvik AK, Putnis A, Gerald JDF, Austrheim H (2008) Albitisation of granitic rocks: the mechanism of replacement of oligoclase by albite. The Canadian Mineralogist 46: 1401-1415.

Fàbrega C, Parcerisa D, Rossell JM, Gurenko A, Franke C (2017) Predicting instrumental mass fractionation (IMF) of stable isotope SIMS analyses by response surface methodology (RSM). J Anal At Spectrom 32:731–748. https://doi.org/10.1039/C6JA0 0397D

Fàbrega C, Parcerisa D, Thiry M, Franke C, Gurenko A, Gòmez-Gras D, Solé J, Travé A. (2019) Permian–Triassic red-stained albitized profiles in the granitic basement of NE Spain: evidence for deep alteration related to the Triassic palaeosurface. International Journal of Earth Sciences 108: 2325-2347.

Farmer VC, Lumsdon DG (1994) An assessment of complex formation between aluminium and silicic acid in acidic solutions. Geochimica et Cosmochimica Acta 58: 3211-3334.

Feist-Burkhardt S, Götz A, Szulc J, Borkhataria R, Geluk M, Haas J, Hornung J, Jordan P, Kempf O, Michalík J, Nawrocki J, Reinhardt L, Ricken W, Röhling H-G, Rüffer T, Török Á, Zühlke R (2008) Triassic. In: McCann (ed.), The Geology of Central Europe, Volume 2, Mesozoic and Cenozoic. Geological Society of London, pp 749-821.

Ferry JM (1979) Reaction mechanisms, physical conditions, and mass transfer during hydrothermal alteration of mica and feldspar in granitic rocks from south-central Maine, USA. Contributions to Mineralogy and Petrology 68:125-139.

Fiebig J, Hoefs J (2002) Hydrothermal alteration of biotite and plagioclase as inferred from intragranular oxygen isotope-and cation-distribution patterns. European Journal of Mineralogy, 14, 49-60.

Fisher RA (Ed.) (1953) Dispersion on a Sphere. Philosophical Transactions of the Royal Society of London. Series A, vol. 217. 295 pp.

Fisher NI, Lewis T, Embleton BJJ 1987) Statistical Analysis of Spherical Data, Cambridge Univ. Press, Cambridge 1-329.

Głuszyński, A., Aleksandrowski, P. (2022) Late Cretaceous–Early Palaeogene inversion-related tectonic structures at the northeastern margin of the Bohemian Massif (southwestern Poland and northern Czechia). Solid Earth, 13(8): 1219-1242.

Goldsmith JR, Laves F (1954) The microcline-sanidine stability relations. Geochimica et Cosmochimica Acta 5: 1-19.

González-Acebrón L, Arribas J, Mas R (2010) Role of sandstone provenance in the diagenetic albitization of feldspars. A case study of the Jurassic Tera Group sandstone (Cameros Basin, NE Spain). Sedimentary Geology 229: 53-63.

González-Acebrón L, Götze J, Barca D, Arribas J, Mas R, Perez-Garrido C (2012) Diagenetic albitization in the Tera Group, Cameros Basin (NE Spain) recorded by trace elements and spectral cathodoluminescence. Chemical Geology 312, 148-162.

Götze J., Krbetschek M.R., Habermann D., Wolf D. 1999: High-resolution cathodoluminescence studies of feldspar minerals. [In]: Cathodoluminescence in geosciences. Ed.: Pagel M., Barbin V., Blanc Ph., Ohnenstetter D., Springer-Verlag, Berlin Heidelberg New York: 271-302.

Götze J, Krbetschek MR, Habermann D, Wolf D (2000) High-resolution cathodoluminescence studies of feldspar minerals. In: Cathodoluminescence in geosciences. Ed.: Pagel M., Barbin V., Blanc Ph., Ohnenstetter D., Springer-Verlag, Berlin Heidelberg New York: 245-270.

Grimaud J-L, Chardon, Metelka V, Beauvais A, Bamba O (2015) Neogene cratonic erosion fluxes and landform evolution processes from regional regolith mapping (Burkina Faso, West Africa). Geomorphology 241: 315-330.

Guy B (1993) Mathematical revision of Korzhinskii's theory of infiltration metasomatic zoning. European Journal of Mineralogy 5: 317-339.

Hövelmann J, Putnis A, Geisler T, Schmidt BC, Golla-Schindler U (2010) The replacement of plagioclase feldspars by albite: observations from hydrothermal experiments. Contribution to Mineralogy and Petrology 159: 43-59.

Jean A, Beauvais A, Chardon D, Arnaud N, Jayananda M, Mathe PE (2020) Weathering history and landscape evolution of Western Ghats (India) from 40Ar/39Ar dating of supergene K–Mn oxides. Journal of the Geological Society, 177(3): 523-536.

Jenkin GRT, Fallick AE, Leake BE (1992) A stable isotope study of retrograde alteration in SW Connemara, Ireland. Contributions to Mineralogy and Petrology 110: 269-288.

Jokubauskas P, Bagiński B, MacDonald R, Awdankiewicz M (2014) Field trip to the Kłodzko – Złoty Stok intrusion. Mineralogia, Mineralogical Society of Poland, Kraków, Special Papers 42: 127-134.

Jokubauskas P, Bagiński B, Macdonald R, Krzemińska E (2018) Multiphase magmatic activity in the Variscan Kłodzko–Złoty Stok intrusion, Polish Sudetes: evidence from SHRIMP U–Pb zircon ages. International Journal of Earth Sciences 107:1623–1639.

Kadzialko-Hofmokl M, Kruczyk J, Mazur S, Siemiatkowski J (2003) Paleomagnetism of the Upper Paleozoic and devonian rocks from the Kłodzko metamorphic Complex in the West Sudetes (SWPoland): tectonic implications for the Variscan Belt of Central Europe. Tectonophysics 177 : 83-99.

Kelley, D.S., Robinson, P.T., Malpas, J.G. (1992) Processes of brine generation and circulation in the oceanic crust: fluid inclusion evidence from the Troodos ophiolite, Cyprus. Journal of Geophysical Research: Solid Earth, 97(B6): 9307-9322.

Kirschvink JL (1980) The least-square line and plane and the analysis of paleomagnetic data, Geophys. J. R. Astron. Soc. 62: 699-718.

Kloppmann W, Girard J-P, Négrel P (2002) Exotic stable isotope compositions of saline waters and brines from the crystalline basement. Chemical Geology 184: 49–70. https://doi.org/10.1016/S0009-2541(01)00352-7

Koržhinskii DS, Oestreich W (1965) Abriss der metasomatischen Prozesse. Akademie-Verlag Berlin: 195 p.

Kowalski A (2020) Triassic palaeogeography of NE Bohemian Massif based on sedimentological record in the Wleń Graben and the Krzeszów Brachysyncline (SW Poland). Annales Societatis Geologorum Poloniae 90: 125–148.

Kozłowski A, Karwowski Ł, Olszyński W (1975) Tungsten-tin-molybdenum mineralization in the Karkonosze massif. Acta Geologica Polonica 25: 415-430.

Kroner U, Mansy J-L, Mazur S, Aleksandrowski P, Hann HP, Huckriede H, Lacquement F, Lamarche J, Ledru P, Pharaoh T, Zedler H, Zeh A, Zulauf G (2008) Variscan Tectonics. In: McCann, T. (ed.): The Geology of Central Europe. The Geological Society, London: 599-664.

Kryza R, Crowley QG, Larionov A, Pin Ch, Oberc-Dziedzic T, Mochnacka K (2012) Chemical abrasion applied to SHRIMP zircon geochronology: An example from the Variscan Karkonosze Granite (Sudetes, SW Poland). Gondwana Research 21: 757-767.

Kryza R, Schaltegger U, Oberc‐Dziedzic T, Pin Ch, Ovtcharova M (2014) Geochronology of a composite granitoid pluton: a high‐precision ID‐TIMS U–Pb zircon study of the Variscan Karkonosze Granite (SW Poland). International Journal of Earth Sciences 103: 683-696.

Kusiak M.A, Williams IS, Dunkley DJ, Konečny P, Słaby E, Martin HM (2014) Monazite to the rescue: U-Th-Pb dating of the intrusive history of the composite Karkonosze pluton, Bohemian Massif. Chemical Geology 364: 76-92.

Lee MR, Parsons I (1997) Dislocation formation and albitization in alkali feldspars from the Shap granite. American Mineralogist, 82: 557-570.

Leichmann J, Broska I, Zachovalová K (2003) Low‐ grade metamorphic alteration of feldspar minerals: a CL study. Terra Nova, 15: 104-108.

Lewandowski, M., Werner, T., Nowoz˙yn´ski, K., 1997. PDA—a package of Fortran programs for paleomagnetic data analysis. Inst. Geophys. Pol. Ac. Sci. (Personal communication).

Lorenc M (1994) Rola magm zasadowych w ewolucji intruzji granitoidowych (studium porównawcze wybranych masywów hercyńskich). Geologia Sudetica 28: 1-130.

Ludwig KR (2003) User’s Manual for Isoplot 3.00 - A Geochronological Toolkit for Microsoft Excel. 940 Berkeley Geochronological Centre Spec Publ Special Pu: 25–32

McFadden PL, McElhinny MW (1988) The combined analysis of remagnetization circles and direct observations in paleomagnetism, Earth Plan. Sci. Letts. 87: 161-172.

Machowiak K, Armstrong R (2007) SHRIMP U-Pb zircon age from the Karkonosze granite. Mineralogia Polonica Special Papers 31: 193-196.

MacQuarrie KTB, Mayer KU, Jin B, Spiessl SM (2010) The importance of conceptual models in the reactive transport simulation of oxygen ingress in sparsely fractured crystalline rock. Journal of contaminant hydrology 112: 64-76.

Majzlan J, Grevel KD, Navrotsky A (2003) Thermodynamics of Fe oxides: Part II. Enthalpies of formation and relative stability of goethite (α-FeOOH), lepidocrocite (γ-FeOOH), and maghemite (γ-Fe2O3). American Mineralogist 88: 855-859.

Marheine D., Kachlik V., Maluski H., Patočka F., Żelaźniewicz A. 2002. The 40Ar/39Ar ages from the West Sudetes (NE Bohemian Massif): constraints on the Variscan polyphase tectonothermal development. Geol. Soc. Spec. Publ., 201, 133-155

Marshall DJ (1988) Cathodoluminescence of Geological Materials. Unwin Hyman, Boston, 146 p.

Matte Ph, Maluski H, Rajlich P, Franke W (1990) Terrane boundaries in the Bohemian Massif: results of large scale Variscan shearing. Tectonophysics 177: 151–170.

Matthews A, Goldshmith JR (1984) The influence of metastability on reaction kinetics involving zoisite formation from anorthite at elevated pressures and temperatures. American Mineralogist 69: 848-857.

Mazur S, Aleksandrowski P, Kryza R, Oberc-Dziedzic T (2006) The Variscan orogen in Poland. Geological Quarterly 50: 89-118.

Mazur S, Aleksandrowski P, Turniak K, Awdankiewicz M (2007) Geology, tectonic evolution and late Paleozoic magmatism of the Sudetes-an overview. In Kozłowski A., Wiszniewska J (eds). In Granitoids in Poland. Archiwum mineralogiczne Monograph 1: 59-87.

Migoń P, Lidmar-Bergström K (2001) Weathering mantles and their significance for geomorphological evolution of central and northern Europe since the Mesozoic. Earth-Science Reviews 56: 285–324.

Migoń P, Danišík M (2012) Erosional history of the Karkonosze Granite Massif – constraints from adjacent sedimentary basins and thermochronology. Geological Quarterly 56: 440–454.

Mikulski SZ, Williams IS, Baginski B (2013) Early Carboniferous (Visean) emplacement of the collisional Kłodzko–Złoty-Stok granitoids (Sudetes, SW Poland): constraints from geochemical data and zircon U–Pb ages. International Journal of Earth Sciences 102: 1007-1027.

Mikulski S.Z, Bagińsky B, Dzierżanowski P (2004) The CHIME age calculations on monazite and xenotime in aplogranite from the Szklarska Poręba Huta. Miner. Ass. Pol. Spec. Pap., 24: 287–290.

Milewicz J., 1968. Karbon górny: niecka północnosudecka. In: Budowa Geologiczna Polski, t.1, cz. 1. Prekambr i paleozoik. Wyd. Geologiczne, Warszawa, 439-441

Milewicz J., 1970. The Cretaceous of the Jerzmanice Graben (Sudetes). Biul. Inst. Geol., 239, 37-66

Morad S, El-Ghaly MAK, Caja MA, Sirat M, Al-Ramadan K, Mansurbeg H (2010) Hydrothermal alteration of plagioclase in granitic rocks from Proterozoic basement of SE Sweden. Geological Journal 45: 105-116.

Oelkers EH, Schott J, Devidal JL (1994) The effect of aluminum, pH, and chemical affinity on the rates of aluminosilicate dissolution reactions. Geochimica et Cosmochimica Acta 58: 2011-2024.

Parcerisa D, Thiry M, Schmitt J-M (2009) Albitisation related to the Triassic inconformity in igneous rocks of the Morvan Massif (France). International Journal of Earth Science 99: 527-544.

Perez RJ, Boles JR (2005) An empirically derived kinetic model for albitization of detrital plagioclase. American Journal of Science 305: 312-343.

Peulvast J-P, Sales VC, Bétard F, Gunnell Y (2008) Low post-Cenomanian denudation depths across the Brazilian Northeast: implications for long-term landscape evolution at a transform continental margin. Global and Planetary Change, 62(1-2): 39-60.

Pillans B (2007) Pre- Quaternary landscape inheritance in Australia. Journal of Quaternary Science: Published for the Quaternary Research Association, 22(5): 439-447.

Plümper O., Putnis A (2009) The Complex Hydrothermal History of Granitic Rocks: Multiple Feldspar Replacement Reactions under Subsolidus Conditions. Journal of Petrology 50(5): 967-987.

Powolny, T., Dumańska-Słowik, M., Anczkiewicz, A. A., & Sikorska-Jaworowska, M. (2022). Origin and timing of spilitic alterations in volcanic rocks from Głuszyca Górna in the Intra-Sudetic Basin, Poland. *Scientific reports*, *12*(1), 1-26. https://doi.org/10.1038/s41598-022-15644-2.

Putnis A, Hinrichs R, Putnis CV, Golla Schindler U, Collins LG (2007) Hematite in porous red-clouded feldspars; evidence of large-scale crustal fluid-rock interaction. Lithos 95: 10-18.

Putnis CV, Ruiz-Aguido E (2013) The mineral-water interface: Where minerals react with the environment. Elements 9: 177-182.

Ramseyer K, Boles JR, Lichtner PC (1992) Mechanism of plagioclase albitization. Journal of Sedimentary Petrology 62: 349-356.

Reicherter K, Froitzheim N, Jarosiński M, Badura J, Franzke H-J, Hansen M, Hübscher H, Müller R, Poprawa P, Reinecker J, Stackebrandt W, Voigt T, Von Eynatten H, Zuchiewicz W (2008). Alpine tectonics north of the Alps. In: McCann (ed), The Geology of Central Europe, Volume 2: Mesozoic and Cenozoic. Geological Society, London, pp 1233-1285.

Richter L., Diamond LW (2022) Characterization of hydrothermal fluids that alter the upper oceanic crust to spilite and epidosite: Fluid inclusion evidence from the Semail (Oman) and Troodos (Cyprus) ophiolites. Geochimica et cosmochimica acta, *319*: 220-253.

Ricordel C, Parcerisa D, Thiry M, Moreau M-G, Gómez-Gras D (2007) Triassic magnetic overprints related to albitization in granites from the Morvan massif (France). Palaeogeography Palaeoclimatology Palaeoecology 251: 268-282. https://doi.org/10.1016/j.palaeo.2007.04.001.

Ruffet G, Innocent C, Michard A, Féraud G, Beauvais A, Nahon D, Hamelin B (1996) A geochronological 40Ar39Ar and 87Rb87Sr study of K–Mn oxides from the weathering sequence of Azul, Brazil. Geochimica et Cosmochimica Acta 60: 2219–2232.

Saigal GC, Morad S, Bjørlykke K, Egeberg PK, Aagaard P (1988) Diagenetic albitization of detrital K-feldspars in Jurassic, Lower Cretaceous, and Tertiary clastic reservoir rocks from offshore Norway, I Textures and origin. Journal of Sedimentary Petrology 58:1003-1013.

Sandström B, Annersten H, Tullborg EL (2010) Fracture-related hydrothermal alteration of metagranitic rock and associated changes in mineralogy, geochemistry and degree of oxidation: a case study at Forsmark, central Sweden. International Journal of Earth Science 99: 1-25.

Schmitt J-M (1986) Albitisation triasique, hydrothermalisme jurassique et altération supergène récente: métallogénie des gisements uranifères du Rouergue. Doct. ès Sciences Thesis, Strasbourg, Louis Pasteur University: p 240.

Schmitt J-M (1992) Triassic albitization in southern France: an unusual mineralogical record from a major continental paleosurface. In: Schmitt JM, Gall Q (eds) Mineralogical and geochemical records of paleoweathering. ENSMP, Mémoires des Sciences de la Terre, Paris, pp 115–131

Schmitt J-M (1994) Geochemical modeling and origin of the Triassic albitized regolith in Southern France. 14th International Sedimentological Congress, Aug. 20-28, Recife, Brazil, Abstracts S8, p. 19-21.

Schmitt J-M Baubron JC, Bonhomme MG (1984) Pétrographie et datations K–Ar des transformations minérales affectant le gîte uranifère de Bertholène (Aveyron-France). Mineralium Deposita 19:123–131.

Schmitt J-M, Clement JY (1989) Triassic regolithization: a major stage of pre-enrichment in the formation of unconformity related deposits in Southern France. Metallogenesis of uranium deposits. IAEA Technical Committee Meeting, Vienna 542(8): 93-113.

Simon K, Hoefs J (1987) Effects of meteoric water interaction on Hercynian granites from the Südschwarzwald, southwest Germany. Chemical Geology 61: 253-261.

Słaby E, Götze J (2004) Feldspar crystallization under magma-mixing conditions shown by cathodoluminescence and geochemical modelling–a case study from the Karkonosze pluton (SW Poland). *Mineralogical Magazine*, *68*(4), 561-577

Słaby E, Martin H (2008) Mafic and felsic magma interaction in granites: the Hercynian Karkonosze pluton (Sudetes, Bohemian massif). Journal of Petrology 49: 353-391.

Słaby E, Galbarczyk-Gąsiorowska E, Baszkiewicz A (2002) Mantled alkali-feldspar megacrysts from the marginal part of the Karkonosze granitoid massif (SW Poland). Acta Geologica Polonica 52: 501-519.

Słaby E, Galbarczyk-Gąsiorowska E, Seltmann R, Müller A (2007) Alkali feldspar megacryst growth : Geochemical modelling. Mineralogy and Petrology 89: 1-29.

Sobczyk A, Danišík M, Wojewoda J, Śliwiński W, Raczyński P, August C (2013) Zircon (U-Th)/He thermochronology of the Permian Weissliegendes sandstone in the Fore-Sudetic Homocline (SW Poland). Mineralogia - Special Papers 41: 81.

Sobczyk A, Danišík M, Aleksandrowski P, Anczkiewicz A (2015) Post-Variscan cooling history of the central Western Sudetes (NE Bohemian Massif, Poland) constrained by apatite fission-track and zircon (U-Th)/He thermochronology. Tectonophysics 649: 47-57.

Sobczyk A, Sobel ER, Georgieva V (2020) Meso-Cenozoic cooling and exhumation history of the Orlica-Śnieżnik Dome (Sudetes, NE Bohemian Massif, Central Europe): Insights from apatite fission-track thermochronometry. Terra Nova 32 (2): 122–133.

Steinthorsson S, Helgason O (1992) Maghemite in Icelandic basalts. Mineralogical Magazine 56: 185-199.

Stillings LL, Brantley SL (1995) Feldspar dissolution at 25°C and pH 3: Reaction stoichiometry and the effect of cations. Geochimica et Cosmochimica Acta 59: 1483-1496.

Stober I, Bucher K (1999a) Origin of salinity of deep groundwater in crystalline rocks. Terra Nov 11:181–185. https://doi.org/10.1046/j.1365-3121.1999.00241.x

Stober I, Bucher K (1999b) Deep groundwater in the crystalline basement of the Black Forest region. Applied Geochemistry 14: 237–254. https://doi.org/10.1016/S0883-2927(98)00045-6

Sun SS, Eadington PJ (1987) Oxygen isotope evidence for the mixing of magmatic and meteoric waters during tin mineralization in the Mole Granite, New South Wales, Australia. Economic Geology 82: 43-52.

Suzuki K, Adachi M (1994) Middle Precambrian detrital monazite and zircon from the hida gneiss on Oki-Dogo Island, Japan: their origin and implications for the correlation of basement gneiss of Southwest Japan and Korea. Tectonophysics 235: 277–292. https://doi.org/10.1016/0040-1951(94)90198-8

Suzuki K, Adachi M, Tanaka T (1991) Middle precambrian provenance of Jurassic sandstone in the Mino Terrane, central Japan: Th-U-total Pb evidence from an electron microprobe monazite study. Sedimentary Geology 75: 141–147. https://doi.org/10.1016/0037-0738(91)90055-I

Suzuki K, Adachi M, Kajizuka I (1994) Electron microprobe observations of Pb diffusion in metamorphosed detrital monazites. Earth and Planetary Science Letters 128: 391–405. https://doi.org/10.1016/0012- 1079 821X(94)90158-9

Taylor HP (1977) Water/rock interactions and the origin of H_2O in granitic batholiths. Journal of Geological Society of London 133: 509-558.

Taylor HP (1977) Water/rock interactions and the origin of H2O in granitic batholiths: Thirtieth William Smith lecture. J Geol Soc London 133:509–558. doi: 10.1144/gsjgs.133.6.0509

Thiry M, Liron MN, Dubreucq P, Polton J-C (2017) Curiosités géologiques du massif de Fontainebleau, Guide géologique, BRGM Editions., 115 p.

Thiry M, Milnes AR, Rayot V, Simon-Coinçon R (2006) Interpretation of palaeoweathering features and successive silicifications in theTertiary regolith of Inland Australia. Journal of the Geological Society 163: 723-736.

Vasconcelos PM, Becker TA, Renne PR, Brimhall GH (1994) Direct dating of weathering phenomena by 40Ar39Ar and K–Ar analysis of supergene K–Mn oxides. Geochimica et Cosmochimica Acta 58: 1635–1665.

Vercruysse C (2011) Mise en évidence et datation de la paléosurface crétacée dans le massif des Vosges. Rapport No O110620CVER, Centre de Geosciences, Ecole des Mines de Paris, Fontainebleau, France, 75 p.

Waychunas GA (1991) Oxide Minerals: Petrologic and magnetic significance. Reviews in Mineralogy 25: 38-46.

Wierzchołowski B (1976) Granitoidy kłodzko-złotostockie i ich kontaktowe oddziaływanie na skały osłony (studium petrograficzne). Geologia Sudetica 11: 7-147.

Wilamowski A, (2002) Chloritization and polytypism of biotite in the Łomnica granite, Karkonosze Massif, Sudetes, Poland: Stable isotope evidence. Chemical Geology 182(2-4): 529-547.

Williams ML, Jercinovic MJ, Goncalves P, Mahan K (2006) Format and philosophy for collecting, 1096 compiling, and reporting microprobe monazite ages. Chemical Geology 225: 1–15. https://doi.org/1097 10.1016/j.mce.2005.09.009

Wojdyr M (2010) Fityk: A general-purpose peak fitting program. Journal of Applied Crystallography 43: 1126-1128.

Yao KFE (2013) Albitization and oxidation of the granitoïd rocks related to the Triassic paleosurface in the Sudetes (SW Poland). Thesis École Nationale Supérieure des Mines de Paris in Paris (France) and Państwowy Instytut Geologiczny - Państwowy Instytut Badawczy in Warsaw (Poland). 164 p. http://pastel.archives-ouvertes.fr/pastel-00971314

Yerle J.-J, Thiry M (1979) Albitisations et minéralisations uranifères dans le socle et les sédiments permo-houillers du bassin de Brousse-Broquiès (Aveyron, France). Bulletin BRGM 4: 275-290.

Žak J, Klominsky J (2007) Magmatic structures in the Krkonoše–Jizera Plutonic Complex, Bohemian Massif: evidence for localized multiphase flow and small-scale thermal–mechanical instabilities in a granitic magma chamber. Journal of Volcanology and Geothermal Research 164: 254-267.

Žák J, Verner K, Sláma J, Kachlík V, Chlupáčová M (2013) Multistage magma emplacement and progressive strain accumulation in the shallow- level Krkonoše- Jizera plutonic complex, Bohemian Massif. Tectonics 32: 1493-1512.

Zheng Y-F (1993) Calculation of oxygen isotope fractionation in anhydrous silicate minerals. Geochim Cosmochim Acta 57:1079–1091. doi: 10.1016/0016-7037(93)90042-U.

Zijderveld, JDA. (1967) A.C. demagnetisation of rocks: analysis of results. In: Collinson, DW, Creer, KM, Runcorn, SK (Eds.), Methods in Paleomagnetism. Elsevier, Amsterdam, pp. 254–286.

Albitization and oxidation of Variscan granitoid rocks related the to Post-Variscan paleosurface in the Sudetes (Bohemian Massif, SW Poland)

Médard Thiry(1*), Christine Franke(1), Kouakou F.E Yao(1), Adam Szuszkiewicz(2), Carles Fàbrega(3), Maria Jeleńska(4), Magdalena Kądziałko-Hofmokl(4), Andrey Gurenko(5), David Parcerisa(3), Artur Sobczyk(2), Krzysztof Turniak(2), Paweł Aleksandrowski(6)

(1) MINES Paris - PSL, Center of Geosciences and Geoengineering, 35 rue St Honoré 77305 Fontainebleau Cedex, France
(2) Institute of Geological Sciences, University of Wrocław, pl. M. Borna 9, 50-204 Wrocław, Poland
(3) Universitat Politècnica de Catalunya, Manresa, Spain
(4) Institute of Geophysics, Polish Academy of Sciences, Ks. Janusza 64, 01-452 Warsaw, Poland
(5) Centre de Recherches Pétrographiques et Géochimiques, UMR 7358, Université de Lorraine, F-54501 Vandoeuvre-lès-Nancy, France
(6) Polish Geological Institute – National Research Institute, Lower Silesia Branch, Al. Jaworowa 19, 53-122 Wrocław, Poland

*corresponding author: medard.thiry@free.fr https://orcid.org/0000-0003-2534-8882

Abstract:

The reddened granitoid facies in the basement of the Polish Sudetes exhibits two categories of alteration spatially arranged with respect to fractures: (1) saussuritization and sericitization within light-colored facies in the interior of fracture-bounded blocks and (2) albitization and hematitization in a reddened facies occurring adjacent to fracture walls. These alterations are associated with chloritization of primary ferromagnesian minerals and the development of secondary minerals such as quartz, K-feldspar, apatite, prehnite, calcite, and titanite. We link these parageneses and the observed zonation to a unique alteration event consisting of an interplay of chemical reactions of variable spatial extent. The complete albitization of the feldspars (plagioclase and K-feldspar) adjacent to fractures points to a significant supply of Na for the albite neoformation and availability of oxygen to form the associated hematite. The dating of the iron oxides by paleomagnetism and the secondary monazite associated with the albitized facies by U-Th-Pb$_{total}$ unambiguously indicates their Post-Variscan ages. In this context, the alterations are related to regionally widespread Post-Variscan paleosurface. Weathering profiles formed in phreatic groundwater environments downgradient of highlands that provided a hydrological head. Sodium supply was likely to origin from the gigantic salt playas that characterized Permian and Triassic lowlands. Weathering was interrupted by an advance of the Mesozoic transgression. The recognition of these weathering profiles over extensive parts of the Variscan Belt provides the basis for reconstructing the Post-Variscan paleosurface and constraining Triassic and Post-Triassic geodynamics, including erosion rates and geomorphological evolution of the Paleozoic massifs in Europe.

Keywords:

albitization, oxidation, granitoid, dating, paleosurface, Post-Variscan, Poland.

Running title:

Albitization related to the Post-Variscan paleosurface

Statements and declarations:

The authors declare that they have no known competing financial interests or personal relationships that could have appeared to influence the work reported in this paper.

Acknowledgements:

This work is the result of a quest that was started more than 40 years ago at the Ecole des Mines de Paris. The French team likes to acknowledge the two participating Polish Institutions for the organization of the field work campaigns and for two scientific stays of K.Y. in the labs with access to CL. We acknowledge the IPGP Paleomagnetism group for access and help with *2G* cryogenic magnetometer paleomagnetic and rock magnetic measurements as well as the CLIMAG group at the LSCE for access to the rock magnetic measurements performed in their laboratories. The authors thank Jean-Bernard Edel from the University of Strasbourg and an anonymous reviewer for their thoughtful comments, which significantly strengthened the earlier version of the article. Authors are also indebted to Tony Milnes from University of Adelaide for his discussions and language edition.

INTRODUCTION

In crystalline rocks, albitization is commonly considered to be a deep and high-temperature metasomatic alteration linked to granite cooling during exhumation (e.g. Putnis et al. 2007; Engvik et al. 2008; Sandström et al. 2010; Morad et al. 2010). Besides, in basaltic rocks, albitization with typical albite, chlorite, and epidote assemblage is considered to be relatated to pervasive alteration by deep circulation of heated seawater (spilitization) under relative lower temperature (Kelley et al. 1992; Alt et al. 2010; Richter and Diamond 2022). Studies of albitization in granitic and other basement rocks have been mostly undertaken by petrologists who usually consider its petrographical aspects and recognise the late-stage nature of the parageneses. However, the geometric aspects of the albitization phenomenon have never been thoroughly investigated. In this paper we describe the albitization as a result of superficial weathering, spatially and temporally associated with the Post-Variscan paleosurface, by analogy with situations described locally in the French Massif Central (Yerle and Thiry 1979; Schmitt 1986, 1992; Schmitt and Clement 1989; Parcerisa et al. 2009) and in NE Spain (Fàbrega et al. 2019).

We focus our study on the Polish Sudetes where paleomagnetic dating of Post-Variscan remagnetization overprints of the Paleozoic crystalline basement has already been well-reported in the literature (e.g. Edel et al. 1997). Our aim is to sort out whether the albitization observed in the Sudetic granitoids could have been of superficial (a weathering phenomenon) rather than of deep-seated hydrothermal origin. For this purpose, we describe detailed mineralogical and petrographical features of the albitized facies rocks. Special attention is payed to the petrographic evolution of the granitoids in relation to the reddened facies adjacent to fractures. The relationship between primary and secondary mineral phases is emphasized with the focus to establish a specific mineral paragenesis and geochemical conceptual model for the albitization, and to understand its association with the contemporaneous formation of hematite. Subsequently, the results of paleomagnetic dating of iron oxides and U-Th-Pb$_{total}$ dating of monazites in the reddened facies are presented in order to explore their respective links with the Post-Variscan paleosurface.

GEOLOGICAL SETTING

Regional frame

The mountain range of the Sudetes is the topographic expression of a regional-size fault block, about 300 km long and 50 to 80 km wide, at the NE margin of the Bohemian Massif (Fig. 1). The Sudetic block was uplifted, together with the entire Bohemian Massif, in Late Cenozoic times along major NW-SE and NE-SW trending faults at the foreland of the Eastern Alps and Carpathians (e.g. Reicherter et al. 2008), while to the NE it is accompanied by the geologically similar Fore-Sudetic block that is currently not elevated.

The Sudetes occur on the norteastern periphery the internal zone of the Variscan belt of Europe, whose mostly crystalline, Late Neoproterozoic to Carboniferous basement rock complexes are arranged in a mosaic of a complex tectonic collage, amalgamated and deformed during Late Devonian through to Carboniferous Variscan tectonic events (Matte et al. 1990; Aleksandrowski and Mazur 2002; Kroner et al. 2008). The collage is intruded by syn- to late orogenic Carboniferous granitoid plutons, the most voluminous of which are those of Karkonosze, Strzegom-Sobótka and Kłodzko - Złoty Stok (e.g. Mazur et al. 2006, 2007).

The basement rocks are locally overlain by syn- to late-tectonic Carboniferous intramontane basins and remnants of a now much eroded post-orogenic Permo-Mesozoic sedimentary-volcanic cover (Fig. 1), which during Late Cretaceous – Early Paleogene times underwent compressional deformation: gentle folding and inversion-related faulting (Głuszyński and Aleksandrowski 2022). To the south, in the Intra-Sudetic Basin, Early Permian red beds and shales with volcanics up to 1250 m thick are followed by Late Permian and Early Triassic fluviatile deposits of Buntsandstein facies, wich do not exceed a few tens of meters in thickness (e.g. Dziedzic and Teisseyre 1990). To the north, in the North Sudetic Basin, there is a dominantly sedimentary series including Early Permian red beds with volcanics and Late Permian Zechstein facies carbonates, sulphates and clastics, averaging about 1000 m in thickness. The Early Triassic Buntsandstein of variegated sandstones, totalling about 600 m in thickness, are capped by Röt dolomites and later Keuper evaporites and Muschelkalk limestones (e.g. Baranowski et al. 1990; Chrząstek and Wojewoda 2011). In south-western and western Poland and eastern and northern Germany, the Early Triassic clastics that are accompanied locally by the Buntsandstein exceed 1000 m in thickness (Feist-Burkhardt et al. 2008). The Early Permian and Early Triassic clastic deposits reflect intense erosion and denudation of the southerly located Variscan internal massifs, including those of the Sudetes. The Late Permian Zechstein carbonates and sulphates as well as the late-Early to Middle Triassic carbonates, on the other hand, mark the episodes of marine transgression. The Late Permian transgression apparently left in the Sudetes only a thin sedimentary sequence of tens of metres thick, whereas that of the late-Early to Middle Triassic might have resulted in an originally much thicker sedimentary succession, similar to those in the adjacent areas (cf. e.g. Feist-Burkhardt et al. 2008). This is suggested by increasingly deepening facies of the now up to 100 m-thick Muschelkalk deposits towards their erosive top (Chrząstek and Wojewoda 2011). Also, the original presence of a relatively thick and extensive cover of marine Jurassic sediments in the Sudetes cannot be entirely ruled out, despite their present absence possibly due to pre-Cenomanian erosion.

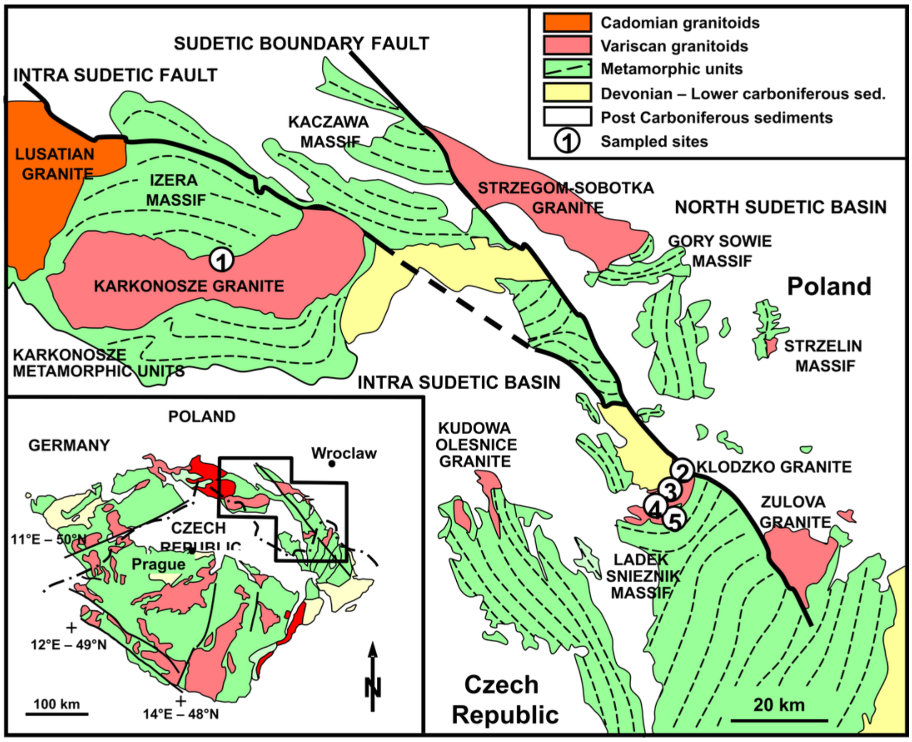

Fig. 1 Geological map of the Sudetes (modified after Aleksandrowski et al. 1997). (1) Szklarska Poręba Huta quarry; (2) Laski quarry; (3) Laski village; (4) Chwalisław valley; (5) Mt Kopciowa

Sampling

Our sampling was concentrated on the reddened granitic rocks in the quarry at Szklarska Poręba Huta on the Karkonosze pluton and in several exposures in the eastern part of the Kłodzko - Złoty Stok pluton, at Laski and in the Chwawlisław valley (Fig. 1). The focus was put on large exposures of rocks with distinct signs of reddening that are typically bound to fractures. In this study we use the term fracture to any brittle discontinuities in a rock, whether or not they imply fracture-parallel or -perpendicular displacement, i.e. various types of both joints and faults. Non-reddened rocks were also sampled in order to characterise differences between the reddened and non-reddened facies.

Karkonosze granitoid massif

The late-orogenic Karkonosze granitoid massif in the western part of the Sudetes is composed of a number of granitic facies thought to correspond to fractional crystallization, mixing with mafic magmas and hybridization processes (Žák and Klomínský 2007; Słaby and Martin 2008). The pluton resulted from sequential emplacement over a brief period of time at ca. 320-310 Ma (Machowiak and Armstrong 2007; Žák et al. 2013; Kryza et al. 2012, 2014; Kusiak et al. 2014).

Sampling of the Karkonosze pluton was undertaken in the Szklarska Poręba Huta quarry (N50°49’39’’, E15°29’38’’) on the NW margin of the Karkonosze massif, close to its contact with the metamorphic envelope

(Fig. 1). Samples were obtained from a steep northern wall of the quarry where there was an exposure of two rock types in sharp intrusive contact: (1) a fine-grained equigranular leucocratic granite (so called aplogranite) and (2) a medium- to coarse-grained porphyritic biotite granite. Both granites contain thick (up to 25 cm) aplite veins and centimetre-wide quartz veins. According to Słaby et al. (2007), the granite from Szklarska Poręba Huta belongs to the geochemically furthest evolved granite types in the Karkonosze composite pluton.

The porphyritic granite from the Szklarska Poręba Huta quarry contains large phenocrysts (up to 10 cm) of perthitic K-feldspar (about 65-99% Or) mantled by plagioclase (about Ab ≥ 83%) and enclosed in medium-grained groundmass (Borkowska 1966; Słaby et al. 2002). Relative to the porphyritic granite, the aplogranite is enriched in quartz and plagioclase and impoverished in biotite and alkali-feldspar (Kozłowski et al. 1975).

The Kłodzko - Złoty Stok pluton

The Kłodzko - Złoty Stok (KZS) pluton, the largest composite intrusion in central Sudetes (Fig. 1), is composed off strongly diversified high-K metaluminous rocks, rich in mafic components (e.g. Lorenc 1994; Bachliński and Bagiński 2007; Jokubauskas et al. 2014). The small magma batches were emplaced between 349.0 ± 3.7Ma and 331.5 ± 2.6Ma. Short-lived late Carboniferous rejuvenation of magmatic activity along major fault zones caused intrusion of the the Laski monzogranite at 303.3 ± 3.8/4.2Ma (Jokubauskas et al. 2018 and references therein).

Exposures of reddened granitic rocks were sampled in the Laski quarry (N50°28'25" E16°48'34"), Laski village (N50°27'40" E16°48'12") and a small old quarry near the creek of Mąkolnica (Chwalisław valley; N50°25'54" E16°49'42"). Jointly were sampled non reddened, relatively dark-grey medium-grained granodiorite wih relatively uniform plagioclase composition (36-46% An) typical of the Laski area (Wierzchołowski 1976). The quarry in the Chwalisław valley exposes granodiorite intruded by dykes (up to about. 1 m wide) of spessartite. Both rocks had been previously dated, yielding ages of 336.7 ± 2.3Ma and 321.1 ± 3.1Ma, respectively (Mikulski et al. 2013). Non-reddened granodiorite is a grey, medium- to fine-grained, equigranular rock with relative anorthite-rich plagioclase (39-44% An), whereas the fine-grained microporphyritic spessartite is composed of more sodic plagioclase (Wierzchołowski 1976; Awdankiewicz and Awdankiewicz 2010; Mikulski et al. 2013).

ANALYTICAL METHODS.

Powder X-ray diffraction (XRD) analyses were carried out at Mines-Paris, using a PANalytical X'Pert system fitted with a Cu-anode and X'celerator detector, on fragments of larger K-feldspar crystals separated by hand-picking from the bulk rock samples. XRD scans were run from 2 to 60° (2θ). The XRD diagrams were interpreted using the EVA© Bruker software. In the case of overlapping (131) and (1-31) peaks, deconvolution was undertaken using the FITYK software (Wojdyr 2010) with Pearson VII function applied to fit the peak shapes. Al-Si ordering of the K-feldspar structure was evaluated on the basis of the triclinicity parameter according to the method of Goldsmith and Laves (1954).

Selected thin sections from the reddened rock samples were studied using conventional petrographical microscopy and cathodoluminescence (CL) techniques at the Institute of Geological Sciences, University of Wrocław. The CL study made use of a CL MK3 cold cathode gun mounted on a polarizing optical microscope.

Systematic sampling for paleomagnetic analysis was performed focused on the reddened facies at four principal outcrops, three of them situated in the Kłodzko – Złoty Stok Massif (Laski quarry, Laski village, Chwalisław valley) and one in Szklarska Poręba Huta area. The samples for paleomagnetic analyses were drilled in the vicinity of principal fractures. The samples were collected as oriented drill cores using a petrol-driven hand drilling machine and as block samples oriented in field by measuring dip and dip azimuth.

They were cut into standard 2.5 x 2.5 cm cylinders for paleomagnetic experiments. Thermal demagnetization was subsequently performed on the cylinders either in the paleomagnetic laboratory of the Institute du Physique du Globe de Paris using a vertical three-axial 2G cryogenic magnetometer and at the Institute of Geophysics of the Polish Academy of Sciences in Warsaw using a 2G Enterprise SQIUD magnetometer. Stepwise demagnetization of the NRM was applied on the samples, starting at room-temperature, and if possible, embracing the complete temperature range up to the hematite temperature interval around 700°C. Alternatively, some selected samples were demagnetized using the alternating field technique at the Institute of Geophysics of the Polish Academy of Sciences in Warsaw. The resulting data are systematically corrected for the geographic position of each individual sample.

Further data processing was performed using either the PaleoMac5 software (Cogné 2003) or the PALMAG software provided by Lewandoski et al. (1997) Characteristic paleomagnetic directions were determined by a least-square fit of linear segments (Kirschvink, 1980) in orthogonal Zijderveld diagrams (Zijderveld 1967; see also supplementary material 2, Fig. S1 to S3), either on equal areas or in great circle fits. The PaleoMac5 and PALMAG software offer the opportunity to choose the groupped directions and to calculate respective site-mean directions and paleomagnetic pole statistics (Fischer, 1953; Mc Fadden and McElhinny 1988). The analyses of thermal demagnetization of NRM curves and thermomagnetic experiments (magnetization and saturation remanence during heating curves) allow the identification of magnetic carriers of the paleomagnetic directions (for instrumental details and rock magnetic results please see also supplementary material 2, Fig. S4 and S5).

The chemical compositions of feldspars and micas were analysed by EPMA (Electron Probe Micro Analysis) at the Scientific and Technological Centers of the Universitat de Barcelona (CCiTUB), using Cameca

SX-51 and JEOL JXA-8230 electron microprobes, both operating at 15 kV and 1.5 nA. The CL images of the samples were used to guide the placing of the analyses. The table of EPMA results is included in the supplementary material 1.

Monazite dating was carried out using the EPMA U-Th-Pb$_{total}$ method following the recommendations included in Cocherie et al. (1998), Cocherie and Albarede (2001), and Williams et al. (2006). Monazite grains suitable for EPMA analysis were found by means of BSE imaging using a Hitachi TM-1000 electron microscope at the Manresa School of Engineering (Spain). U-Th-Pb$_{total}$ EPMA analyses were undertaken at the Scientific and Technological Centers of the Universitat de Barcelona (Spain) using a Jeol JXA-8230 electron microprobe operating at 15 kV, 40 nA of current intensity and a beam diameter of 1 µm. An in-house reference monazite from the Petaca District (Mexico), with an age of 1332 ± 5 Ma (2σ), was analyzed as a control standard jointly with the monazite samples. The age of each analysed monazite was calculated using the MonaziteAge software based on the works of Suzuki and Adachi (1991, 1994) and Suzuki et al. (1994) and which is included with the Jeol JXA-8230 instrument. The initial acquired data were prepared for subsequent statistical age analysis by eliminating the analyses which presented oxide totals higher and lower than 100 ± 5%. Subsequently, age outliers were discarded using a stepwise process based on box-plot graphs. The final ages of the different monazite generations were determined by deconvolution of the ages histogram using the Microsoft Excel add-in ISOPLOT 4.15 from the Berkeley Geochronology Center (Ludwig 2003). A total of 189 EPMA analyses were made and 147 analyses (77% of the total) were retained including 18 from the Szklarska Poręba Huta quarry and 129 from the Chwalisław valley section. The table of monazite EPMA results is included in the Electronic Supplementary material 1.

The oxygen isotope composition of plagioclase and K-feldspar was determined by Seconday Ion Mass Spectrometry (SIMS) using a CAMECA IMS 1280HR ion microprobe at the Centre de Recherches Pétrographiques et Géochimiques (CRPG), Vandœuvre-lès-Nancy, France. Samples were mounted in 25 mm diameter epoxy mounts and the surface was metallographically polished. Afterwards the samples surfaces were imaged under optical cathodoluminescence to differentiate textural domains within the crystals. The detailed analytical conditions during the SIMS session are described in Fàbrega et al. (2017). The granite samples were analysed jointly with in-house plagioclase and K-feldspar standards. The analyses were placed in homogeneous luminescent domains in crack- and inclusion-free areas of the crystals. A total of 28 and 31 analyses were carried out on plagioclase and K-feldspar grains, respectively. Afterwards, the craters of the SIMS analyses were observed under BSE-imaging and analyzed by EPMA to check that the craters were homogeneously excavated and determine the chemical composition linked to each isotopic analysis. The instrumental mass fractionation (IMF) of the raw results was corrected by means of response surface methodology (RSM) following the procedures and using the response surface models described in detail by Fàbrega et al. (2017). The SIMS results including the instrumental setting, the raw and IMF-corrected δ^{18}O values, and the CL-images of the samples are included in the Electronic Supplementary Information. All the δ^{18}O values of this paper are relative to VSMOW.

SPATIAL DISTRIBUTION OF THE REDDENING

A process of granite reddening has resulted in both a pervasive coloration homogeneously distributed within the rock volume at some area and a more localised development of red to pinkish granite facies allied to the fracture network at other areas. The most typical and widespread type of alteration is a **fracture controlled reddening** with reddish/pinkish coloration restricted to narrow bands along fracture planes. The granodiorite of the Laski quarry and the aplogranite of the Szklarska Poręba Huta quarry are typical examples for this. The most intense alteration is a **pervasive and homogeneous reddening** with the entire rock impregnated by the reddish pigments, and fracture planes coated with dark red iron oxides. The Laski village section is typical of this pervasive reddened facies. The less intense alteration is a **red spotted facies** with pinkish spots distributed within non-reddened rock. The granite of Chwalisław valley outcrop is typical of this weakly altered facies.

In the Laski quarry the fractures are metre-spaced, cutting the rock into well-defined 0.5 to 1 m^3 blocks (Fig. 2a). The extent of fracture controlled reddening is closely related to the rank of the fracture, i.e. it is weak along minor fractures and more intense along major ones. The reddening penetrates the rock as deep as 1-10 cm. The coloration is most intense along fracture walls but fades further away from the fractures. There is also a direct relation between the frequency of the fractures and the intensity of coloration. In the SE part of the quarry, the most intensive reddened facies occur along a weakly defined metre-wide zone, characterized by particularly dense fracturing. Similarly, the porphyritic granodiorite exposed on Mt Kopciowa has fracture controlled reddening restricted to weak, narrow staining fronts, where its large K-feldspar phenocrysts are partly or entirely pink along the fractures.

In the Szklarska Poręba Huta quarry, the porphyritic granite is generally not reddened. However, the fine to medium-grained aplogranite exhibits a light pink reddening along steep N40° major and N135° related fractures, which penetrates the rock to a distance of 5-15 cm to 30-40 cm away from the fractures. Where fractures are sparse, the aplogranite is greenish in the center of the blocks (Fig. 2b) but in densely fractured ("chopping fractures") zones the rock is pervasively pink.

The Chwalisław valley granodiorite outcrop is a typical example of the red spotted facies (Fig. 2c). A weak fracture controlled pinkish coloration has developed in narrow zones along fractures but further away from the fracture planes there is a scatter of spots together with small pinkish patches in the non-reddened rock. There is no obvious direct relationship between lamprophyre dikes and the reddening of the granodiorite. In fact the lamprophyre also has a faint pinkish coloration along the fracture planes, but their observance is hindered by the dark color of the rock.

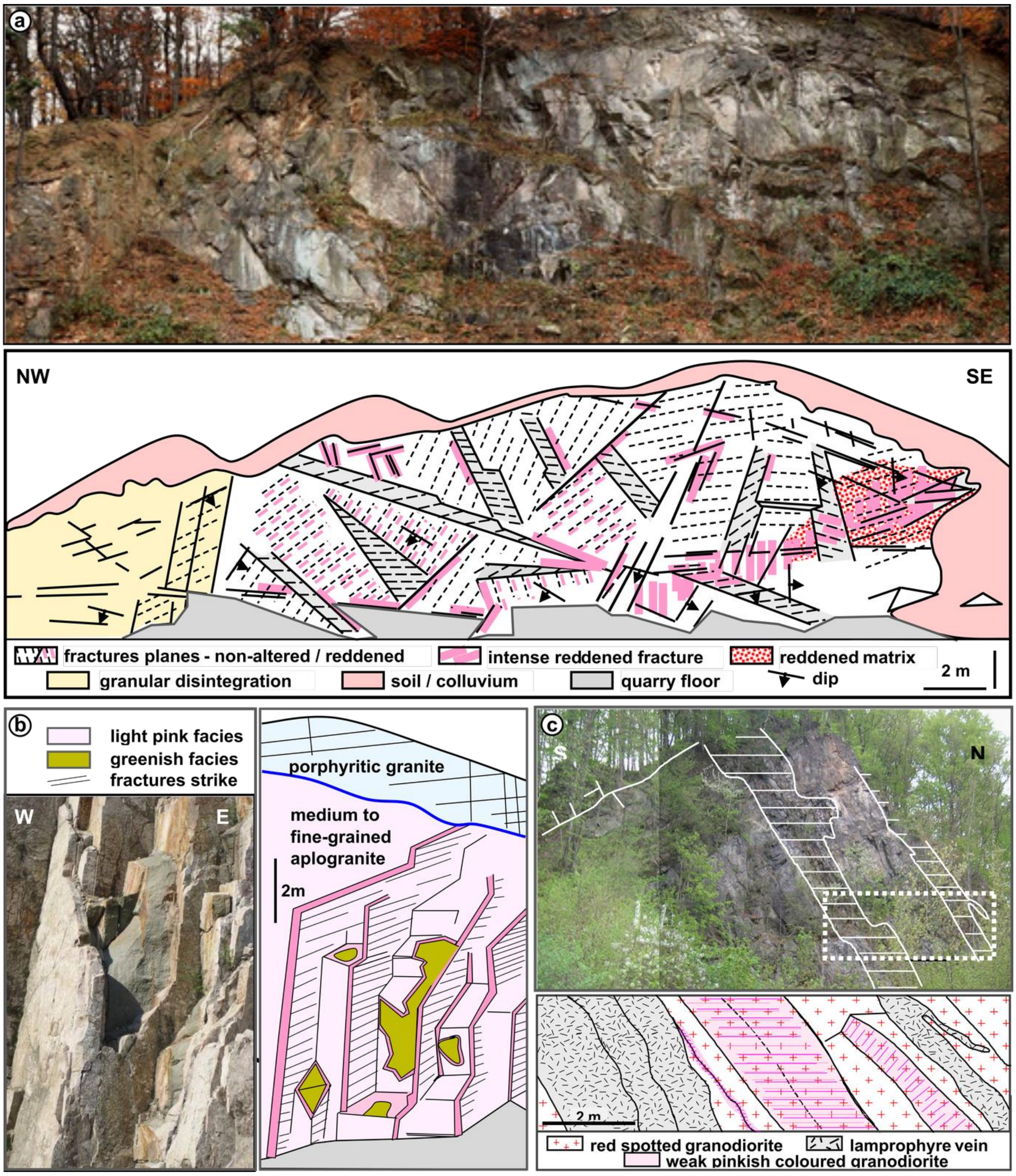

Fig. 2 Spatial arrangement of the reddening. (a) Photo and sketch of the fracture-controlled reddening in the Laski quarry. The highly fractured zones in the SE of the quarry are the most reddened. (b) Szklarska Poręba Huta quarry facies. The reddening proceeds along the steep fractures that cut the fine-grained aplogranite. (c) Sketch of the reddish alteration facies in the Chwalisław valley outcrop. The alteration is parallel to the lamprophyre veins that intruded the granodiorite

MICROSCOPIC ASPECTS OF REDDENING

Optical and cathodoluminescence petrography reveal some systematic differences between the non-reddened and reddened rock facies. We present petrographical comparison of the affected mineralogical constituents, but thoses that are neither affected by nor related to the staining phenomenon are omitted from the comparison.

Plagioclase

In non-reddened granites plagioclase appears white to the naked eye. Large crystals are often normal-zoned with Ca-enriched cores and Ca-poor margins: some crystals are also rimmed with nearly pure albite. Polysynthetic twinning is common. It also occurs as inclusions in the K-feldspar phenocrysts (in porphyritic rock types) and constitutes most of the rock groundmass. The luminescence is typical for igneous plagioclase with yellow-green CL (Fig. 3a and 3b), that turns blue in the albitic rims. Regions with increased intensity of yellow-green CL correlates with a higher Ca content (cf. Słaby et al. 2002; Słaby and Götze 2004). Partial sericitization of primary plagioclase is often observed, especially in the Ca-enriched cores.

In reddened granites plagioclase appears pink to the naked eyes, due to hematite pigments which confer a red cloudiness to spots where primary plagioclase has been thoroughly altered to secondary untwined albite (i.e. albitization). While the hematite-free domains retain their primary CL characteristics, the pigmented plagioclase is non-luminescent (Fig. 3a and 3b), which is typical of neogenic feldspars formed at low temperatures (e.g. Marshall 1988; Götze et al. 2000; Leichmann et al. 2003; Powolny et al. 2022). Contrasting CL conveniently mark out the geometrical relationship between primary plagioclase and secondary albite: Ca-enriched crystal cores may be albitized leaving the outer Na-enriched zones unaffected (Fig. 3a) or secondary albite may be associated with microcracks, twinning and/or cleavage planes (Fig. 3b).

Primary plagioclase compositions range from An_{26} to An_{84}, and An_{14} to An_{51}, in the Chwalisław biotite-hornblende granodiorite and Laski valley granodiorite, respectively (Table 1). The oxygen isotope composition of the primary plagioclase, determined in the biotite-hornblende granodiorite of Chwalisław, shows $\delta^{18}O$ values ranging from +3 to +7 ‰ (Fig. 3c and Table 2), with no aparent correlation with the composition of plagioclase determined by EPMA in the SIMS points, that ranges from An_{36} to An_{43}.

Secondary albite shows a widespread micro porosity and a typical composition about An_{0-2}, independently of the type of parent rock and of the primary plagioclase composition (Table 1). In crystals were the completeness of albitization has not been totally reached, a slightly higher Ca content was observed, with An% values ranging from 6 to 14% (Table 1). The oxygen isotope composition of the secondary albite, determined in the Chwalisław sector, is significantly heavier than the primary plagioclase, with $\delta^{18}O$ values ranging from +7 to 11‰ (Fig. 3d and Table 2).

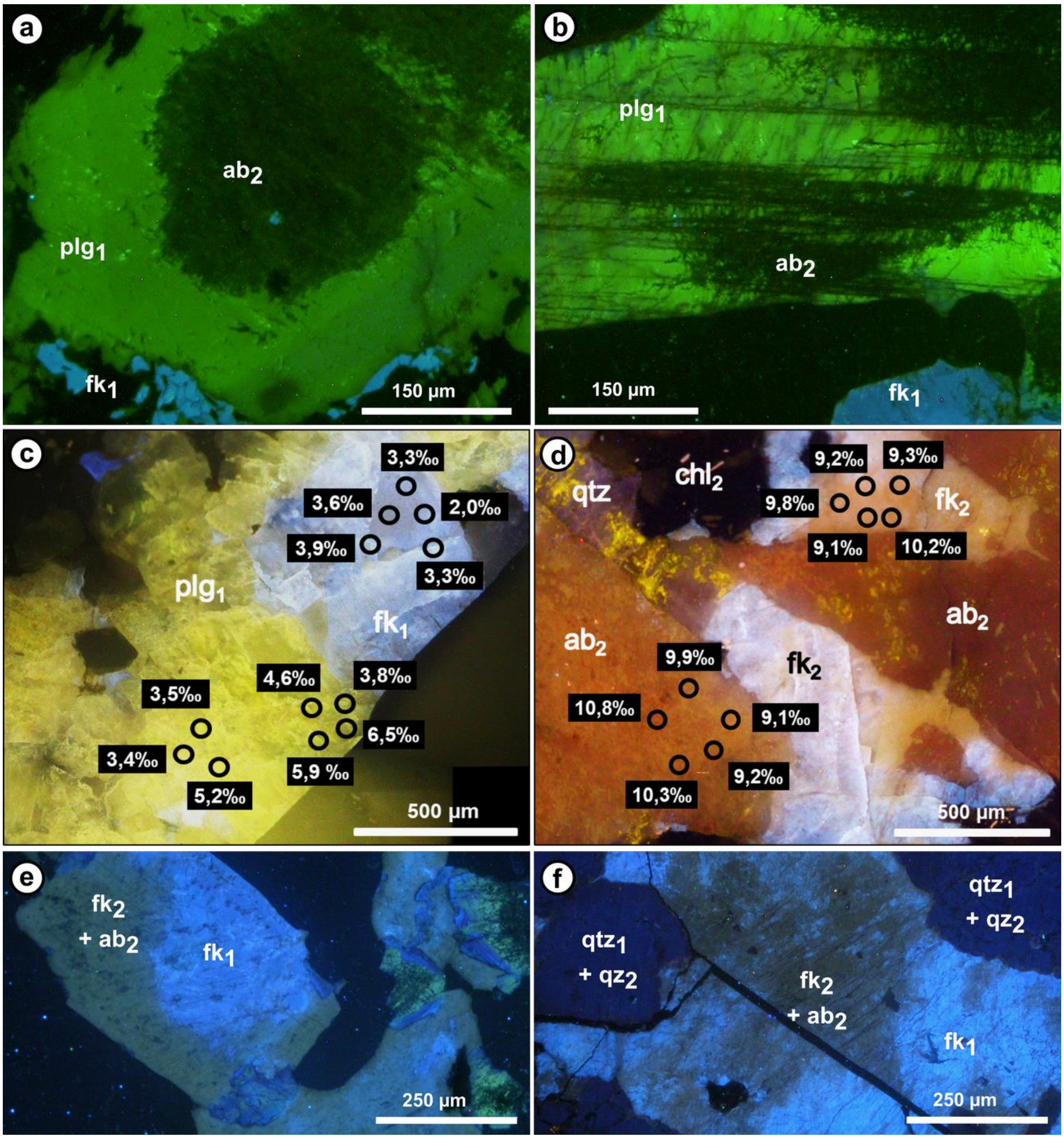

Fig. 3 CL Petrography and oxygen isotope composition of albitized plagioclase and K-feldspar. (a) Plagioclase with a non-luminescent albitized core and yellow luminescent rim. (b) Albitization along the major twinning planes and micro-fractures. (c) δ18O values of yellow luminescent primary plagioclase and blue luminescent primary K-feldspar and (d) non-luminescent secondary albite and turbid microclinized K-feldspar. (e) Cathodoluminescence images of partially albitized K-feldspar showing non-luminescent areas containing secondary microcline, patch perthites and quartz patches on the crystal rims. (f) Albitization of K-feldspar along microfractures. plg$_1$: primary plagioclase; ab$_2$: secondary stained albite; fK$_1$: primary K-feldspar; fK$_2$: secondary K-feldspar; qtz$_1$: primary quartz; qtz$_2$: secondary quartz

Table 1 Mole % of feldspar components of plagioclase and K-feldspar

site	rock	plagioclase		K-feldspar	
		primary / albitized	**An %**	**primary / microclinized**	**Or %**
Reddened facies					
Szklarska Poręba	porphyritic granite	primary albitized	1 - 3 0 - 3	microclinized	94 - 98
Laski Quarry	granodiorite	albitized	0 - 2	microclinized	95 - 98
Spotted facies					
Szklarska Poręba	porphyritic granite	primary albitized	8 - 14 4 - 6	partially microclinized	78 - 93
Laski Quarry	granodiorite	primary albitized	21 - 59 6 - 14	partially microclinized	79 - 92
Fresh rock					
Laski Valley	granodiorite	primary	14 - 51	primary	85 - 91
Chwalislaw Valley	hornblende-biotite granodiorite	primary	26 - 84	primary	72 - 93

* EPMA analyses converted to mole percent of the feldspar components by normalizing to eight oxygen atoms per formula unit.

Table 2 $\delta^{18}O$ ‰ results of plagioclase and K-feldspar

site	rock	plagioclase		K-feldspar	$\delta^{18}O$ ‰
		primary / albitized	**$\delta^{18}O$ ‰**	**primary / microclinized**	
Reddened facies					
Chwalislaw Valley	hornblende-biotite granodiorite	albitized	6 - 11	microclinized	5 - 11
Fresh rock					
Chwalislaw Valley	hornblende-biotite granodiorite	primary	3 - 7	primary	2 - 4

Apart from hematite pigments, neogenic albite is sometimes associated with calcite and prehnite. Secondary albite is not twinned - its development erased the polysynthetic twinning in the primary plagioclase. This is in contrast to "classical" saussuritization in which the petrographic features of the primary plagioclase are preserved, at least partially (de la Roche 1957; Sandström et al. 2010; Jenkin et al. 1992; Morad et al. 2010).

K-feldspar

In non-reddened granites, K-feldspar is white to grey and often Carlsbad-twinned with varying amounts of microperthitic albite. In the porphyritic granitoids it is present as large (several centimeters) phenocrysts and as a constituent of the groundmass (<< 1 cm). Cross-hatch twinning is not a common feature but, if present, is developed in domains rather than whole crystals.

As observed using CL, any alteration of primary crystals is manifested by a change in the blue luminescence typical of igneous K-feldspar (cf. Słaby et al. 2002; Słaby and Götze 2004; Powolny et al. 2022). The hematite-stained parts of K-feldspar crystals correspond to regions of quenched, sometimes dark-brownish luminescence, similar to the previously shown secondary albite (Fig. 3e and 3f). Such CL characteristics match secondary feldspars formed in low-temperature diagenetic and supergenic environments (e.g. Götze et al. 1999; González-Acebrón et al. 2010; González-Acebrón et al. 2012).

There is a clear relationship between hematite staining and albitization of K-feldspar. Semi-quantitative measurements of the intensity of XRD reflections from the two feldspar species reveal that a low and rather constant albite content in K-feldspar phenocrysts in non-reddened granitoids increases and becomes highly variable in the reddened facies (Yao 2013). Primary light-colored K-feldspar phenocrysts are predominantly formed of orthoclase but an increase in albite content is generally marked by its transformation (recrystallization) to microcline, as indicated by an increasing triclinicity. Since triclinicity reflects the state of Al-Si ordering of K-feldspar structure it is likely that the increase of Al-Si ordering, albitization and hematite-staining of the K-feldspar are interrelated processes.

The composition of the primary K-feldspar ranged from Or_{72} to Or_{93} in the the Chwalisław sector and from Or_{85} to Or_{91} in the Laski valley (Table 1). The oxygen isotope composition of the primary K-feldspar (Table 2), determined in crystals from the biotite-hornblende granodiorite of Chwalislaw valley, present $\delta^{18}O$ values ranging from +2 to +4 ‰. The $\delta^{18}O$ values show a positive trend versus the increase in K^+ content of the K-feldspar (see Electronic Supplementary Information). In the quenched luminescence regions, the primary orthoclase is replaced by secondary microcline showing aboundant micro porosity, with typical composition varying from Or_{94} to Or_{98}, indepentdently of the parent rock and the composition of the primary K-feldspar. The microclinization process is accompanied by the development of patch perthites of highly pure albite, with typical composition of An_0. The oxygen isotope composition of the microclinized K-feldspar (Table 2), also determined in the biotite-hornblende granodiorite of Chwalislaw, presents $\delta^{18}O$ values, ranging from +5 to +11 ‰ and also shows a positive trend versus the orthoclase content (0r %) of the K-feldspar.

Albitization propagation

Albitization of primary plagioclase occurred along microcracks and cleavage planes (Fig. 4a). The albitized zones are patchy and amoeboid, with no relation to the crystallographic directions in the primary plagioclase. Often albitization developed from the margins towards the central parts of a crystal, leaving the core as well as the primary albitic outer rim unaffected (Fig. 4b). A common albitization pattern is observed in some of the compositionally zoned plagioclases in which the Ca-enriched core has been altered but the Ca-poor rims remains unaffected (Fig. 4c). The albitized core often contains scattered sericite which corresponds to an earlier phenomenon than albitization as it is also observed in non-albitized plagioclase from the non reddened facies. In most altered facies, primary plagioclase is perversavely albitized exept outer rims composed of primary albite (Fig. 4d). These altered facies are intensely reddened and often show micro-fractures filled with iron oxides.

Albitization of primary K-feldspar proceeds in a similar way as in palgioclases: from the margins of the crystals along microcracks, twinning and/or cleavage planes. In the reddened granitoids, euhedral to sub-euhedral K-feldspar phenocrysts are partly or entirely pink (Fig. 4e and 4f). There is a direct correlation between the intensity of staining in the granitoids and the amount and distribution of hematite pigmenting phenocrysts and smaller K-feldspar crystals.

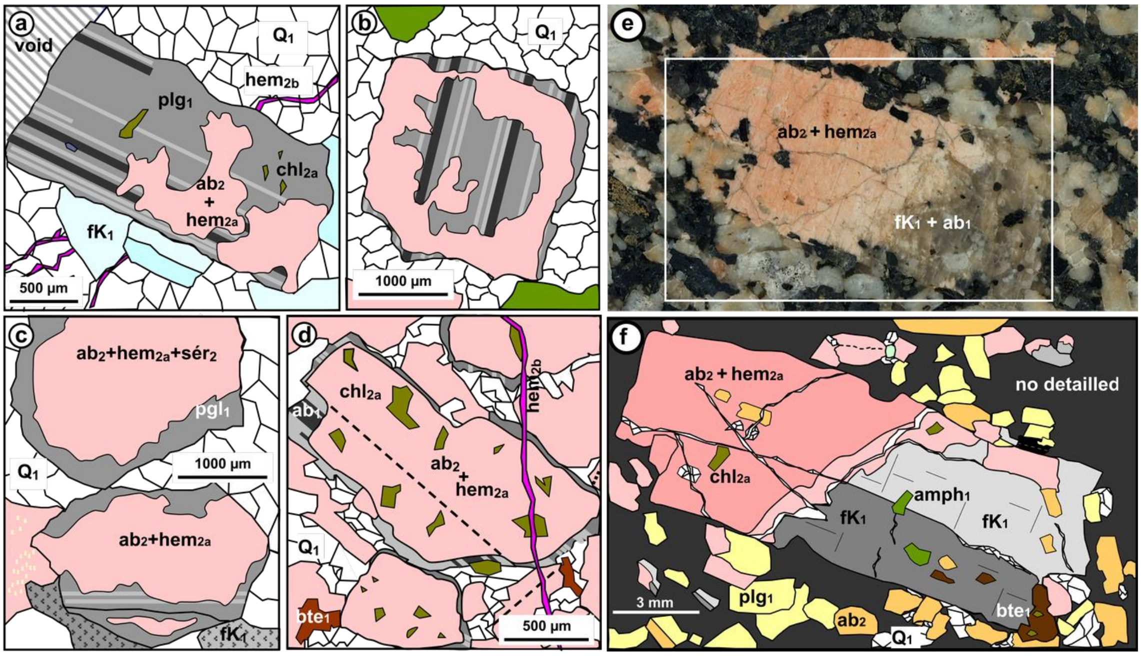

Fig. 4 Sketches of albitized red/pinkish plagioclase and K-feldspar. (a) Plagioclase albitization along microfractures. (b) Irregular albitization of the outer rim of the primary plagioclase: the primary albitic rim remains unaffected. (c) Albitization of the seritized core of the primary plagioclase. (d) Complete albitization of the primary plagioclase crystal except the outer rim which is composed of primary albite. (e) Polished section of a partially reddened orthoclase phenocryst. The upper part of the phenocryst is pink and dull whereas the lower part is translucent. (f) Sketch of (e). The orthoclase phenocryst exhibits classic Carlsbad twinning in the translucent part and has inclusions of hornblende, chlorite, biotite, and plagioclase. In the pinkish part the twinning is erased, and the orthoclase is albitized and hematized. fK_1: primary K-feldspar; plg_1: primary plagioclase; Q_1: primary quartz; bte_1: biotite; amph1: amphibole; ab_2: untwined secondary albite; chl_{2a}: secondary chlorite after biotite; hem_{2a}: pigmentary hematite; hem_{2b}: coarser-crystalline hematite

Fe-Mg minerals

Light to dark brown biotite is the main mafic mineral and minor greenish hornblende is commonly present in samples from the Kłodzko - Złoty Stok massif. In non-reddened samples both biotite and hornblende show signs of chloritization, though hornblende appears more resistant to this alteration.

Chloritization is significantly more intensive in the reddened granitoids where all stages of the replacement process, from initial weak alteration along the edges and cleavage planes of the primary crystals to the formation of complete chlorite pseudomorphs, could be observed. Biotite inclusions in hematite-stained plagioclase are invariably replaced by chlorite. There is no clear evidence for a volume change during the chloritization of the primary Fe-Mg minerals. Secondary microcrystalline and flaky chlorite also occurs in microfractures and intergranular boundaries. Pyrite, Ti-oxides and titanite are often associated with secondary chlorite.

Fe-minerals

Fe-sulphides and oxides in the granitoids include pyrite, hematite, maghemite, and magnetite. Pyrite occurs irrespective of hematite pigmentation as relatively large (50-200 µm) euhedral crystals and lens-shaped aggregates in the cleavages of chloritized biotite and hornblende. Late anhedral grains fill also microfractures. The margins of most of the observed pyrite grains are replaced by hematite.

Pigmentary hematite is responsible for red cloudiness observed in plagioclase from the reddened granitoïd facies under microscope. In the red spotted facies plagioclase exhibits coexisting hematite-pigmented and hematite-free domains which are primary igneous plagioclase (Fig. 5a) and in pervasively reddened facies and in fracture controlled reddened facies the plagioclase is entirely hematite-stained (Fig. 5b). Dusty hematitic pigment is confined to albitized domains in plagioclase and K-feldspar. Some observations suggest that the hematitic pigments are not directly related to microporosity in the altered feldspars. Firstly, the pigment is absent from the porous saussuritized feldspars of the non-reddened granitoid facies. Secondly, it is not concentrated along the albitization front which is enriched in micropores that relate to the volume-loss replacement of the primary feldspar by secondary albite. Instead, hematite is distributed more or less homogeneously through all of the albitized feldspar. Microscopic flaky aggregates and subhedral larger grains of hematite are often observed in intergranular boundaries located close to chloritized biotite and hornblende (Fig. 5b) and in microfractures (Fig. 5c) and, as well as in the cleavage of some chloritized biotite (Fig. 5e), sometimes together with secondary quartz and/or calcite.

Maghemite and magnetite could not be recognized unequivocally under the microscope nor by XRD analyses but their presence was unmistakably detected by thermal demagnetization experiments (paleomagnetic experiments, this study). In contrast to hematite, magnetite is restricted to the non-reddened facies. Maghemite, on the other hand, was detected mainly in the weakly reddened facies. Thus, maghemite may be regarded as a 'transitional' Fe-mineral between the magnetite-dominated non reddened granitoids and hematite-dominated reddened facies.

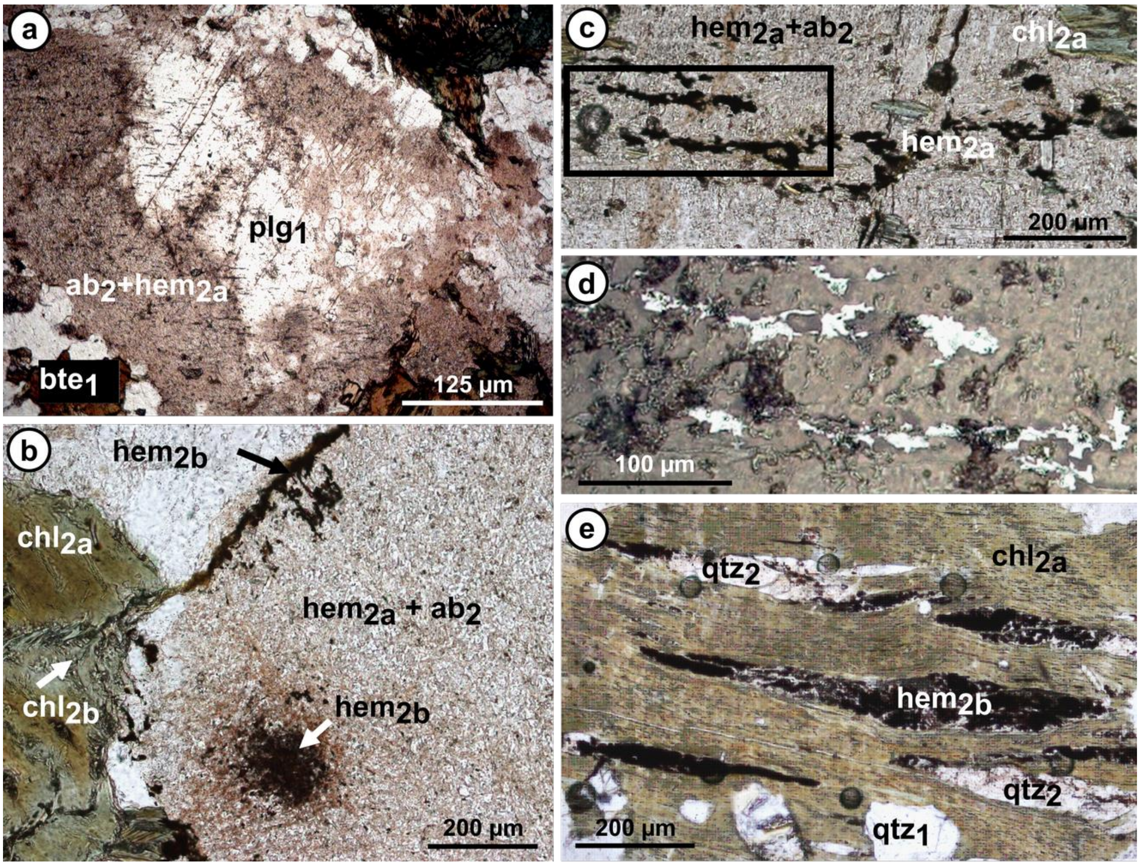

Fig. 5 Hematite occurrences within albitized granitoids. a) Light pink albitized plagioclase away from reddened fracture walls with light colored relict of primary plagioclase. (b) Plagioclase entirely reddened and albitized from pervasively reddened facies; hematite appears as pigments within the secondary albite and as granules within microfractures. (c) Fine red hematite pigments and elongated hematite flakes within secondary

albite; plane polarized. (d) Enlargement of (c); reflected light. (e) Hematite lenses within the cleavage of a chloritized biotite crystal, notice lenses of secondary quartz in similar position; plane polarized. plg_1: primary plagioclase; ab_2: secondary albite; bte_1: primary biotite; chl_{2a}: secondary chlorite after biotite; chl_{2b}: neogenic chlorite in micro-fracture; hem_{2a}: secondary hematite pigment; hem_{2b}: secondary granular and flaky subhedral hematite

Other minerals

Quartz of the non-reddened facies is essentially unaltered, presenting a homogeneous dull-luminescence. Differently, the quartz grains of the reddened facies are significantly altered, presenting a network of micron sized non-luminescent veins of secondary quartz displaying in a cobweb texture. Internal zoning of quartz have already been described in the chloritized facies of the Sudetic Karkonosze granite (Wilamowski 2002), and similar quartz alteration has been observed in the red albitized facies of NE Spain (Fàbrega et al. 2019).

Sericite is more abundant in non-reddened samples and in weakly-reddened rock away from fractures. It occurs mostly in plagioclase and emphasizes the compositional zoning as it has preferentially developed in the Ca-enriched plagioclase cores but is entirely absent from the albitic rims. Sericitization obliterates the primary polysynthetic twinning in the plagioclase host. Tiny sericite crystals (5 µm) occur in plagioclase in the aplogranite of Szklarska Poręba Huta and less fractured granodiorites of the Kłodzko – Złoty Stok massif. This form of sericite is associated with secondary albite but not with Ca-bearing minerals such as prehnite and epidote. However, larger sericite flakes (10-20 µm) formed at the expense of Ca-enriched plagioclase in the reddened granodiorite from Chwalisław and Laski are associated with secondary prehnite, albite, and sometimes also calcite. Sericite is rare in K-feldspars.

Prehnite and less commonly calcite are either present as secondary minerals associated with saussuritization of plagioclase and chloritization of Fe-Mg minerals or as late primary phases healing fractures. While calcite is observed exclusively in the reddened rock facies, disseminated prehnite is more abundant in the non-reddened granitoids. Secondary prehnite, apart from prehnite-sericite-albite aggregates in the saussuritized Ca-enriched plagioclase cores, occurs also as monomineralic fan- and bowtie-shaped aggregates in intergranular boundaries and as elongated lenses in biotite. The latter are concordant with cleavage and the inflation of the lenses disturbs the parallel alignment of the mica flakes. They are observed only in partially chloritized biotite in the non-reddened granitoids but are absent in the proximity of reddened fracture walls. Similar lenses of secondary calcite are present in chloritized biotite and hornblende in the reddened rock facies. Both prehnite and calcite, sometimes accompanied by laumontite, are also observed as late primary minerals healing microfractures cutting across the mineral framework of the reddened granitoids.

Magmatic apatite is commonly present as small inclusions in biotite and hornblende or as inherited inclusions in their chlorite pseudomorphs. Nonetheless, in some chlorite pseudomorphs, we also observe apatite inclusions that were considerably larger and at the same time less abundant than typical apatite inclusions in unaltered primary Fe-Mg minerals. They are likely a second generation of apatite resulting from recrystallization and also dissolution of smaller crystals during chloritization, such as those shown in the albitized facies in the Morvan (Parcerisa et al., 2009) and in NE Spain (Fàbrega et al.,2019) and those linked to low-temperature spilitic albitization in the Intra-Sudetic Basin (Powolny et al. 2022).

REE-bearing minerals, mostly epidote and monazite, are typically subhedral to euhedral crystals around 50-200 µm in size, in the non-reddened. The REE-rich epidote is more abundant in the reddened facies than in the unaltered rocks and occurs as larger grains up to 200-400 µm. Monazite in the reddened facies occurs in two different forms depending on its position with respect to the reaction front. The crystals in a cm-scale zone inside the reddish/pinkish facies in contact with the albitization reaction front are mostly pseudomorphed by secondary monazite. This secondary monazite has corroded grain boundaries and micron-sized porosity, suggesting that the replacement occurs via a dissolution-reprecipitation process. In contrast, in strongly reddened rocks, monazite grains can be pseudomorphed by secondary apatite.

Summary of petrographic observations

Petrographic analyses of the reddened and non-reddened granitoids provide a basis for discerning major differences in the mineralogical composition of the two granitoid facies. Apart from hematite, which is responsible for the red pigmentation, and quartz, the content of which is fairly constant, the relative abundances of major and some minor constituents vary with increasing reddening (Fig 6). In particular, the amount of Ca-enriched plagioclase decreases largely at the expense of secondary albite and is practically undetectable in the most intensely reddened sample. While plagioclase in the non-reddened rocks is partially sericitized, the plagioclase in the reddened facies is predominantly albitized. To some extent K-feldspar follows the same pattern, with albitization and microclinization of primary K-feldspar in the reddened facies. Weak chloritization of biotite and amphibole is observed already in the non-reddened granitoids but the process is dramatically more intense with increasing reddening and leads to a complete disappearance of the primary Fe-Mg minerals in the most reddened facies. Chloritization of biotite, in particular where the alteration is intense, is often coupled with the formation of secondary titanite and Fe-minerals along cleavage planes and microfractures. Similarly, chloritized amphibole often contains calcite along cleavages, indicating the removal of Ca from the chloritized crystal.

Small amounts of prehnite occur in the unpigmented granitoids but it becomes more abundant with reddening. However, its presence also depends on the initial rock type as it is absent from the aplogranite of Szklarska Poręba Huta and the granodiorite of Laski village, irrespective of the extent of staining. The sericite content seems to be unaffected by reddening. Dispersed calcite and laumontite are detected exclusively in the reddened facies, though they are present as late fracture fillings in both stained and unstained granitoids.

The presence of hematite pigments in feldspars is directly related to albitized domains. For instance, we have not observed albitized plagioclase that is hematite-free. Also, hematite pigments in K-feldspars were not observed in non-albitized regions. The crystallization of hematite pigments seems to be synchronous with albitization. If hematite formed later in micropores within secondary albite, it is expected that the migration of the hematitizing fluids followed some pathways. No such possible pathways were observed. Thus, assuming that hematite and secondary albite are contemporaneous, the albitization must have taken place under oxidizing conditions. Furthermore, secondary minerals related to albitization near the fractures are stained with iron oxides whereas secondary saussuritization minerals, corresponding to albite-sericite-prehnite aggregates, are not affected by the reddening. Albitization-saussuritization alterations grade progressively from fractures inwards into the fracture blocks; they do not overlap or cut across each other as expected if they were distinct unrelated alteration stages.

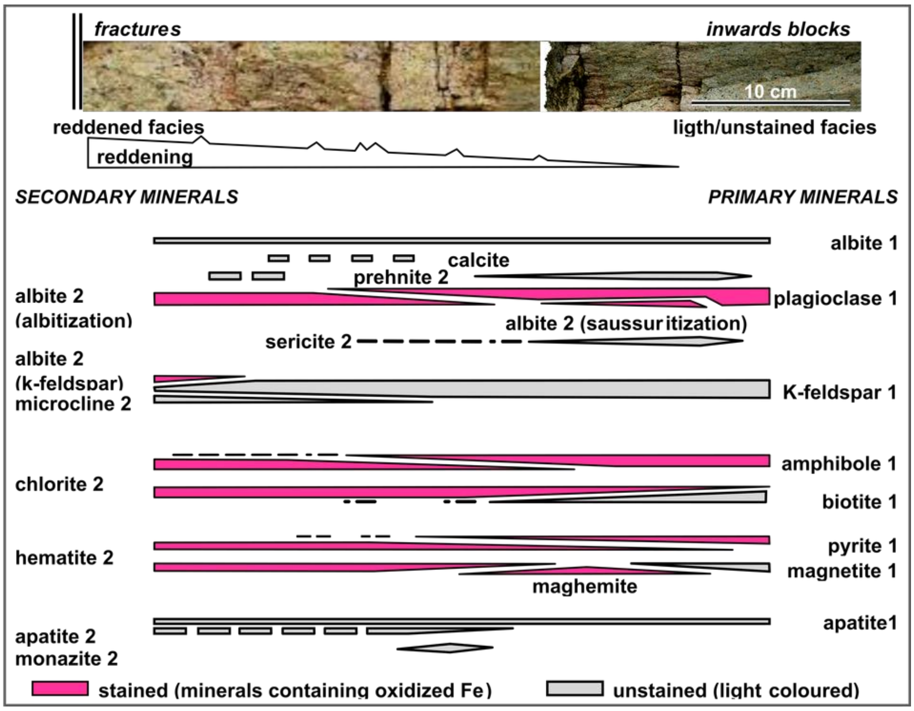

Fig. 6 Spatial distribution of mineral parageneses in relation to marginal fractures and core of granitoid fracture blocks

AGE DATING AND GEODYNAMICS

Dating of the albitization provides a clear tool for determining if it could be related to deep, high-temperature metasomatic processes linked to granite cooling or alternatively a product of weathering on uplift and exposure of the granitoid mass. We compared the results of two independent methods of dating: on one hand paleomagnetic dating of iron minerals and on the other hand U-Th-Pb_{total} radiochronology of monazite, a phosphate able to incorporate high U and Th concentrations.

Monazite dating

The Szklarska Poręba Huta quarry section provided only one sample containing mainly unaltered monazite. Deconvolution of the monazite U-Th-Pb_{total} ages histogram (Fig. 7a) provides an average age of 314 ± 56 Ma (2σ). Although we cannot discard the possibility that some of these points could represent a mix of primary and secondary mineral ages. The Chwalisław valley section provided two samples containing numerous monazite grains for U-Th-Pb_{total} radiochronology. The deconvolution of the monazite U-Th-Pb_{total} ages histogram (Fig. 7b) yields two distinct age peaks, one at 254 ± 24 Ma (2σ) and a second at 321 ± 8 Ma (2σ) with a relative misfit of 0.988.

The textural analyses of samples from the Chwalisław valley section show that the older ages occur in well preserved grains from the non-reddened facies as well as in primary domains preserved within altered grains of the slightltly reddened/pinkish facies. On the other hand, the younger ages (centered around 254 Ma) are almost observed in the monazite grains with dissolution-reprecipitation features in the reddish/pinkish facies close to the reaction front (Fig. 7d and 7e). The resseting of the monazite geochronometer is accompanied with compositional changes, including an increase in the Huttonite component [Th,Si(PO_4)], Fe and Al, and a loss of REE+Y (Fig. 7c). These compositional changes in relationship with younger ages, and the systematic occurrence of the younger ages in the more altered monazite grains close to the reaction front strongly support that primary monazite in the reddish/pinkish albitized facies were variably recrystallized at about 254 Ma. The broad distribution observed in the 254

Ma peak relative to the 321 Ma peak is caused by less younger age data (in comparison with older age data).

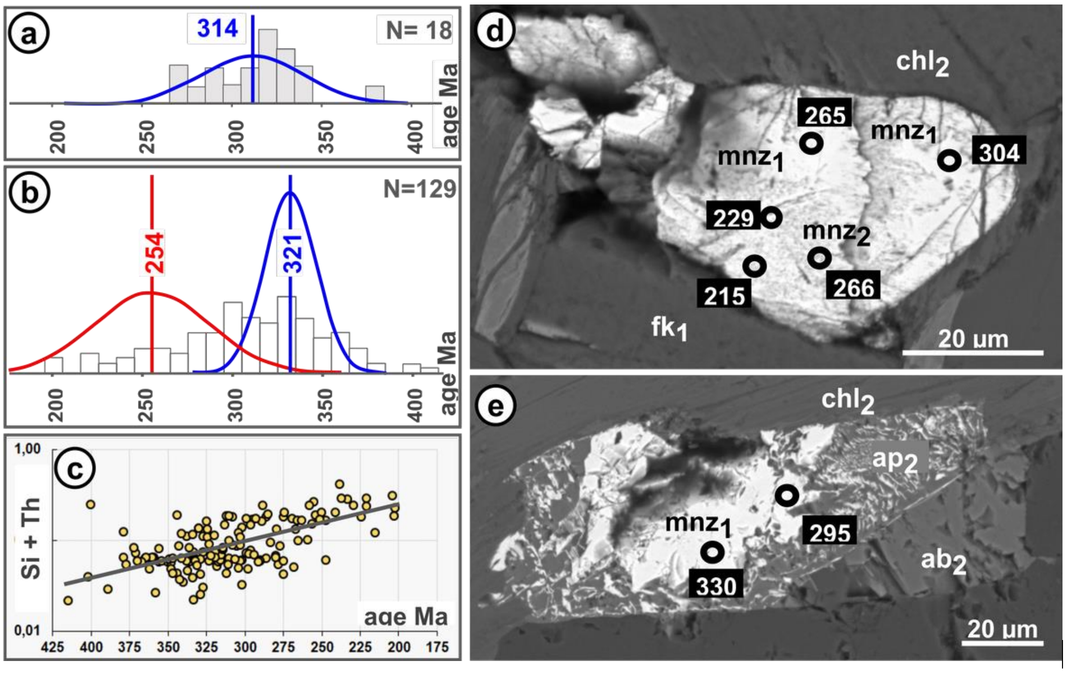

Fig. 7 Dating of monazite. (a) Mean age obtained from the histogram of ages of samples from the Szklarska Poręba Huta quarry, sample WL 006. (b) Deconvolution ages obtained from the histogram of ages of samples from the Chwalisław valley section, samples WL 018 and WL 018a. (c) Single U-Th-Pb$_{total}$ age of a monazite grain in the pinkish facies near the albitization front showing primary monazite (clear patches) partially replaced by microporous secondary monazite, BSE image. (d) Single U-Th-Pb$_{total}$ age of a monazite grain in the strongly reddened rocks partially replaced by secondary apatite, BSE image. mnz_1: primary monazite; mnz_2: secondary monazite; ap_2: secondary apatite; ch_2: chloritized biotite; fk_1: primary K-feldspar, ab_2: secondary albite

Paleomagnetic dating

Albitization and reddening caused by the presence of hematite, are shown to be closely associated as they reveal no spatial discrepancy at outcrop or microscope scale. We thus consider albitization and hematization to be cogenetic. The dating of the hematite formation is possible by dating the paleomagnetic secondary remagnetization signal. This would then allow to date the albitization event.

The different components of the paleomagnetic signal recorded within the analyzed oriented samples have been separated by stepwise thermal demagnetization experiments and are related to their specific magnetic carriers (see also supplementary material 2). According to the respective temperature interval at which a specific decay in the magnetic intensity curve was observed, one or a sucession of several magnetic carriers were identified in the sample. In principle, thermomagnetic and microscopic analysis showed three different types of magnetic mineral assemblages were observed within the analyzed samples: (1) hematite dominated in pervasive reddened facies and in fracture controlled reddened facies; (2) coexisting hematite-maghemite mostly in fracture controlled reddened facies further away from the fractures; and (3) maghemite dominated mainly in spotted facies.

In addition, maghemite-bearing mineral assemblages sometimes register residual, presumably primary magnetite. This was mainly observed in samples distant from fracture zones and in the less reddened spotted facies. As well, a weak contribution of goethite was sometimes observed which was demagnetized after application the 120°C demagnetization step. Goethite is considered as negligible component compared to the other magnetic carrier minerals and is most likely linked to a weak recent overprint by surface weathering of the outcropping rock sections.

The stepwise thermal demagnetization allowed us to obtain the vector directions recorded by the magnetic carrier minerals at the moment of their formation. These directions were considered to be characteristic for either the maghemite or hematite components, or both, if their inclination and declination values were stable according to the respective considered temperature intervals. It is thus possible to sometimes extract two slightly different directional intervals from one single sample if the two main carriers diverge in their mean direction. The results were 'sub-grouped' according to their directional information.

The extracted directional information was then transformed into magnetic paleopoles (e.g. Butler 1998) that were subsequently projected onto the apparent polar wander path (APWP) reference curve for Eurasia

(Edel and Duringer 1997; Besse and Courtillot 2003). In total 275 individual samples were analyzed for the calculation of the mean paleopoles carried by hematite or hematite-maghemite.

The severe rejection criteria for paleomagnetic samples in our dataset are mainly due to high error defined by values of α 95 (Kirschvink 1980; Fisher et al. 1987). Additionally, we eleminated samples that did not show any linear segments of the demagnetization vector on a Zijderveld diagram or a clear stable endpoint near the origin of a Zijderveld plot, as described by McFadden and McElhinny (1988). The resulting 18 averaged paleopoles all show acceptable α 95 values (< 15) according to the recommendations of e.g. Fisher et al. (1987) and very often plot directly on or close to the Apparent Polar Wander Path (APWP; Table 3). Six paleopoles were calculated for one or two directions only. For these paleopoles the mean angle deviation (MAD) values are given instead. All poles were listed in the Table 3. The paleomagnetic data set also includes additional paleopoles that correspond to the primary Devonian magnetization of the granitoid rocks, carried by primary magnetite (not shown here).

Table 3 Results from paleomagnetic data analyses, corresponding to the averaged site-wise paleopoles plotted in Fig. 8. MAD = mean angle deviation; TH = thermal demagnetization; AF = alternating field demagnetization; mgt = magnetite; mhm = maghemite; hm = hematite; goe = goethite; LC = low coercivity compounds; HC = high coercivity compounds.

paleo-poles	**site outcrop**	**age**	**Nb of samples**	**α 95**	**MAD**	**type of analysis**	**pole latitude**	**pole longitude**	**magnetic carriers**
1	Sklaska Poreba	Late Carboniferous	3	8.9		TH	20	125	mgt, mhm, hm
2	Chwalisław	Late Carboniferous	2		10.1	AF	23	126	LC+HC
3	Laski quarry	Late Carboniferous	3	8.7		TH	27	141	mgt, mhm, hm
4	Laski quarry	Middle Permian	4	8.7		TH	41	182	mhm, hm
5	Laski quarry	Late Permian	2		6.7	TH	53	161	goe*, hm
6	Laski village	Late Permian	1		3.8	TH	55	170	hm
7	Sklaska Poreba	Late Permian	3	10.1		TH	47	157	mhm
8	Laski quarry	Late Triassic	4	5.1		AF	54	127	LC+HC
9	Laski quarry	Triassic/Jurassic	2		7.7	AF	51	107	HC
10	Chwalisław	Triassic/Jurassic	3	3.3		AF + TH	49	118	mhm
11	Chwalisław	Triassic/Jurassic	3	7.3		TH	42	99	mhm, hm, goe*
12	Sklaska Poreba	Triassic/Jurassic	3	7.2		TH	36	104	mhm, hm
13	Laski quarry	Early Jurassic	4	9.1		TH	53	74	mhm
14	Chwalisław	Early Jurassic	8	5.9		TH	58	83	mhm, goe*
15	Laski quarry	Early Jurassic	2		6.6	AF + TH	73	93	mhm, hm
16	Sklaska Poreba	Early Jurassic	3	5.9		AF	74	67	LC+HC
17	Laski village	Middle Jurassic	6	5.0		TH	73	170	hm
18	Laski village	Middle Jurassic	1		10.4	TH	79	114	hm

Figure 08 shows the mean paleopoles for all four studied outcrops including Laski quarry, Laski village, Chwalisław valley, and Szklarska Poręba Huta. Four main groups of paleopoles and some ’isolated’ average paleopoles plot along the APWP curve for Eurasia

(1) Samples from paleopoles 1, 2, and 3 have a mixed magnetic assemblage which is dominated by primary magnetite. These represent the oldest group with Late Carboniferous ages (between 320 to 303 Ma) and are represented in all outcrops (with exception of Laski Village, that exhibits exclusivly pervasive reddened facies) whichpresumambly correspond to the primary age of the granitoid. All other paleopoles record secondary remagnetization ages.

(2) An ‘isolated’ average paleopole of Middle Permian age near the 270 Ma reference point from Laski quarry (paleopole 4).

(3) A cluster of Late Permian ages close to 258 Ma from the Szklarska Poręba Huta quarry, Laski quarry and the basal part of the Laski village section (paleopoles 5, 6, 7).

(4) A relatively ‘isolated’ average paleopole of Late Triassic age close to 225 Ma from Laski quarry (paleopole 8).

(5) A group of ages near Triassic/Jurassic boundary (arround 205 Ma) comprising four sets of paleopoles from the Laski quarry (paleopole 9), Chwalisław valley (paleopoles 10 and 11) and Szklarska Poręba Huta (paleopole 12) samples.

(6) A group of paleopoles of Middle Jurassic ages (between 175-165 Ma; paleopoles 17 and 18). This group is clearly different because it is solely carried by samples from the upper part of the Laski village section that is pervasively reddened/hematized. The intense remagnetization of these samples seems to have erased the primary magnetization carried by magnetite and the potential Permo-Triassic overprint. The lower part of the section still retains the Permo-Triassic signal.

(7) A group of Early Jurassic paleopoles (13, 14, 15, 16) plots between the 195 to 187 Ma reference point, but they show a significant S to SW offset from the APWP. Part of this directional offset may be due to the fact that these samples (from the Laski quarry, Chwalisław valley, and Szklarska Poręba Huta) may have been remagnetized successibly multiple times during the Permo-Triassic and later again during Early Jurassic times. If so, the hematite in these samples could carry a mixed cumulative age signal that is probably less well extractable than the initial remagnetization from primary magnetite to maghemite and/or hematite during the Permo-Triassic alteration phase.

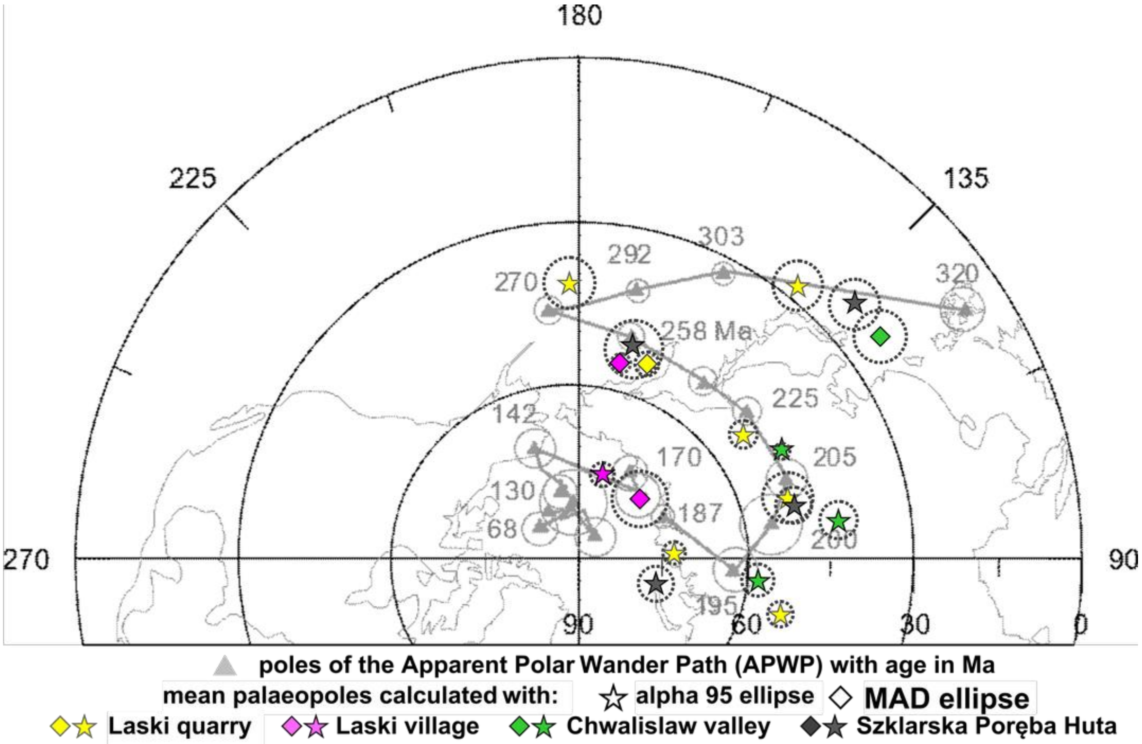

Fig. 8 Stereographic projection of the paleomagnetic results for the calculated average paleopoles for the study sites. The paleopoles are compared to the APWP for Eurasia (grey line) using the combined curve of Edel and Duringer (1997) from the Permian to Middle Jurassic (grey circles) and Besse and Courtillot (2003) from the Middle Jurassic until present (grey triangles). Star symbols represent mean poles with their respective α 95 confidence circle, diamond symbols are paleopoles with their respective MAD confidence circle, corresponding to Table 3

In our petrographic studies magnetite was solely found in the non-reddened facies whereas the magnetite detected by thermal demagnetization in samples of the weakly reddened facies probably relates to residual tiny crystals included in quartz. Maghemite is mainly detected in the weakly to intermediately pigmented facies distant from the reddened fractures at Laski and Szklarska Poręba Huta and in red spotted facies from Chwalisław valley. According to the literature, maghemite is metastable with respect to hematite and is considered to have formed by the slow oxidation of magnetite under weak oxidative conditions (Steinthorsson and Helgason 1992; Bowles et al. 2011). Hematite is dominant in the pervasively reddened facies in the Laski village section and is indicative of strong oxidative environments.

A chronology appears between the different magnetic facies of alteration. The less reddened spotted facies which is mainly dominated by maghemite carries the oldest remagnetization ages while the pervasively reddened and albitized facies shows the youngest ages. In the mean time, incipient reddening and albitization appears as the less intensely altered facies and conversely the pervasively reddened and even pervasively albitized without primary plagioclase and K-feldspar relict appears as the most intensely altered facies. This conjonction and the fracture controled reddening that diminish obvioully from most intensely altered facies towards the less altered spotted facies led us to consider that these various gradiens agree with a succession of facies from the base to the top of the alteration profiles. This suggests also that, with time, the active alteration front progressively retreated upwards into shallower weathering horizons.

It is of particular note that the Late Permian U-Th-Pb_{total} age at 254 ± 24 Ma obtained for secondary monazites in samples from the Chwalisław valley section corresponds to the paleomagnetic poles 10, 11, and 14 near 258 Ma on the Eurasian APWP (Fig. 8). These paleomagnetic poles, were obtained for weakly pigmented facies from Lasky quarry, Sklarska Proeba Huta, and Laski village, from samples taken further away from reddened fractures that contain significant amounts of maghemite. On one hand, maghemite developed in the early stages of albitization, under less oxidative conditions. On the other hand, secondary monazite formed in the immediate vicinity of the albitization front and was rapidly altered away from this front. The consistency in independed ages of the albitizing and oxidizing environments obtained from completely different secondary minerals and by means of distinctly different dating methods provide confidence in datation results. This does not contradict with the younger paleomagnetic ages obtained in this study for which we do not have access to separately datable minerals.

Links to other age determinations

The older age obtained for monazite from the Chwalisław valley section (321±8 Ma) is within the range of the previously published primary crystallization ages for the Kłodzko - Złoty Stok (KZS) Pluton between 349.0±3.7 Ma and 331.5±2.6 Ma (U-Pb, zircon; Jakubauskas et al. 2018 and references therein). The younger age (254±24 Ma) reflects growth of secondary monazite via dissolution-reprecipitation process. Similar Permian K-Ar ages between 256-268 Ma (K-Ar isochron age, 4 points: 261 Ma) were reported by Depciuch (1972) for KZS diorites from Mąkolno affected by chloritization/sericitization and interpreted as time of hydrothermal solutions activity. Unaltered samples representing main varieties of KZS igneous rocks provided significantly older K-Ar ages ranging from 291 to 303 Ma (K-Ar isochron age, 14 points: 295 Ma).

Our mean value of the monazite age (314 Ma) for Szklarska Poręba Huta aplogranite is consistent with high precision ID-TIMS U-Pb zircon ages 312.5 ± 0.3 Ma and 312.2 ± 0.3 Ma indicating crystallization of two main granite varieties (porphyritic and equigranular) of the Karkonosze Pluton (Kryza et al. 2014). Similar 40Ar/39Ar ages of 312 ± 4 Ma reported by Marheine et al. (2002) suggest fast cooling below closure temperature of the K-Ar system. It has to be mentionned, even if of poor quality, an age of 271 ± 20 Ma obtained on monazite from the same aplogranite at Szklarska Poręba Huta (Mikulski et al. 2004). This dating deserves to be linked to the 254 ± 24 Ma obtained on the secondary monazite of the Chwalisław valley section. The Karkonosze granite underwent fast uplift to the surface as evidenced by granitic detrital material in Upper Carboniferous sediments of the North Sudetic Basin (Milewicz 1968, Milewicz 1970).

Previous paleomagnetic dating aimed to determine the primary age of the emplacement of several Carboniferous plutonic units of the Polish Sudetes and led to the detection of Permo-Triassic (re)magnetizations (Edel et al. 1997). Even if the study did not plan to determine the age of the albitization, and even if sampling of the obviously altered (reddened) facies was avoided, re-magnetization events, younger than the age of the emplacement of the granitoïd, were present in some of the samples from the Chwalisław valley amphibolites in contact with the Kłodzko - Złoty Stok intrusion and in the~~ ~~Izera dolerite close to the the Szklarska Poręba Huta quarry (Edel et al. 1997). The authors identified paleomagnetic carriers of these Permo-Triassic paleopoles as hematite and maghemite, while the

Carboniferous paleopoles reported by Edel et al. (1997) are carried by (primary) magnetite. Further paleomagnetic studies on the Kłodzko Metamorphic Complex report on Triassic and Jurassic directions for similar magnetic mineral assemblages (Kądziałko-Hofmokl et al. 2003).

The Permian-Triassic age in the Kłodzko – Złoty Stok massif and the Szklarska Poręba area recurs systematically despite the different dating techniques. Thus, there is consistency between the results of paleomagnetic dating of the reddened/albitized facies in this study and other published age determinations on the various facies which were simply described as 'altered' but not clearly characterized as albitized.

Link to the Post-Variscan paleosurface

The Sudetic area, together with the southern part of the Germanic Basin of central Europe, is assed to have been emergent during Permian and Trias on the basis of stratigraphic and sedimentological evidence (Feist-Burkhardt et al. 2008; Głuszyński and Aleksandrowski 2022). At the same time, Permian and Triassic ZHe cooling ages reported by Danišik et al. (2010) and Sobczyk et al. (2015) are consistent with the idea of exposure of some parts of the Karkonosze granite during the Triassic (see also Migoń and Danišik 2012). Similarly, Carboniferous to Triassic ZHe data reported by Danišik et al. (2012) show that certain parts of the Kłodzko - Złoty Stok granitoid massif may have been close to the Earth surface during the Triassic (249.8 ± 20.0 – 209.4 ± 4.1 Ma) and reflect the record of progressive cooling through the zircon helium partial retention zone.

Results of zircon (U-Th)/He (ZHe) dating available for the Western Sudetes area revealed i.a. Triassic (248.2 ± 16.6 – 212 ± 14.2 Ma) cooling signals (Sobczyk et al. 2015). They have been interpreted as a record of bedrock slow exhumation or alternatively as an apparent ages due to zircon thermal system rejunevation, as a result of burial (see discussion in Sobczyk et al. 2020) or an advective heat flow under crustal extensional conditions (Botor et al. 2017). Noteworthy, ZHe datings for the Permian sandstones from the Fore-Sudetic Homocline (Sobczyk et al. 2013) provided a single Mid-Triassic cooling age (244 ± 5.0 Ma) within a Weissliegendes series, correlating with paleomagnetic datation which was interpreted, due to its clear post-depositional origin, as a probable age of Kupferschiefer mineralization. Therefore, low-temperature thermochronological data, even if not providing indisputable proof for the Post-Variscan paleosurface exposure during Trias, give some arguments for linking Triassic bedrock cooling with a regional crustal instabillity during the post-orogenic unroofing. Also the local sedimentological record for the Early Triassic lithofacies within the Intra-Sudetic and North Sudetic synclinoriums indicates channel flow and river bed depositionial environments (Kowalski 2020), suggesting the predominance of continental conditions for this period with local source areas located mainly in the Karkonosze-Izera Massif. Noteworthy, strongly kaolonized undisturbed Triassic (Buntsandstein) sandstones from the Sudetes are interpreted as a record of *in situ* chemical weathering profiles at the Triassic paleosurface (Kowalski 2020 and references therein). Finally, regional review studies indicate that during the Late Triassic to Early Cretaceous the Sudetes landforms were steaty sustained by the Post-Variscan paleosurface that formed a vast land mass undergoing slow erosion and denudation resuling i.a. in formation of deep weathering mantles, known also from central and northern Europe (Migoń and Lidmar-Bergström 2001). Powolny et al. (2022) advocated a late to post-magmatic low-temperature fluid-rock interactions controlling the process of albitization within the Permian trachyandesites from the Intra-Sudetic Basin. Based on apatite fission-track central ages obtained for three samples, these authors proposed a Jurassic (182 – 161 Ma) time interval for this thermal event. Closer inspection of apatites analyzed by Powolny et al. (2022) show that >50% of all dated grains revealed a Triassic cooling age, which indicates a possible two stage post-Variscan albitization in the Sudetes.

In the absence of any major Triassic magmatic event in the Sudetes and adjacent areas, we link the reddening alteration of the Kłodzko – Złoty Stok and of the Karkonosze granites, as well as their albitization, to a Post-Variscan/Pre-Triassic paleosurface, similar as described for the French Massif Central (e.g. Schmitt and Clement 1989; Parcerisa et al. 2009) and in NE Spain (Fàbrega et al. 2019). It follows then that the most pervasively reddened/albitized facies were formed near the paleosurface while at depth the granites were progressively less affected by the alteration process. It is of note that the conspicuous reddened and albitized fractures are never cut by any fractures that do not exhibit this alteration. Hence, we regard the lack of non-albitized fractures as evidence that the alteration is relatively recent and post-dates the exhumation of the granite bodies.

Moreover, the superficial origin of albitisation and reddening via weathering explains the spread of the paleomagnetic data along the APWP curve for 100 Ma from the Permian to the Jurassic. This distribution of palaeomagnetic ages is not the result of successive phases of alteration, but rather a single event that is heterogeneously recorded in the rock. It relates to the progression of weathering along fractures and even around kilometer sized massive rock volumes. But presumably there were times of more active and less active phases during this long period, mainly under the influence of climate and eustatic sea level changes, which could explain some clustering of paleomagnetic ages during distinct periods.

INTERPRETATION OF THE PARAGENESES

In general, our observations agree with earlier data on fracture related hydrothermal alterations with the development of albitization and saussuritization (e.g. De Jong and Williams 1995; Lee and Parsons 1997; Engvik et al. 2008; Plümper and Putnis 2009; Sandström et al. 2010; Morad et al. 2010; Powolny et al. 2022). The direct relationship of albitization and related alterations with the Post-Varisacan paleosurface completely changes the paleoenvironmental conditions that prevailed for these alterations compared to quoted studies that ascribe them a deep and relatively high temperature environment. Nevertheless, in the context of a direct relationship with the Post-Varisacan paleosurface, the alterations discussed in this study do not exhibit any typical regolith features, such as illuviation structures related to water percolation in vadose environments, bioturbation, or pallid or iron stained mottles. On the contrary, the isotropic structures around blocks evoke an aquifer environment and recall saprolite from the lower zones of regolith horizons corresponding to deep weathering of bedrock. The most astonishing characteristic is the alteration around the fracture blocks. This occurs without modification of the primary fabric of the rock and without any obvious development of porosity. However, the alteration developed systematically via a hierarchical net of fracturing from the macro-scale, demarking fracture blocks, to intergrain microcracks, giving to the albitization front at outcrop scale a dendritic aspect of fresh unaltered blocks surrounded by reddened fractures (Fig. 9a). Here we examine the geochemical grades, coupled dissolutions, precipitations and water-rock interactions in order to identify the nature of the fluids that triggered these alterations and ultimately the nature of the related paleoenvironment.

Fracture-bound geochemical grades

The alteration primarily and intensively affects the plagioclase and only to a lesser extent K-feldspar and ferromagnesian minerals (biotite and amphibole). The alteration of plagioclase is of three kinds (Fig. 9a and 16b).

1) Albitization of the primary feldspars is causally linked to proximity to the fractures. Some late Ca-bearing silicates may be associated with this alteration, but they rather fill in microcracks and their origin may not be directly related to the albitized plagioclases.

2) Saussuritization of the primary plagioclases accompanied by the development of Ca-bearing prehnite is typical of the non reddened and lightly reddened facies away from fractures. Secondary albite has developed along with saussuritization of the primary plagioclase.

3) Invasive development of sericite (sericitization) affects in places the primary plagioclases from the non reddened and lightly reddened facies and is associated with the formation of small neogenic albite but without any Ca-bearing silicates.

The alteration of ferromagnesian minerals is connected to the alteration of plagioclase. There is a progressive chloritization of biotite in the non reddened and lightly reddened facies as the fractures are approached. Chloritization seems to occur either under volume conservation or with a slight decrease of the volume of the biotite with secondary minerals such as quartz, K-feldspar, prehnite, and iron-bearing minerals embedded in the cleavage planes. The amphiboles appear to be less sensitive to chloritization than biotite, remaining practically unaltered in the unaltered and lightly reddened saussuritized facies.

These alterations result in a strong geochemical overprint between the core and the boundaries of the fracture-isolated blocks (Fig. 9c). The margins of the blocks are strongly Na-enriched due to albitization of plagioclase, and depleted in K due to chloritization of biotite and partial albitization of K-feldspar. The cores of the blocks are relatively enriched in K, Ca and Al compared to the albitized facies (taking into consideration the saussuritization of the plagioclases).

The secondary mineral parageneses, especially albitization and sausuritization, never exhibit an interruption or clear alteration front but appear rather as continuum, grading from one to another. There is no obvious temporal succession between the parageneses. By contrast, the parageneses are overlapping, with small sericites in the albitized/hematitized plagioclase crystal cores formed due to alteration of the plagioclase before albitization. The secondary parageneses appear more like an expression of the geochemical gradients between fluids circulating within the fractures and the massive granitoid blocks. Thus, the observed sequences of neogenic minerals result from the progressive encroachment of the reaction front towards the cores of the fracture blocks while their outer margins are gradually altered in equilibrium with the interstitial fluids. It is appropriate at this juncture to refer to metasomatic sequence or zonation rather than paragenesis involving successive or different alteration processes.

The albitization as well as the iron oxide pigmentation becomes less intense away from the walls of the fractures towards the inner parts of the fracture blocks. This gradient reflects a decreasing Na^+ and O_2 (and/or Fe) content of the fluids circulating in the intergranular crystal boundaries (Fig. 9d). In contrast, the K^+ and Ca^{++} content of the interstitial fluids would have decreased in the opposite direction: K-bearing minerals (K-feldspar, biotites) and Ca-bearing plagioclases were altered by leaching of K^+ and Ca^{++} at the fracture walls and sericite formed within the lightly reddened and unaltered facies progressively more distant from them.

Coupled dissolution-precipitation reactions

It is well known, plagioclase with a high An content is susceptible to preferential dissolution due to enhanced instability in the presence of water (Matthews and Goldsmith 1984; Stillings and Brandtley 1995). Thus, destabilization of plagioclase could be a trigger resulting in a chain of reactions in the altered granitoids.

Albitization of plagioclase proceeds at constant volume (with low porosity) given a Na-supply, additional silica, and with the release of Ca and some Al (Ramseyer et al. 1992; Parcerisa et al. 2009; Hövelmann et al. 2010). In the vicinity of the fractures, the released cations would have been leached and evacuated by the circulating fluids. As the reaction continued, fluid circulating in the rock by diffusion and convection would have become gradually depleted in Na, and albitization diminished and or even ceased at low Na-content (Fig. 9d).

Biotites are destabilized and transfromed into chlotite in the vicinity of the fractures, probably through a double effect of the leaching of the K interlayer cations and oxidation of the Fe2+ in octahedral sheets (Fig. 9e). Here leaching of $Si(OH)_4$ takes place because the cation/Si ratio is equal to ~1 within the biotite, whereas it is between 1 and 1,5 within the replacement chlorite. Detailled study of the Karkonosze granite's chloritization (Wilamowski 2002) showed that "The rate of potassium removal from biotite during the progress of chloritization is not constant. The rapid removal of K is observed at initial stages of chloritization. After the replacement of 20% of the biotite, K removal is much slower." The released silica could have nourished the albitization of the plagioclase. If the chloritization occurred without an additional cation supply, the volume loss would have been about 30%, whereas if additional cations were introduced (such as the Al released by plagioclase alteration) the volume loss may have been less substantial (Ferry 1979).

Amphiboles appear to be less "sensitive" to chloritization than the biotites, probably because their structure does not contain any unstable or mobile cations such as K^+. The destabilization of the amphiboles is most likely a result of leaching of Mg and perhaps oxidation of Fe^{2+}. It might be that amphiboles, and in particular hornblendes (which are calcic), are relatively protected against chloritization because of the Ca liberated by albitization of the plagioclase. For that reason the chloritization of amphiboles occurs only in the more intensively altered facies in which plagioclases are albitized and therefore no longer provide Ca^{++} to the fluids.

Hematitization is systematically associated with the albitization. Hematite occurs mainly as pigments within the neogenic albite or as coarser crystalline material associated with the ferromagnesian minerals. There is no iron oxide precipitation in the fractures, so the fluids circulating in the fractures appear unlikely to have been iron-bearing. Hematite has likely been nourished by the iron released by alteration of ferromagnesian minerals.

The formation of sericite depended mainly on the availability of K^+. Chloritization of biotite was the quasi-exclusive source of K in the system because albitization of K-feldspar was not pervasive. Besides, K released by chloritization in the early stage of the alteration and in the vicinity of fractures would have been evacuated by convective fluid flow. Sericitization is present away from the fractures where diffusion was dominant with respect to the movement of the chemical elements. Thus, sericitization is dominant in the non reddened and moderately reddened facies where the Na-content was lowered in the interstitial fluids due the increasing distance from the fractures that are the major source of Na. Yet, where the K/Na ratio was higher, albitization was limited and K competed with Na to form K-bearing silicates (mainly secondary K-feldspars and/or sericite) in combination with Si and Al (Ben Baccar et al. 1993; Perez and Boles 2005).

Euhedral crystals of prehnite within altered plagioclase indicate epigenetic replacement with the main chemical component directly supplied in situ by the plagioclase. On the other hand, prehnite finning in microfractures witnesses the mobility of these components over some distance. If the mobility of Ca and Si is to be expected, it is rather unusual for Al , typical fairly immobile in a medium close to neutral pH, except in presence of complexing agents (Castet et al. 1993; Farmer and Lumsdon 1994 ; Oelkers et al. 1994). In any case, Al appears to have been fairly mobile, at least in some cases, but it is difficult to assess whether or not Al was evacuated from the fractures by fluid circulation.

Recrystallization of monazite was also apparently triggered by calcium availability. Initially, primary monazite recrystallized into secondary monazite at the early stages of albitization but later, during advanced stages of the albitization, primary and secondary monazite recrystallized into apatite in concert with the increase in calcium availability in the system.

These alterations can be considered to be topochemical: the saussuritization of plagioclase provided Ca for prehnite development and the chloritization of biotite is the likely source of K for sericitization. However, the complete albitization of the plagioclases and in particular the albitization of the K-feldspars in the vicinity of the fractures testify for the supply of Na, and the hematite associated with albite registers the oxidative capacity of the alteration and therefore a supply of oxygen.

Fluid-rock interactions

The geochemical exchanges between reaction zones are determined by the transport of the ions in the fluids. Exchanges in fractures record the circulation of the transport fluids by convection. The circulation may have been relatively rapid in the major fractures but slower as the dimensions of the fractures decreased. Away from the open micro-fractures, the quantity of fluid is reduced and mainly limited to ‘thin films’ at the boundaries of mineral grains and the dissolution-recrystallization interface. Such confined fluids may be very different in chemical composition and behavior from bulk fluids (Putnis and Ruiz-Agudo 2013). Within thin films, the circulation would have been minimal, diffusion prevailed over convection and ion mobility was extremely reduced.

In this context, the coupled-reactions described above are not part of a global geochemical equilibrium related to the fluids in the fractures but they are rather part of a spatially-linked dynamic geochemical equilibrium. The balances are not determined by the kinetics of the mineralogical reactions but rather by the kinetics of the diffusion of ions in the rock. The system was only partially open. A geochemical zoning developed and progressed in a chromatographic way: with displacement of ions at diverse rates and according to fronts governed by distinct reactions. This is characteristic of a metasomatic system (Korzhinskii and Oestreich 1965; Brinhall and Dietrich 1987; Guy 1993). Thus, thermodynamic reactions that originally seem incompatible with a global context may occur. Temperature is not a limiting factor but it allows speeding up of the reactions by accelerating diffusion. The reaction rate is controlled by the diffusion rate and is extremely slow, but not impossible from a thermodynamical point of view.

Thus, within a block of massive rock bounded by fractures, a zoning of the ion transport that determines the geochemical zoning is primary established (Fig. 9g). Along the fracture walls, exchanges by convection prevail and are relatively fast; the mineralogical parageneses formed in equilibrium with the fluid and thereby reveal the geochemical characteristics of the fluid. Further away from the fracture walls, exchanges are slow and are driven by diffusion; the mineralogical parageneses are controlled by local balances that are far from the balance within the fluid. This alteration of massive blocks differs entirely from alteration of porous rock where ion mobility is practically exclusively provided by fluid flowthrough.

Geochemistry of the fracture fluids.

Albitization of plagioclase and K-feldspar reflects an interaction with Na-enriched and relatively K-depleted fluids (Saigal et al. 1988; Aagaard et al. 1990; Ben Baccar et al. 1993; Schmitt 1994; Perez and Boles 2005). The association with hematite indicates that the fluids were also enriched in oxygen. There seems to have been a relatively low CO_2 fugacity since only minor calcite was formed, in spite of the abundance of Ca released during plagioclase alteration. The fluids were also relatively under-saturated in SiO_2, Al and Mg, since chlorite coating the fractures is sometimes entirely altered to hematite. On exiting the system, fluids were depleted in Na and O_2. However, they were enriched in K because, in the early stages of the alteration, little or no sericite was formed within plagioclases during the chloritization of biotite. The chemical balance is more difficult to establish for SiO_2, Al and Ca. Significant amounts of silica were liberated during chloritization of biotite so it is likely that it was exported from the system, at least in the granodioritic facies that is rich in biotite. It could be that Al and Ca were in balance between the altered plagioclases and the formation of prehnite and calcite, even if a quantified balance is not available. Nevertheless, it is obvious that the Ca was easily exported from the cortical reactional zones during the early stage of the alteration. The mobility of Al is unlikely to have occurred on a significant scale because the major fractures never show any alumino-silicate mineralization. In conclusion, it appears clear that the fluids responsible for the alteration were oxidized, Na-rich and relatively depleted in K in comparison to Na.

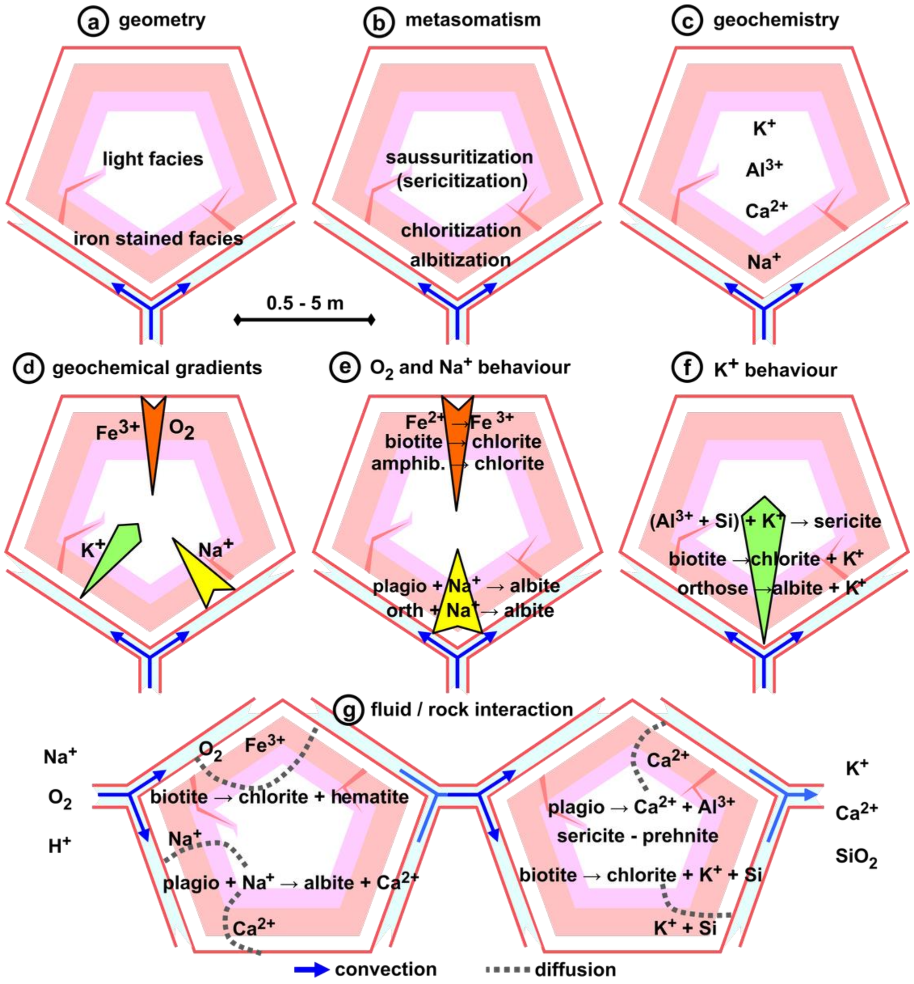

Fig. 9 Schematic interpretative sketch of the various petrographic parageneses related to reddening and albitization of the granitoid rocks in the Sudetes at the outcrop scale

Iron oxide behavior

Maghemite is considered to be metastable with respect to hematite (Waychunas 1991; Majzlan et al. 2003). In addition, it is generally admitted that slow and incomplete oxidation of magnetite favours the topotactic formation of maghemite whereas faster oxidation of magnetite, under highly oxidizing conditions, results in hematite formation (Steinthorsson and Helgason 1992; Bowles et al. 2011). The maghemite-hematite transition during albitization may be attributed to changes in the alteration environment during the oxidation of magnetite. In this case the alteration commenced with the formation of maghemite under low oxidizing conditions in the non-reddened and slightly reddened granitoids and continued with the formation of hematite in the reddened facies under stronger oxidizing conditions, when ferrous silicates (biotite and amphibole) were being oxidized. Thus, the occurrence of maghemite and hematite suggests that the oxidizing conditions changed during the alteration of the granitoid and the spatial distribution of hematite and maghemite provides a tool to estimate the gradient of these conditions. The distribution of the alteration environments substantiates the idea that reddened albitized facies and non reddened saussuritized/sericitized facies reflect gradational changes during a single event.

From a geochemical point of view there is no contradiction in the spatial discrepancy between the zones of alteration of the silicate minerals and the distribution of the iron oxides. The physico-chemical properties that constrain their reactions are not the same. A key-factor in the alteration and crystallization of the silicates is the pH, whereas Eh and the oxygen fugacity controls the oxidation state of the iron oxides. Theses two parameters may vary independently. Nevertheless, the precipitation of iron oxides is also facilitated by the elevated pH. Thus, local lowering of the H^+ activity at the sites of feldspar alteration will favour the localized precipitation of hematite as inclusions within the feldspars (Boone 1969). This also explains the local distribution of pigmentary hematite inclusions in albite during the alteration of both plagioclase and K-feldspar. On the other hand, the intensity of the reddening, or the abundance of the pigmenting hematite, is related to oxygen fugacity and therefore is likely to decrease away from the fractures. From the geochemical point of view, the hematite distribution is consistent with the alteration sequence of the silicate minerals.

Origin of the oxidizing fluids

In general, post-magmatic alterations are explained by a hydrothermal model which uses large convective circuits to bring the superficial fluids in contact with the warm rock complexes, in particular granitic intrusions, in which the alterations then take place (Taylor 1977; Jenkin et al. 1992; Putnis et al. 2007; Drake et al. 2008). The magmatic intrusions provide heat to the fluids and the subsequent loss in fluid density causes the upwelling, maintaining the circulation between the landsurface and depth. Fluids with a deeper origin may be also mixed into this circulation model.

In the hydrothermal model, the superficial origin of the fluids, or at least the participation of meteoric water, has been evoked by oxygen and hydrogen isotope studies on the alteration minerals (Simon and Hoefs 1987; Sun and Eadington 1987; Jenkin et al. 1992; Boyce et al. 2003). These models usually consider superficial oxygen-rich fluids descending very deeply (more than 10 km) before they interact with the rock matrix. However, some reactive transport models strongly suggest that this form of fluid percolation leads to a rapid depletion of the oxygen fugacity in the circulating fluids, so fluids at great depths are very likely to be under-saturated in oxygen (MacQuarrie et al. 2010).

Here we have documented the Permian-Triassic-Jurassic age of the alteration and provided arguments that it is necessarily related to the Post-Variscan paleosurface and *de facto* involved infiltration of weathering solutions and/or groundwater flow.

Temperature and depth of formation

The $\delta^{18}O$ results allow to estimate the fluid temperature during plagioclase albitization and K-feldspar microclinization. Assuming a local isotopic equilibrium between minerals and the fluid at the reaction interface, the isotopic mass balance was calculated for each reaction using the equation of Taylor (1977), by (Eq. 1):

$$\delta^{18}O_f^w = \delta^{18}O_i^w + \frac{R}{W} \times \left(\delta^{18}O_i^m - \delta^{18}O_f^m\right) \qquad (1)$$

Where $\delta^{18}O^w{}_i$ and $\delta^{18}O^w{}_f$ $\delta^{18}O^w{}_i$ are the initial and final oxygen isotope compositions of the fluid, respectively, R and W the percentage of oxygen atoms in the rock (or mineral) and water, respectively, and $\delta^{18}O^m{}_i$ and $\delta^{18}O^m{}_f$ the oxygen isotope composition of the initial and final minerals, respectively. For the rock-to-water oxygen mass ratio (R/W), conservative estimates of 0.5 and 1 were applied. The applied values for the oxygen isotope composition of the initial fluid ($\delta^{18}O^w{}_i$) were -8 and -12‰ (VSMOW), which are typical $\delta^{18}O$ values observed in deep groundwaters hosted in stable granitic basements (Stober & Bucher 1999a and b; Barth 2000; Kloppmann et al. 2002).

Two options of reactions paths were considered, (1) sequential reactions, with a fluid moving across a steeped sequence of albitization and microclinization, so that the mass balance of albitization is calculated first and subsequently the mass balance of microclinization is calculated using as initial fluid isotopic composition the $\delta^{18}O$ value of the final fluid obtained from the mass balance of previous albitization or, (2) concomitant reactions, were the fluid is renewed at the beginning of each reaction. After the isotopic mass balance estimation for each reaction, a temperature was calculated for each reaction using the plagioclase-water (Eq. 2) and K-feldspar-water (Eq. 3) equilibrium fractionation equations of Zheng (1993).

$$1000 \ln \alpha_{Ab-H2O} = \frac{4.33}{T^2} \times 10^6 - \frac{6.15}{T} \times 10^3 + 1.98 \qquad (2)$$

$$1000 \ln \alpha_{Kfs-H2O} = \frac{4.32}{T^2} \times 10^6 - \frac{6.27}{T} \times 10^3 + 2.00 \qquad (3)$$

Using the two reaction paths and the crossed combinations of the different applied values for R/W and $\delta^{18}O^{w}_{i}$, the estimated interaction temperatures of water during albitization and microclinization range between 32 and 89°C (average of 60°C). Significantly, and despite the large relative variations in the values applied to R/W and $\delta^{18}O_{if}$, and the two different reaction paths, the temperature estimates present a narrow range of variability, supporting that the mineral reactions developed in by interaction with "low" temperature groundwaters. Thus, considering the Permian-Triassic age and the relatively low temperature of the alteration, the hypothesis that the alteration fluids were closely related to the paleosurface and *de facto* "vertical" infiltrations of a weathering solution is a plausible possibility. Similar reaction temperatures (45 to 65°C) were obtained for plagioclase albitization and K-feldspar microclinization in Permian-Triassic age red-stained albitized profiles in NE Spain (Fàbrega et al. 2019), that are similar in field layout, petrographic characteristics and age to the Polish sections of this study.

Regardless of the lack of accuracy of these temperature estimates, these estimated values show that the temperatures of the reactions associated with the development of red-stained albitized rocks are significantly below temperatures suggested for albitization formed under hydrothermal alteration (Cathelineau 1986; Boulvais et al. 2007) and tardi-magmatic alteration (Lee and Parsons 1997; Fiebig and Hoefs 2002). Instead, the low temperature range accords with the geological settings, age and association of the red-stained albitized profile developped on the Post-Variscan paleosurface during the Permian-Jurassic period. We suggest that the albitized profile developed a few hundred metres beneath the Post-Variscan paleosurface by interaction with relatively ‘low’ temperature groundwaters, and was subsequently exposed at the landsurface after erosion of the uppermost weathering mantle.

PALEOENVIRONMENTAL SETTING OF THE ALBITIZATION

The absence of mesoscale- and microscale-geopetal structures, together with clues of directional water flow combined with the isotropic structures around fracture blocks within the macro-scale profiles, evoke an aquifer environment at the origin of the albitization. Boreholes in the Massif Central (Schmitt 1986) and field exposures in the Morvan (Parcerisa et al. 2009) and NE Spain (Fàbrega et al. 2019) show that the albitized profiles may generally reach 100 m in thickness and may even exceed 200 m. Such profiles are comparable to those of weathering profiles with thick basal saprolite horizons in tropical soils (Boulangé 1984; Vasconcelos et al. 1994; Ruffet et al. 1996; Grimaud et al. 2015) and deep groundwater saprolites in dry saline environments as well as in periglacial environments (Thiry et al. 2006; Thiry et al. 2017). Nevertheless, the primary profiles were probably much thicker because only the deep indurated horizons have survived the erosion that preceded the Mesozoic transgression. The profiles were certainly at some stage surmounted by non-indurated horizons and regolith materials. On the other hand, the functioning of the albitization profiles and thus landscape stability spreading over ~50 Ma in the Sudetes is comparable to the duration of the deep tropical weathering profiles and related landscapes rooted in old cratons mentioned above.

Reaction temperatures calculated from the oxygen isotope composition of minerals, and hypotheses about the oxygen isotope composition of reactant fluids and their circulation, led us to an estimation of the mean temperature of albitization and associated reactions of about 60°C in the Sudetes albitized profiles and 55°C in the Catalan albitized profiles (Fàbrega et al. 2019). Based on this temperature, and considering a geothermal gradient of about 25–30°C km^{-1} and a surface temperature of ~30°C, in consideration of the high paleotemperature proposed at the Permian–Triassic boundary, led to calculate a mean depth of about 1 km for the environment in which albitization occurred.

There is indeed a systematic vertical profile organization for the sections we have studied, specifically with a more albitized and ferruginized upper part, a less-altered and reddened lower part where albitization occurred under weakly oxidizing conditions, and the progressive weakening and disappearance of alteration with depth. In connecting this geometry to the Pre-Triassic paleosurface, its is clear that the albitization represents a climatic weathering process of great magnitude. The low mobility of most of the involved chemical elements could point to deep groundwater table with very low outflow. But even if the alteration occurred at a greater depth, reactant solutions would have to have been renewed to provide at least sufficient O_2 and Na^+. Therefore, there must have been water flow within fractures between the fractured blocks which implies a hydraulic gradient. In particular, a regional hydraulic gradient with meteoric water infiltrating the upstream profiles and groundwater outflowing downstream would have been necessary. As albitization developed, water changed composition from entrance to outflow with loss of O_2, Na^+, and H^+ and a likely increase in K^+, Ca^{++}, and possibly SiO_2 content, as deduced from the geochemistry of the mineral transformations (Fig. 9g). The lateral evolution of such albitized profiles has been documented in the SW of the French Massif Central (Yerle and Thiry 1979; Clément 1986; Schmitt 1986). Here, (1) profiles on basement heights are thin and albitization is mainly restricted to fracture walls (such as described herein), and (2) lowland profiles rooted in Carboniferous and Permian deposits are much thicker with upper horizons albitised and oxidized whereas deeper albitized horizons remain anoxic and are the site of K-feldspar neoformations (Fig. 10).

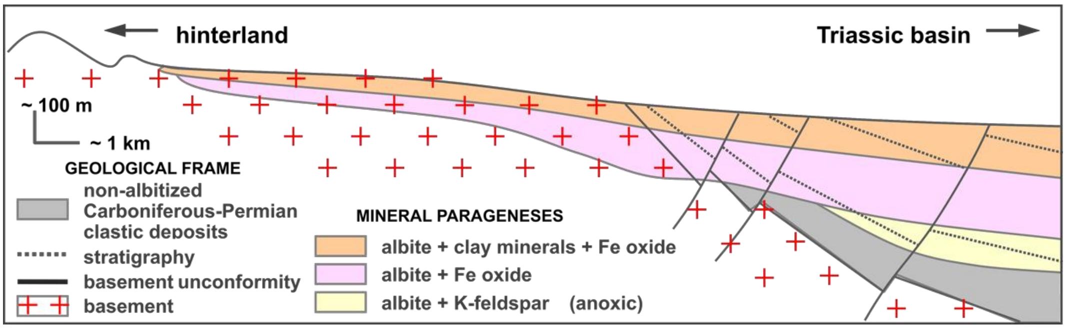

Fig. 10 Arrangement of mineral parageneses on the southern edge of the Massif Central. Albitized profiles thicken from crystalline heights towards Carboniferous and Permian basin lowlands where K-feldspar forms at depth. Modified after Clément (1986)

Two fundamental elements must be taken into account: (1) the presence of relief to ensure the hydrological gradient, and (2) the origin of sodium that triggers the whole chain of alteration. In terms of the groundwater dynamics, it could be that albitization developed in landscapes of intermediate relief, perhaps on large piedmonts between a mountain range and sea level. Petrographic data indicate that sodium was imported without potassium enrichment. Early modeling attempts (Schmitt 1994) also indicated that a high Na^+/K^+ ratio was probably required. The Na^+ enrichment is most likely to be linked with the peculiar geochemical setting of the Permian-Triassic environments in the region. Sodium could have originated from the gigantic salt deposits of these periods and may have been imported in large quantities and over long distances by successive phases of eolian reworking from littoral and endoreric basins during dry periods (Bourquin et al. 2011).

It should be stressed that the albitization started long before the recorded dating, possibly as early as Mid-Permian, with the development of the Zechstein evaporite deposits in the Germanic basin. It is the final stage that we have dated: previous stages have likely been overprinted by succeeding reactions. Classically, weathering profiles progress from top to base and result in older ages in the uppermost horizons and younger ages at depth, as evidenced in numerous long-lasting paleoweathering sequences (Vasconcelos et al. 1994; Dammer 1995; Ruffet et al. 1996). However, paleomagnetic dating of the profiles we have studied here show an inverse polarity, with the oldest ages in the weakly albitized and reddened bottom horizons and the youngest ages in the more albitized and ferruginized uppermost horizons. This points to a 'regressive' weathering sequence, in which the weathering profile did not continue to deepen but was 'blocked' with only the upper horizons continuing to be weathered. This profile form relates in some way to the specific evolution of the landscape in the region in relation to the widespread Mesozoic transgression. It would have corresponded to a rise in basal hydrological level which induced rising watertables across the continent. The rising watertables would have limited the infiltration of surficial waters, changed the hydrodynamic gradients and effectively stopped the alteration at depth. Thus, the regional geodynamics during the Late Permian and Triassic period strongly influenced weathering and regolith processes while the climate was steadily warm and semi-arid.

Weathering toposequences should be considered on a continental scale as shown by Fàbrega et al. (2019). In the case of our study area, the toposequence is arranged between the relief of the Varsican Belt that provided the hydraulic gradient and the Permian and Triassic basins that probably supplied the salt. Albitization was initiated and probably gradually invaded the entire Post-Varisacan paleosurface across several 10's of Ma during which both landscape and climate were relatively stable. Indeed, the overall ages determined up to now for the albitization span a relatively long period, between 270 and 170 Ma, that corresponds to the Middle Permian to the Middle Jurassic (Table 4). The distribution of the now-dated albitized profiles along the Post-Variscan paleosurface between the Zechstein Sea in the North and the Tethys in the South (Fig. 11), shows that:

4) the profiles closest to the marine environments, namely the Sudetes and NE Spain, show the oldest ages (this study; Fàbrega et al. 2019);

5) the Vosges massif, which was connected to the marine environment through the threshold passage of the Triassic transgression coming from the North, also show relatively old albitized profiles (Vercruysse 2011);

6) the area most distant from the sea, namely the Rouergue heights overlay by infra-Jurassic deposits, comprises the youngest albitized profiles (Schmitt et al. 1984) while the Permian graben covered with coarse Triassic deposits on lower plateaux in Rouergue (Bonhomme et al. 1980) and Morvan (Ricordel et al. 2007) have older ages; and

7) in the Sudetes, the highly evolved ferruginous albitized facies currently in hillside positions are relatively young while the valley-bottom sections are older. This differentiation is possibly related to local morphologies whereby raised tectonic blocks remained emerged during the Mesozoic transgression.

The concordance between age and relative position in the Triassic paleogeography is striking. The areas covered early by the Triassic transgression have the oldest albitized profiles whereas the highlands distant from the sea have the youngest ages. It is actually the interruption of weathering by the Triassic transgression that is dated. These datings could in future be used as a tool to better enhance the mapping of the Triassic transgression and the geodynamics of the basement as well as its post-Triassic evolution.

Paleolandscape and paleoweathering features of the Post-Varican paleosurface in Western Europe may be compared to regolith features existing today on the African, Australian and South American cratons inherited from Pangea break out. Combined radiogenic dating and geomorphological analyses allowed us to document paleolandscape and paleoweathering profiles that functioned for more than 100 Ma in these cratonic regions (Vasconcelos et al. 1994; Dammer 1995; Ruffet et al. 1996; Pillans, 2007; Beauvais et al. 2008; Peulvast et al. 2008 ; Beauvais and Chardon 2013; Jean et al. 2020). This is the spatial and temporal scale of the albitization and hematization paleoweathering profiles we studied on the Western European Post-Variscan paleosurface. Persistance of the Post-Variscan paleosurface is conforted by the widespread magnetic overprinting phase due to secondary hematite formation (related or not to albitization) that affected widely the Variscan belt during the 235-250 Ma time-span Edel et al. (2018).

Table 4 – Age of the reddened/albitized rocks related to the Post-Variscan paleosurface on the Variscan Belt

area	location	geomorph	rockl	sample	method	age	reference
Sudetes	Szklarska Poręba	hill	granitoide	2.5 x 2.5 cm	palaeomag	256-190	herein
	Laski quarry	valley	granitoide	2.5 x 2.5 cm	palaeomag	270-190	herein
	Laski village	hill slope	granitoide	2.5 x 2.5 cm	palaeomag	258-170	herein
	Chwalisław	valley	granitoide	2.5 x 2.5 cm	palaeomag	205-195	herein
	Chwalisław	valley	granitoide	monazite	U-Th-Pb$_{tot}$	254	herein
	Chwalisław	valley	granitoide	2.5 x 2.5 cm	palaeomag	250	Edel et al. (1997)
Vosges			granitoide	2.5 x 2.5 cm	palaeomag	255-235	Vercruysse (2011)
Morvan			granitoide	2.5 x 2.5 cm	palaeomag	235	Ricordel et al. (2007)
Rouergue	Bertholène	high	orthogneiss	minerals	K-Ar	210-200	Schmitt et al. (1984)
	Brousse	basin	sediments	clay fraction	K-Ar	230	Bonhomme et al. (1980)
NE Spain	Guilleries Massif		granite	monazite	U-Th-Pb$_{tot}$	251	Fàbrega et al. (2019)
	Roc Frausa Mass.		granite	monazite	U-Th-Pb$_{tot}$	254	Fàbrega et al. (2019)
	Hortmoier Massif		granite	K-F crystals	K-Ar	240	Fàbrega et al. (2019)

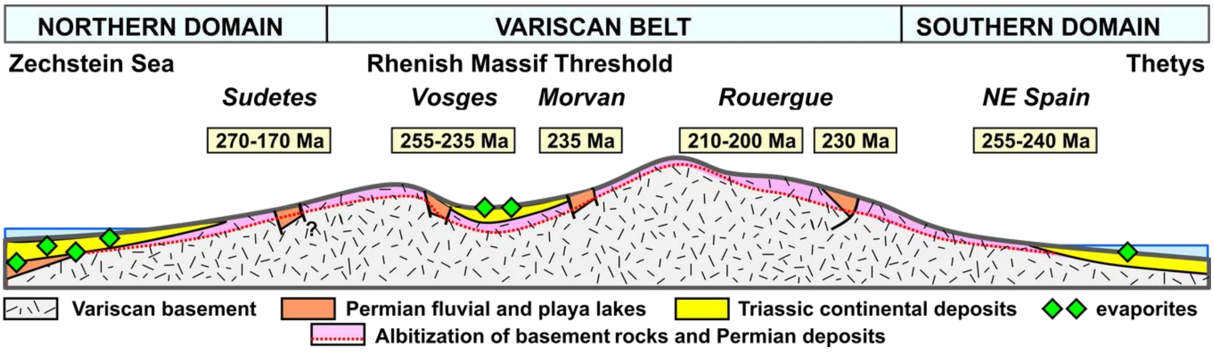

Fig. 11 Position and age of the studied albitized profiles on a schematic N-S geomorphological section of the Post-Variscan paleosurface and

associated sedimentary basins during Permian-Triassic times. The oldest ages occur nearest the sea and youngest away the sea and in highland areas that were later buried. Paleogeography after Bourquin et al. (2011)

CONCLUSIONS

The oxidized and albitized facies of the Polish Sudetes granitoids exhibit ~~t~~wo types of ‘classical’ petrographical parageneses: a saussuritization-sericitization and an albitization-hematitization. The chloritization of amphiboles and biotites that is associated to these alterations is intermediate between both. These alterations are always closely associated without any break or spatial discordance between them. They are controlled by the presence of fractures and are spatially arranged with respect to the configuration of these fractures. Albitization and hematitization are preferentially intense close to the walls of the fractures whereas the saussuritization and the sericitization of plagioclase become more important further away from the fractures and towards the center of the massive blocks. These alterations can be considered as topochemical. However, the complete albitization of the plagioclase and K-feldspar in the vicinity of the fractures signifies a supply of Na. Hematite associated with albite is an indication of oxidative capacity and therefore the supply of oxygen via the alteration.

Paleomagnetic dating of the reddened and albitized facies reveal Late Permian to Early Jurassic ages for the iron-oxides and radiochronological dating of associated monazite using the U-Th-Pb$_{total}$ method indicates Late Permian recrystallization ages. Given the ages of the alteration, it can clearly be related to the extensive Post-Variscan paleosurface in the region, since the altered granitoids were already outcropping during from Late Permian to Early Jurassic. Therefore, these reddened and albitized profiles can be considered a consequence of deep weathering.

As there was clearly a requirement to renew solutions to feed chemical reactions, it is likely that the alteration profiles were downstream of highlands in order to generate a hydrological head. The sodium supply that triggered albitization could well have come from the gigantic salt playas that characterized the lowland paleogeography of the Permian and Triassic in the region. Thus, we suggest that the reddened and albitized profiles developed on a wide glacis shaped in the basement rocks upstream of the evaporatic basins. The deep weathering was interrupted and preserved by the Mesozoic transgression.

The age dating shows that the oldest examples of the alteration profiles (Late Permian to Early Triassic) are proximal to the Zechstein and Tethys seas, while the youngest (late Triassic to basal Jurassic) are further away and appear to be located on the highlands that were more recently covered by the Mesozoic transgression. Thus, this alteration of the crystalline rocks is an important marker to constrain Triassic and post-Triassic geodynamics in the region, including erosion rates and the geomorphic evolution of the Paleozoic massifs.

Albitized and oxidized facies of crystalline basement are widespread throughout the world. Until now, this subject has attracted relatively little interest from petrographers. A re-examination of all existing data could involve a reconsideration of questions such as prehnite and sericite paragenesis, particularly from the viewpoint of temperature of formation, since they have in the past been used as an indicator of 'high temperatures'. It may be that the formation of sericite and prehnite is not part of a unique alteration leading to albitization, but the fact remains that proximity to the paleosurface is clearly indicated by the presence of hematite.

We suggest that particular attention should be paid to the radiochronological and paleomagnetic dating results that some have considered to be "obviously too young" in the context of the age of emplacement of the crystalline massifs. These "too young" dates have been systematically rejected as false in the past and rarely noted in publications; consequently this information was lost. A new consideration of these dates may realise their consistency, as shown for example by Edel and Schneider (1995) for the Permian formations that endured a Triassic rejuvenation highlighted by paleomagnetism.

It should be noted that the formation of secondary apatite in the reddened albitized Sudetes rocks has previously been reported in conjunction with albitization and chloritization related to the Triassic paleosurface in the French Massif Central (Parcerisa et al. 2009) and in NE Spain (Fàbrega et al. 2019). It also formed during metasomatic albitization in a metagabbro from Norway (Engvik et al. 2009). The formation of significant amounts of secondary apatite during albitization must be taken into account if fission track analysis or (U–Th)/He dating is carried out on these reddened albitized rocks.

References:

Aagaard P, Egeberg PK, Saigal GC, Morad S, Bjørlykke K (1990) Diagenetic albitization of detrital K-feldspars in Jurassic, Lower Cretaceous, and Tertiary clastic reservoir rocks from offshore Norway, II. Formation water chemistry and kinetic considerations. Journal of Sedimentary Petrology 60:575–581

Aleksandrowski P, Kryza R, Mazur S, Żaba J (1997) Kinematic data on major Variscan strike-slip faults and shear zones in the Polish Sudetes, northeast Bohemian massif. Geological Magazine 133: 727-739

Aleksandrowski P, Mazur S (2002) Collage tectonics in the northeasternmost part of the Variscan Belt: the Sudetes, Bohemian Massif). In: Winchester, J., Pharaoh T. & Verniers J. (eds), Palaeozoic Amalgamation of Central Europe, Geological Society, London, Special Publications 201: 237-277

Alt, J.C., Laverne, C., Coggon, R.M., Teagle, D.A., Banerjee, N.R., Morgan, S., Smith-Duque, C.E., Harris, M., Galli, L. (2010) Subsurface structure of a submarine hydrothermal system in ocean crust formed at the East Pacific Rise, ODP/IODP Site 1256. Geochemistry, Geophysics, Geosystems, 11(10)

Awdankiewicz M, Awdankiewicz H (2010) Spessartites of the Kłodzko Złoty-Stok dyke swarm. Mineralogia Special Papers 37: 135-139

Bachliński R, Bagiński B (2007) Kłodzko-Złoty-Stok granitoids massif. In Kozłowski A., Wiszniewska J (eds) In Granitoids in Poland, Archiwum mineralogiczne, Monograph 1: 261-273

Baranowski Z, Haydukiewicz A, Kryza R, Lorenc S, Muszynski A (1990) Outline of the geology of the Góry Kaczawskie (Sudetes, Poland). Neues Jahrbuch für Geologie und Paläontologie, Abhandlungen 179: 223-257

Barth SR (2000) Geochemical and boron, oxygen and hydrogen isotopic constraints on the origin of salinity in groundwaters from the crystalline basement of the Alpine Foreland. Applied Geochemistry 15:937–952. https://doi.org/10.1016/S0883-2927(99)00101-8

Beauvais A, Chardon F (2013) Modes, tempo, and spatial variability of Cenozoic cratonic denudation: The West African example, Geochem. Geophys. Geosyst., 14, 1590–1608, doi:10.1002/ggge.20093

Beauvais, A., Ruffet G, Henocque O, Colin F (2008) Chemical and physical erosion rhythms of the West African Cenozoic morphogenesis: The 39Ar-40Ar dating of supergene K-Mn oxides, J. Geophys. Res., 113, F04007, doi:10.1029/2008JF000996

Ben Baccar M, Fritz B, Madé B (1993) Diagenetic albitization of K-feldspar and plagioclase in sandstone reservoirs: thermodynamic and kinetic modeling. Journal of Sedimentary Petrology 63:1100–1109

Besse J, Courtillot V (2003) Apparent true polar wander and the geometry of the geomagnetic field over the last 200 Myr: Correction. Journal of Geophysical Research 108: 2300

Bonhomme M, Yerle J.-J, Thiry M (1980) Datation K-Ar de fractions fines associées aux minéralisations. Le cas du bassin uranifère permo-houiller de Brousse-Broquiès (Aveyron, France).- C.R. Académie Sciences Paris 291D: 121-123

Boone GM (1969) Origin of clouded red feldspars, petrology contrasts in a granitic porphyry intrusion. American Journal of Science 267: 633-668

Borkowska M, (1966) Petrografia granitu Karkonoszy (Petrography of the Karkonosze Granite). Geologia Sudetica 2: 7-119. (in Polish with English extended summary)

Botor D, Dunkl I, Anczkiewicz A, Mazur S (2017) Post-Variscan thermal history of the Moravo-Silesian lower Carboniferous Culm Basin (NE Czech Republic - SW Poland). Tectonophysics 712-713: 643-662

Boulangé B (1984) Les formations bauxitiques latéritiques de Côte d'Ivoire. Travaux et Documents ORSTOM 175, 341 p

Boulvais P, Ruffet G, Cornichet J, Mermet M (2007) Cretaceous albitization and dequartzification of Hercynian peraluminous granite in the Salvezines Massif (French Pyrénées). Lithos 93: 89-106.

Bourquin S, Bercovici A, López-Gómez J, Diez J-B, Broutin J, Ronchi A Amour F (2011) The Permian–Triassic transition and the onset of Mesozoic sedimentation at the northwestern peri-Tethyan domain scale: palaeogeographic maps and geodynamic implications. Palaeogeography Palaeoclimatology Palaeoecology 299: 265-280

Bowles JFW, Howie RA, Vaughan DJ, Zussman J (2011) Non-Silicates: Oxides, Hydroxides and Sulphides. Rock-Forming Minerals, 2nd edn, Geological Society of London 5A: 920 p.

Boyce AJ, Fulignati P, Sbrana A (2003) Deep hydrothermal circulation in a granite intrusion beneath Larderello geothermal area (Italy): constraints from mineralogy, fluid inclusions and stable isotopes. Journal of Volcanology and Geothermal Research 126: 243-262

Brinhall G, Dietrich W (1987) Constitutive mass balance relations between chemical composition, volume, density, porosity, and strain in metasomatic hydrochemical systems: Results on weathering and pedogenesis. Geochimica et Cosmochimica Acta 51: 567-587

Butler RF (1998) Paleomagnetism: Magnetic domains to geologic terranes. Electronic edition, 237 p.

Castet S, Dandurand J-L, Schott J, Gout R (1993) Boehmite solubility and aqueous aluminium speciation in hydrothermal solutions (90-350°C): Experimental study and modeling. Geochimica et Cosmochimica Acta 57: 4869-488

Cathelineau M (1986) The hydrothermal alkali metasomatism effects on granitic rocks: quartz dissolution and related subsolidus changes. Journal of Petrology 27: 945-965

Chrząstek A., Wojewoda J (2011) Mezozoik południowo-zachodniej Polski - synklinorium północnosudeckie (Mesozoic of SW Poland, the North Sudetic Synclinorium). In: Żelaźniewicz, A., Wojewoda, J., Ciężkowski, W. (eds), *Mezozoik i kenozoik Dolnego Śląska*. Polskie Towarzystwo Geologiczne, Wrocław, 1-10 (in Polish, English abstract)

Clément J-Y, (1986) Minéralogie, pétrologie et géochimie du Permien de Lodève (Hérault, France) : diagenèse précoce, altération feldspathisante et mise en place des minéralisations uranifères. E.N.S.M.P. Mémoire Sciences de la Terre 2: 137 p.

Cocherie A, Albarede F (2001) An improved U-Th-Pb age calculation for electron microprobe dating of 845 monazite. Geochimica et Cosmochimica Acta 65:4509–4522, https://doi.org/10.1016/S0016-7037(01)00753-0 846

Cocherie A, Legendre O, Peucat J-J, Kouamelan AN (1998) Geochronology of polygenetic monazites 847 constrained by in situ electron microprobe Th-U-total lead determination: Implications for lead 848 behaviour in monazite. Geochimica et Cosmochimica Acta *62*: 2475-2497, https://doi.org/10.1016/S0016-7037(98)00171-9

Cogné J-P (2003) PaleoMac: a Macintosh™ application for treating paleomagnetic data and making plate reconstructions. Geochemistry Geophysics Geosystems 4: 1007.

Dammer D (1995) Geochronology of chemical weathering processes in the northern and western Australian regolith. PhD thesis, Australian National University: 214 p.

Danišík M, Migoń P, Kuhlemann J, Evans NJ, Dunkl I, Frisch W (2010) Thermochronological constraints on the long-term erosional history of the Karkonosze Mts, central Europe, Geomorphology 117: 78–89

Danišík M, Štěpančíková P, Evans NJ (2012) Constraining long-term denudation and faulting history in intraplate regions by multisystem thermochronology: An example of the Sudetic Marginal Fault (Bohemian

Massif, central Europe). Tectonics 31: TC2003, https://doi.org/10.1029/2011TC003012

De Jong G., Williams PJ (1995). Giant metasomatic systems formed during exhumation of mid-crustal Proterozoic rocks in the vicinity of the Cloncurry fault, northwest Queensland. Australian Journal of Earth science 42: 281-290

De La Roche H (1957) Eléments pour l'étude de la saussuritisation. Mémoires de l'Institut Scientifique de Madagascar 7D: 217-223

Depciuch T (1972) Wiek bezwzględny (K-Ar) granitoidów Kłodzko Złotostockich i strefy Niemczy. Kwartalnik Geologiczny 16: 103-111

Drake H, Tullborg EL, Annersten H (2008) Red-staining of the wall rock and its influence on the reducing capacity around water conducting fractures. Applied Geochemistry 23: 1898-1920

Dziedzic K, Teisseyre AK (1990) The Hercynian molasse and younger deposits in the Intra-Sudetic Depression, SW Poland. Neues Jahrbuch für Geologie und Paläontologie, Abhandlungen 179: 285–305

Edel J-B, Schneider J-L (1995) The Late Carboniferous to Early Triassic geodynamics evolution of the Variscan Europe in the light of magnetic overprints in Early Permian rhyolites from the northern Vosges (France) and the central Black Forest (Germany). Geophysical Journal International 122: 858-876

Edel J-B, Duringer P (1997) The apparent polar wander path of the European plate in Upper Triassic-Lower Jurassic times and the Liassic intraplate fracturing of the Pangea: New palaeomagnetic constraints from NW France and SW Germany. Geophysical Journal International 128: 331-344

Edel J-B, Aifa T, Jelenska M, Kadzialko-Hofmokl M, Zelazniewicz A (1997) Réaimantations des formations paléozoïques des Sudètes polonaises et courbe de dérive des pôles géomagnétiques d'Europe du Carbonifère moyen au Jurassique moyen. Comptes Rendus de l'Académie des Sciences - Séries IIA - Earth and Planetary Science Letters 325: 479-486

Edel J B, Schulmann K, Lexa O, Lardeaux J-M. (2018) Late Palaeozoic palaeomagnetic and tectonic constraints for amalgamation of Pangea supercontinent in the European Variscan belt. Earth-science reviews, 177: 589-612

Engvik AK, Golla-Schinder U, Berndt J, Austrheim H, Putnis A (2009) Intragranular replacement of chlorapatite by hydroxy-fluor-apatite during metasomatism. Lithos 112: 236-246

Engvik AK, Putnis A, Gerald JDF, Austrheim H (2008) Albitisation of granitic rocks: the mechanism of replacement of oligoclase by albite. The Canadian Mineralogist 46: 1401-1415

Fàbrega C, Parcerisa D, Rossell JM, Gurenko A, Franke C (2017) Predicting instrumental mass fractionation (IMF) of stable isotope SIMS analyses by response surface methodology (RSM). J Anal At Spectrom 32:731–748. https://doi.org/10.1039/C6JA0 0397D

Fàbrega C, Parcerisa D, Thiry M, Franke C, Gurenko A, Gòmez-Gras D, Solé J, Travé A. (2019) Permian–Triassic red-stained albitized profiles in the granitic basement of NE Spain: evidence for deep alteration related to the Triassic palaeosurface. International Journal of Earth Sciences 108: 2325-2347

Farmer VC, Lumsdon DG (1994) An assessment of complex formation between aluminium and silicic acid in acidic solutions. Geochimica et Cosmochimica Acta 58: 3211-3334

Feist-Burkhardt S, Götz A, Szulc J, Borkhataria R, Geluk M, Haas J, Hornung J, Jordan P, Kempf O, Michalík J, Nawrocki J, Reinhardt L, Ricken W, Röhling H-G, Rüffer T, Török Á, Zühlke R (2008) Triassic. In: McCann (ed.), The Geology of Central Europe, Volume 2, Mesozoic and Cenozoic. Geological Society of London, pp 749-821

Ferry JM (1979) Reaction mechanisms, physical conditions, and mass transfer during hydrothermal alteration of mica and feldspar in granitic rocks from south-central Maine, USA. Contributions to Mineralogy and Petrology 68:125-13

Fiebig J, Hoefs J (2002) Hydrothermal alteration of biotite and plagioclase as inferred from intragranular oxygen isotope-and cation-distribution patterns. European Journal of Mineralogy, 14: 49-60

Fisher RA (Ed.) (1953) Dispersion on a Sphere. Philosophical Transactions of the Royal Society of London. Series A, vol. 217, 295 p.

Fisher NI, Lewis T, Embleton BJJ (1987) Statistical Analysis of Spherical Data, Cambridge Univ. Press, Cambridge, 329 p.

Głuszyński, A., Aleksandrowski, P. (2022) Late Cretaceous–Early Palaeogene inversion-related tectonic structures at the northeastern margin of the Bohemian Massif (southwestern Poland and northern Czechia). Solid Earth, 13(8): 1219-1242

Goldsmith JR, Laves F (1954) The microcline-sanidine stability relations. Geochimica et Cosmochimica Acta 5: 1-19

González-Acebrón L, Arribas J, Mas R (2010) Role of sandstone provenance in the diagenetic albitization of feldspars. A case study of the Jurassic Tera Group sandstone (Cameros Basin, NE Spain). Sedimentary Geology 229: 53-63

González-Acebrón L, Götze J, Barca D, Arribas J, Mas R, Perez-Garrido C (2012) Diagenetic albitization in the Tera Group, Cameros Basin (NE Spain) recorded by trace elements and spectral cathodoluminescence. Chemical Geology 312:: 148-162

Götze J., Krbetschek M.R., Habermann D., Wolf D. 1999: High-resolution cathodoluminescence studies of feldspar minerals. [In]: Cathodoluminescence in geosciences. Ed.: Pagel M., Barbin V., Blanc Ph., Ohnenstetter D., Springer-Verlag, Berlin Heidelberg New York: 271-302

Götze J, Krbetschek MR, Habermann D, Wolf D (2000) High-resolution cathodoluminescence studies of feldspar minerals. In: Cathodoluminescence in geosciences. Ed.: Pagel M., Barbin V., Blanc Ph., Ohnenstetter D., Springer-Verlag, Berlin Heidelberg New York: 245-270

Grimaud J-L, Chardon, Metelka V, Beauvais A, Bamba O (2015) Neogene cratonic erosion fluxes and landform evolution processes from regional regolith mapping (Burkina Faso, West Africa). Geomorphology 241: 315-330

Guy B (1993) Mathematical revision of Korzhinskii's theory of infiltration metasomatic zoning. European Journal of Mineralogy 5: 317-339

Hövelmann J, Putnis A, Geisler T, Schmidt BC, Golla-Schindler U (2010) The replacement of plagioclase feldspars by albite: observations from hydrothermal experiments. Contribution to Mineralogy and Petrology 159: 43-59

Jean A, Beauvais A, Chardon D, Arnaud N, Jayananda M, Mathe PE (2020) Weathering history and landscape evolution of Western Ghats (India) from 40Ar/39Ar dating of supergene K–Mn oxides. Journal of the Geological Society, 177(3): 523-536

Jenkin GRT, Fallick AE, Leake BE (1992) A stable isotope study of retrograde alteration in SW Connemara, Ireland. Contributions to Mineralogy and Petrology 110: 269-288

Jokubauskas P, Bagiński B, MacDonald R, Awdankiewicz M (2014) Field trip to the Kłodzko – Złoty Stok intrusion. Mineralogia, Mineralogical Society of Poland, Kraków, Special Papers 42: 127-134

Jokubauskas P, Bagiński B, Macdonald R, Krzemińska E (2018) Multiphase magmatic activity in the Variscan Kłodzko–Złoty Stok intrusion, Polish Sudetes: evidence from SHRIMP U–Pb zircon ages. International Journal of Earth Sciences 107: 1623–1639

Kadzialko-Hofmokl M, Kruczyk J, Mazur S, Siemiatkowski J (2003) Paleomagnetism of the Upper Paleozoic and devonian rocks from the Kłodzko metamorphic Complex in the West Sudetes (SWPoland): tectonic implications for the Variscan Belt of Central Europe. Tectonophysics 177: 83-99

Kelley, D.S., Robinson, P.T., Malpas, J.G. (1992) Processes of brine generation and circulation in the oceanic crust: fluid inclusion evidence from the Troodos ophiolite, Cyprus. Journal of Geophysical Research: Solid Earth, 97(B6): 9307-9322

Kirschvink JL (1980) The least-square line and plane and the analysis of paleomagnetic data, Geophys. J. R. Astron. Soc. 62: 699-718

Kloppmann W, Girard J-P, Négrel P (2002) Exotic stable isotope compositions of saline waters and brines from the crystalline basement. Chemical Geology 184: 49–70. https://doi.org/10.1016/S0009-2541(01)00352-7

Koržhinskii DS, Oestreich W (1965) Abriss der metasomatischen Prozesse. Akademie-Verlag Berlin: 195 p.

Kowalski A (2020) Triassic palaeogeography of NE Bohemian Massif based on sedimentological record in the Wleń Graben and the Krzeszów Brachysyncline (SW Poland). Annales Societatis Geologorum Poloniae 90: 125 – 148

Kozłowski A, Karwowski Ł, Olszyński W (1975) Tungsten-tin-molybdenum mineralization in the Karkonosze massif. Acta Geologica Polonica 25: 415-430

Kroner U, Mansy J-L, Mazur S, Aleksandrowski P, Hann HP, Huckriede H, Lacquement F, Lamarche J, Ledru P, Pharaoh T, Zedler H, Zeh A, Zulauf G (2008) Variscan Tectonics. In: McCann, T. (ed.): The Geology of Central Europe. The Geological Society, London: 599-66

Kryza R, Crowley QG, Larionov A, Pin Ch, Oberc-Dziedzic T, Mochnacka K (2012) Chemical abrasion applied to SHRIMP zircon geochronology: An example from the Variscan Karkonosze Granite (Sudetes, SW Poland). Gondwana Research 21: 757-767

Kryza R, Schaltegger U, Oberc‐Dziedzic T, Pin Ch, Ovtcharova M (2014) Geochronology of a composite granitoid pluton: a high‐precision ID‐TIMS U–Pb zircon study of the Variscan Karkonosze Granite (SW Poland). International Journal of Earth Sciences 103: 683-696

Kusiak M.A, Williams IS, Dunkley DJ, Konečny P, Słaby E, Martin HM (2014) Monazite to the rescue: U-Th-Pb dating of the intrusive history of the composite Karkonosze pluton, Bohemian Massif. Chemical Geology 364: 76-92

Lee MR, Parsons I (1997) Dislocation formation and albitization in alkali feldspars from the Shap granite. American Mineralogist, 82: 557-570

Leichmann J, Broska I, Zachovalová K (2003) Low-grade metamorphic alteration of feldspar minerals: a CL study. Terra Nova, 15: 104-108

Lewandowski, M., Werner, T., Nowoz˙yn´ski, K., 1997. PDA—a package of Fortran programs for paleomagnetic data analysis. Inst. Geophys. Pol. Ac. Sci. (Personal communication)

Lorenc M (1994) Rola magm zasadowych w ewolucji intruzji granitoidowych (studium porównawcze wybranych masywów hercyńskich). Geologia Sudetica 28: 1-130

Ludwig KR (2003) User's Manual for Isoplot 3.00 - A Geochronological Toolkit for Microsoft Excel. 940 Berkeley Geochronological Centre Spec Publ Special Pu: 25–32

McFadden PL, McElhinny MW (1988) The combined analysis of remagnetization circles and direct observations in paleomagnetism, Earth Plan. Sci. Letts. 87: 161-172

Machowiak K, Armstrong R (2007) SHRIMP U-Pb zircon age from the Karkonosze granite. Mineralogia Polonica Special Papers 31: 193-196

MacQuarrie KTB, Mayer KU, Jin B, Spiessl SM (2010) The importance of conceptual models in the reactive transport simulation of oxygen ingress in sparsely fractured crystalline rock. Journal of contaminant hydrology 112: 64-76

Majzlan J, Grevel KD, Navrotsky A (2003) Thermodynamics of Fe oxides: Part II. Enthalpies of formation and relative stability of goethite (α-FeOOH), lepidocrocite (γ-FeOOH), and maghemite (γ-Fe2O3). American Mineralogist 88: 855-859

Marheine D., Kachlik V., Maluski H., Patočka F., Żelaźniewicz A. 2002. The 40Ar/39Ar ages from the West Sudetes (NE Bohemian Massif): constraints on the Variscan polyphase tectonothermal development. Geol. Soc. Spec. Publ., 201: 133-155

Marshall DJ (1988) Cathodoluminescence of Geological Materials. Unwin Hyman, Boston, 146 p.

Matte Ph, Maluski H, Rajlich P, Franke W (1990) Terrane boundaries in the Bohemian Massif: results of large scale Variscan shearing. Tectonophysics 177: 151–170

Matthews A, Goldshmith JR (1984) The influence of metastability on reaction kinetics involving zoisite formation from anorthite at elevated pressures and temperatures. American Mineralogist 69: 848-857

Mazur S, Aleksandrowski P, Kryza R, Oberc-Dziedzic T (2006) The Variscan orogen in Poland. Geological Quarterly 50: 89-118

Mazur S, Aleksandrowski P, Turniak K, Awdankiewicz M (2007) Geology, tectonic evolution and late Paleozoic magmatism of the Sudetes-an overview. In Kozłowski A., Wiszniewska J (eds). In Granitoids in Poland. Archiwum mineralogiczne Monograph 1: 59-87

Migoń P, Lidmar-Bergström K (2001) Weathering mantles and their significance for geomorphological evolution of central and northern Europe since the Mesozoic. Earth-Science Reviews 56: 285–324

Migoń P, Danišík M (2012) Erosional history of the Karkonosze Granite Massif – constraints from adjacent sedimentary basins and thermochronology. Geological Quarterly 56: 440–454

Mikulski SZ, Williams IS, Baginski B (2013) Early Carboniferous (Visean) emplacement of the collisional Kłodzko–Złoty-Stok granitoids (Sudetes, SW Poland): constraints from geochemical data and zircon U–Pb ages. International Journal of Earth Sciences 102: 1007-1027

Mikulski S.Z, Bagińsky B, Dzierżanowski P (2004) The CHIME age calculations on monazite and xenotime in aplogranite from the Szklarska Poręba Huta. Miner. Ass. Pol. Spec. Pap., 24: 287–290

Milewicz J., 1968. Karbon górny: niecka północnosudecka. In: Budowa Geologiczna Polski, t.1, cz. 1. Prekambr i paleozoik. Wyd. Geologiczne, Warszawa: 439-441

Milewicz J., 1970. The Cretaceous of the Jerzmanice Graben (Sudetes). Biul. Inst. Geol., 239: 37-66

Morad S, El-Ghaly MAK, Caja MA, Sirat M, Al-Ramadan K, Mansurbeg H (2010) Hydrothermal alteration of plagioclase in granitic rocks from Proterozoic basement of SE Sweden. Geological Journal 45: 105-116

Oelkers EH, Schott J, Devidal JL (1994) The effect of aluminum, pH, and chemical affinity on the rates of aluminosilicate dissolution reactions. Geochimica et Cosmochimica Acta 58: 2011-2024

Parcerisa D, Thiry M, Schmitt J-M (2009) Albitisation related to the Triassic inconformity in igneous rocks of the Morvan Massif (France). International Journal of Earth Science 99: 527-544

Perez RJ, Boles JR (2005) An empirically derived kinetic model for albitization of detrital plagioclase. American Journal of Science 305: 312-343

Peulvast J-P, Sales VC, Bétard F, Gunnell Y (2008) Low post-Cenomanian denudation depths across the Brazilian Northeast: implications for long-term landscape evolution at a transform continental margin. Global and Planetary Change, 62(1-2): 39-6

Pillans B (2007) Pre‐Quaternary landscape inheritance in Australia. Journal of Quaternary Science: Published for the Quaternary Research Association, 22(5): 439-447

Plümper O., Putnis A (2009) The Complex Hydrothermal History of Granitic Rocks: Multiple Feldspar Replacement Reactions under Subsolidus Conditions. Journal of Petrology 50(5): 967-987

Powolny, T., Dumańska-Słowik, M., Anczkiewicz, A. A., & Sikorska-Jaworowska, M. (2022). Origin and timing of spilitic alterations in volcanic rocks from Głuszyca Górna in the Intra-Sudetic Basin, Poland. *Scientific reports*, *12*(1), 1-26. https://doi.org/10.1038/s41598-022-15644-2

Putnis A, Hinrichs R, Putnis CV, Golla Schindler U, Collins LG (2007) Hematite in porous red-clouded feldspars; evidence of large-scale crustal fluid-rock interaction. Lithos 95: 10-18

Putnis CV, Ruiz-Aguido E (2013) The mineral-water interface: Where minerals react with the environment. Elements 9: 177-182

Ramseyer K, Boles JR, Lichtner PC (1992) Mechanism of plagioclase albitization. Journal of Sedimentary Petrology 62: 349-356

Reicherter K, Froitzheim N, Jarosiński M, Badura J, Franzke H-J, Hansen M, Hübscher H, Müller R, Poprawa P, Reinecker J, Stackebrandt W, Voigt T, Von Eynatten H, Zuchiewicz W (2008). Alpine tectonics north of the Alps. In: McCann (ed), The Geology of Central Europe, Volume 2: Mesozoic and Cenozoic. Geological Society, London, pp 1233-1285

Richter L., Diamond LW (2022) Characterization of hydrothermal fluids that alter the upper oceanic crust to spilite and epidosite: Fluid inclusion evidence from the Semail (Oman) and Troodos (Cyprus) ophiolites. Geochimica et cosmochimica acta, 319: 220-253

Ricordel C, Parcerisa D, Thiry M, Moreau M-G, Gómez-Gras D (2007) Triassic magnetic overprints related to albitization in granites from the Morvan massif (France). Palaeogeography Palaeoclimatology Palaeoecology 251: 268-282. https://doi.org/10.1016/j.palaeo.2007.04.001

Ruffet G, Innocent C, Michard A, Féraud G, Beauvais A, Nahon D, Hamelin B (1996) A geochronological 40Ar39Ar and 87Rb87Sr study of K-Mn oxides from the weathering sequence of Azul, Brazil. Geochimica et Cosmochimica Acta 60: 2219-2232

Saigal GC, Morad S, Bjørlykke K, Egeberg PK, Aagaard P (1988) Diagenetic albitization of detrital K-feldspars in Jurassic, Lower Cretaceous, and Tertiary clastic reservoir rocks from offshore Norway, I Textures and origin. Journal of Sedimentary Petrology 58:1003-1013

Sandström B, Annersten H, Tullborg EL (2010) Fracture-related hydrothermal alteration of metagranitic rock and associated changes in mineralogy, geochemistry and degree of oxidation: a case study at Forsmark, central Sweden. International Journal of Earth Science 99: 1-25

Schmitt J-M (1986) Albitisation triasique, hydrothermalisme jurassique et altération supergène récente: métallogénie des gisements uranifères du Rouergue. Doct. ès Sciences Thesis, Strasbourg, Louis Pasteur University: p 240.

Schmitt J-M (1992) Triassic albitization in southern France: an unusual mineralogical record from a major continental paleosurface. In: Schmitt JM, Gall Q (eds) Mineralogical and geochemical records of paleoweathering. ENSMP, Mémoires des Sciences de la Terre, Paris, pp 115–131

Schmitt J-M (1994) Geochemical modeling and origin of the Triassic albitized regolith in Southern France. 14th International Sedimentological Congress, Aug. 20-28, Recife, Brazil, Abstracts S8, p. 19-21

Schmitt J-M Baubron JC, Bonhomme MG (1984) Pétrographie et datations K–Ar des transformations minérales affectant le gîte uranifère de Bertholène (Aveyron-France). Mineralium Deposita 19:123–131

Schmitt J-M, Clement JY (1989) Triassic regolithization: a major stage of pre-enrichment in the formation of unconformity related deposits in Southern France. Metallogenesis of uranium deposits. IAEA Technical Committee Meeting, Vienna 542(8): 93-113.

Simon K, Hoefs J (1987) Effects of meteoric water interaction on Hercynian granites from the Südschwarzwald, southwest Germany. Chemical Geology 61: 253-261

Słaby E, Götze J (2004) Feldspar crystallization under magma-mixing conditions shown by cathodoluminescence and geochemical modelling–a case study from the Karkonosze pluton (SW Poland). *Mineralogical Magazine*, *68*(4), 561-577

Słaby E, Martin H (2008) Mafic and felsic magma interaction in granites: the Hercynian Karkonosze pluton (Sudetes, Bohemian massif). Journal of Petrology 49: 353-391

Słaby E, Galbarczyk-Gąsiorowska E, Baszkiewicz A (2002) Mantled alkali-feldspar megacrysts from the marginal part of the Karkonosze granitoid massif (SW Poland). Acta Geologica Polonica 52: 501-519

Słaby E, Galbarczyk-Gąsiorowska E, Seltmann R, Müller A (2007) Alkali feldspar megacryst growth: Geochemical modelling. Mineralogy and Petrology 89: 1-29

Sobczyk A, Danišík M, Wojewoda J, Śliwiński W, Raczyński P, August C (2013) Zircon (U-Th)/He thermochronology of the Permian Weissliegendes sandstone in the Fore-Sudetic Homocline (SW Poland). Mineralogia - Special Papers: 41: 81.

Sobczyk A, Danišík M, Aleksandrowski P, Anczkiewicz A (2015) Post-Variscan cooling history of the central Western Sudetes (NE Bohemian Massif, Poland) constrained by apatite fission-track and zircon (U-Th)/He thermochronology. Tectonophysics 649: 47-57

Sobczyk A, Sobel ER, Georgieva V (2020) Meso-Cenozoic cooling and exhumation history of the Orlica-Śnieżnik Dome (Sudetes, NE Bohemian Massif, Central Europe): Insights from apatite fission-track thermochronometry. Terra Nova 32 (2): 122–133

Steinthorsson S, Helgason O (1992) Maghemite in Icelandic basalts. Mineralogical Magazine 56: 185-199

Stillings LL, Brantley SL (1995) Feldspar dissolution at 25°C and pH 3: Reaction stoichiometry and the effect of cations. Geochimica et Cosmochimica Acta 59: 1483-1496

Stober I, Bucher K (1999a) Origin of salinity of deep groundwater in crystalline rocks. Terra Nov 11:181–185. https://doi.org/10.1046/j.1365-3121.1999.00241.x

Stober I, Bucher K (1999b) Deep groundwater in the crystalline basement of the Black Forest region. Applied Geochemistry 14: 237–254. https://doi.org/10.1016/S0883-2927(98)00045-6

Sun SS, Eadington PJ (1987) Oxygen isotope evidence for the mixing of magmatic and meteoric waters during tin mineralization in the Mole Granite, New South Wales, Australia. Economic Geology 82: 43-52

Suzuki K, Adachi M (1994) Middle Precambrian detrital monazite and zircon from the hida gneiss on Oki-Dogo Island, Japan: their origin and implications for the correlation of basement gneiss of Southwest Japan and Korea. Tectonophysics 235: 277–292. https://doi.org/10.1016/0040-1951(94)90198-8

Suzuki K, Adachi M, Tanaka T (1991) Middle precambrian provenance of Jurassic sandstone in the Mino Terrane, central Japan: Th-U-total Pb evidence from an electron microprobe monazite study. Sedimentary Geology 75: 141–147. https://doi.org/10.1016/0037-0738(91)90055-I

Suzuki K, Adachi M, Kajizuka I (1994) Electron microprobe observations of Pb diffusion in metamorphosed detrital monazites. Earth and Planetary Science Letters 128: 391–405. https://doi.org/10.1016/0012- 1079 821X(94)90158-9

Taylor HP (1977) Water/rock interactions and the origin of H_2O in granitic batholiths. Journal of Geological Society of London 133: 509-558

Taylor HP (1977) Water/rock interactions and the origin of H2O in granitic batholiths: Thirtieth William Smith lecture. J Geol Soc London 133:509–558. doi: 10.1144/gsjgs.133.6.0509

Thiry M, Liron MN, Dubreucq P, Polton J-C (2017) Curiosités géologiques du massif de Fontainebleau, Guide géologique, BRGM Editions., 115 p.

Thiry M, Milnes AR, Rayot V, Simon-Coinçon R (2006) Interpretation of palaeoweathering features and successive silicifications in theTertiary regolith of Inland Australia. Journal of the Geological Society 163: 723-736

Vasconcelos PM, Becker TA, Renne PR, Brimhall GH (1994) Direct dating of weathering phenomena by 40Ar39Ar and K–Ar analysis of supergene K–Mn oxides. Geochimica et Cosmochimica Acta 58: 1635–1665

Vercruysse C (2011) Mise en évidence et datation de la paléosurface crétacée dans le massif des Vosges. Rapport No O110620CVER, Centre de Geosciences, Ecole des Mines de Paris, Fontainebleau, France, 75 p.

Waychunas GA (1991) Oxide Minerals: Petrologic and magnetic significance. Reviews in Mineralogy 25: 38-46.

Wierzchołowski B (1976) Granitoidy kłodzko-złotostockie i ich kontaktowe oddziaływanie na skały osłony (studium petrograficzne). Geologia Sudetica 11: 7-147

Wilamowski A, (2002) Chloritization and polytypism of biotite in the Łomnica granite, Karkonosze Massif, Sudetes, Poland: Stable isotope evidence. Chemical Geology 182(2-4): 529-547

Williams ML, Jercinovic MJ, Goncalves P, Mahan K (2006) Format and philosophy for collecting, 1096 compiling, and reporting microprobe monazite ages. Chemical Geology 225: 1–15. https://doi.org/1097 10.1016/j.mce.2005.09.009

Wojdyr M (2010) Fityk: A general-purpose peak fitting program. Journal of Applied Crystallography 43: 1126-1128

Yao KFE (2013) Albitization and oxidation of the granitoïd rocks related to the Triassic paleosurface in the Sudetes (SW Poland). Thesis École Nationale Supérieure des Mines de Paris in Paris (France) and Państwowy Instytut Geologiczny - Państwowy Instytut Badawczy in Warsaw (Poland). 164 p. http://pastel.archives-ouvertes.fr/pastel-00971314

Yerle J.-J, Thiry M (1979) Albitisations et minéralisations uranifères dans le socle et les sédiments permo-houillers du bassin de Brousse-Broquiès (Aveyron, France). Bulletin BRGM 4: 275-290

Žak J, Klominsky J (2007) Magmatic structures in the Krkonoše–Jizera Plutonic Complex, Bohemian Massif: evidence for localized multiphase flow and small-scale thermal–mechanical instabilities in a granitic magma chamber. Journal of Volcanology and Geothermal Research 164: 254-267

Žák J, Verner K, Sláma J, Kachlík V, Chlupáčová M (2013) Multistage magma emplacement and progressive strain accumulation in the shallow‐level Krkonoše‐Jizera plutonic complex, Bohemian Massif. Tectonics 32: 1493-1512

Zheng Y-F (1993) Calculation of oxygen isotope fractionation in anhydrous silicate minerals. Geochim Cosmochim Acta 57:1079-1091. doi: 10.1016/0016-7037(93)90042-U

Zijderveld, JDA. (1967) A.C. demagnetisation of rocks: analysis of results. In: Collinson, DW, Creer, KM, Runcorn, SK (Eds.), Methods in Paleomagnetism. Elsevier, Amsterdam: 254–286